

POLITECNICO DI MILANO

FACOLTÀ DI INGEGNERIA INDUSTRIALE  
CORSO DI LAUREA IN INGEGNERIA AERONAUTICA



Active flutter suppression using the  
receptance method

Relatore: Prof. Ricci Sergio

Tesina di laurea di:  
Chiozzini Alessandro  
matr. 724827

Anno Accademico 2010/2011



# Active flutter suppression using the receptance method



# Contents

<b>List of figures</b>	<b>I</b>
<b>Sommario</b>	<b>VII</b>
<b>Abstract</b>	<b>IX</b>
<b>1 Introduction</b>	<b>1</b>
1.1 Receptance Method . . . . .	2
1.1.1 Theory of the method . . . . .	3
1.1.2 Output-feedback control . . . . .	3
1.1.3 State-feedback control . . . . .	5
<b>2 Rigid wing</b>	<b>9</b>
2.1 Experimental model . . . . .	10
2.2 Numerical model . . . . .	16
2.3 Control by the receptance method . . . . .	20
2.3.1 First pairs of poles placed . . . . .	22
2.3.2 Second pair of poles placed . . . . .	36
2.4 Gains . . . . .	48
<b>3 Cantilever elastic wing</b>	<b>53</b>
3.1 Open loop system . . . . .	54
3.2 Controlled System . . . . .	55
3.2.1 First pairs of poles placed . . . . .	56
3.2.2 Second pairs of poles placed . . . . .	65
3.3 Gains . . . . .	73
<b>4 Conclusions and future work</b>	<b>77</b>
4.1 Conclusions . . . . .	77
4.2 Future work . . . . .	85
<b>Bibliography</b>	<b>87</b>

## CONTENTS

---

# List of Figures

2.1	Geometry of the wing section with pitch and plunge springs . . .	9
2.2	V-stack actuator . . . . .	10
2.3	Outline of the full test section . . . . .	12
2.4	Adjustable vertical spring . . . . .	13
2.5	Vertical stiffness range . . . . .	14
2.6	Adjustable torsional spring . . . . .	15
2.7	Torsional stiffness range . . . . .	16
2.8	Root locus of the uncontrolled system . . . . .	20
2.9	Open loop V-plots . . . . .	20
2.10	Root locus decreasing the real part of the first pair of poles, $V_C = 10 \text{ ms}^{-1}$ , leaving the second pair free . . . . .	22
2.11	Damping plot decreasing the real part of the first pair of poles, $V_C = 10 \text{ ms}^{-1}$ , leaving the second pair free . . . . .	23
2.12	Frequency plot decreasing the real part of the first pair of poles, $V_C = 10 \text{ ms}^{-1}$ , leaving the second pair free . . . . .	23
2.13	Root locus decreasing the real part of the first pair of poles, $V_C = 10 \text{ ms}^{-1}$ , placing the second pair . . . . .	24
2.14	Root locus of the second mode, $-30\%$ first pole real part vari- ation, $V_C = 10 \text{ ms}^{-1}$ , two strategies compared . . . . .	24
2.15	Damping plot, $-30\%$ first pole real part variation, $V_C = 10 \text{ ms}^{-1}$ , two strategies compared . . . . .	25
2.16	Damping plot, $-30\%$ first pole real part variation, fixing the second pair of poles, different $V_C$ compared . . . . .	26
2.17	Root locus increasing the real part of the first pair of poles, $V_C = 10 \text{ ms}^{-1}$ , leaving the second pair free . . . . .	26
2.18	Damping plot increasing the real part of the first pair of poles, $V_C = 10 \text{ ms}^{-1}$ , leaving the second pair free . . . . .	27
2.19	Frequency plot increasing the real part of the first pair of poles, $V_C = 10 \text{ ms}^{-1}$ , leaving the second pair free . . . . .	27
2.20	Root locus increasing the real part of the first pair of poles, $V_C = 10 \text{ ms}^{-1}$ , placing the second pair . . . . .	28

## LIST OF FIGURES

---

2.21	Damping plot increasing the real part of the first pair of poles, $V_C = 10 \text{ ms}^{-1}$ , placing the second pair . . . . .	28
2.22	Damping plot, 30% first pole real part variation, $V_C = 10 \text{ ms}^{-1}$ , two strategies compared . . . . .	29
2.23	Frequency plot, 30% first pole real part variation, $V_C = 10 \text{ ms}^{-1}$ , two strategies compared . . . . .	29
2.24	Root locus decreasing the imaginary part of the first pair of poles, $V_C = 10 \text{ ms}^{-1}$ , leaving the second pair free . . . . .	30
2.25	Damping plot decreasing the imaginary part of the first pair of poles, $V_C = 10 \text{ ms}^{-1}$ , leaving the second pair free . . . . .	30
2.26	Root locus of the first pole decreasing the imaginary part of the first pair of poles, $V_C = 10 \text{ ms}^{-1}$ , leaving the second pair free . . . . .	31
2.27	Root locus decreasing the imaginary part of the first pair of poles, $V_C = 10 \text{ ms}^{-1}$ , placing the second pair . . . . .	32
2.28	Damping plot increasing the imaginary part of the first pair of poles, $V_C = 10 \text{ ms}^{-1}$ , leaving the second pair free . . . . .	33
2.29	Root locus increasing the imaginary part of the first pair of poles, $V_C = 10 \text{ ms}^{-1}$ , leaving the second pair free . . . . .	33
2.30	Root locus increasing the imaginary part of the first pair of poles, $V_C = 10 \text{ ms}^{-1}$ , placing the second pair . . . . .	34
2.31	Frequency plot increasing the imaginary part of the first pair of poles, $V_C = 10 \text{ ms}^{-1}$ , placing the second pair . . . . .	34
2.32	Damping plot, -30% first pole imaginary part variation, leaving the second pair free, different $V_C$ compared . . . . .	35
2.33	Frequency plot, +15% first pole imaginary part variation, placing the second one, different $V_C$ compared . . . . .	35
2.34	Root locus decreasing the real part of the second pair of poles, $V_C = 10 \text{ ms}^{-1}$ , leaving the first pair free . . . . .	36
2.35	Damping plot decreasing the real part of the second pair of poles, $V_C = 10 \text{ ms}^{-1}$ , leaving the first pair free . . . . .	37
2.36	Frequency plot decreasing the real part of the second pair of poles, $V_C = 10 \text{ ms}^{-1}$ , leaving the first pair free . . . . .	37
2.37	Root locus, -30% second pole real part variation, $V_C = 10 \text{ ms}^{-1}$ , two strategies compared . . . . .	38
2.38	Root locus, -20% second pole real part variation, leaving the first pair free, different $V_C$ compared . . . . .	39
2.39	Damping plot, -20% second pole real part variation, leaving the first pair free, different $V_C$ compared . . . . .	39
2.40	Root locus increasing the real part of the second pair of poles, $V_C = 10 \text{ ms}^{-1}$ , leaving the first pair free . . . . .	40



2.41 Damping plot increasing the real part of the second pair of poles, $V_C = 10 \text{ ms}^{-1}$ , leaving the first pair free . . . . .	40
2.42 Root locus, 30% second pole real part variation, placing the first pair, different $V_C$ compared . . . . .	41
2.43 Damping plot, 30% second pole real part variation, placing the first pair, different $V_C$ compared . . . . .	41
2.44 Root locus decreasing the imaginary part of the second pair of poles, $V_C = 10 \text{ ms}^{-1}$ , leaving the first pair free . . . . .	42
2.45 Frequency plot decreasing the imaginary part of the second pair of poles, $V_C = 10 \text{ ms}^{-1}$ , leaving the first pair free . . . . .	43
2.46 Root locus decreasing the imaginary part of the second pair of poles, $V_C = 10 \text{ ms}^{-1}$ , placing the first pair . . . . .	43
2.47 Frequency plot decreasing the imaginary part of the second pair of poles, $V_C = 10 \text{ ms}^{-1}$ , placing the first pair . . . . .	44
2.48 Root locus increasing the imaginary part of the second pair of poles, $V_C = 10 \text{ ms}^{-1}$ , placing the first pair . . . . .	45
2.49 Damping plot increasing the imaginary part of the second pair of poles, $V_C = 10 \text{ ms}^{-1}$ , placing the first pair . . . . .	45
2.50 Root locus increasing the imaginary part of the second pair of poles, $V_C = 10 \text{ ms}^{-1}$ , leaving the first pair free . . . . .	46
2.51 Damping plot increasing the imaginary part of the second pair of poles, $V_C = 10 \text{ ms}^{-1}$ , leaving the first pair free . . . . .	46
2.52 Root locus increasing the imaginary part of the second pair of poles, $V_C = 20 \text{ ms}^{-1}$ , leaving the first pair free . . . . .	47
2.53 Root locus increasing the imaginary part of the second pair of poles, $V_C = 20 \text{ ms}^{-1}$ , placing the first pair . . . . .	47
2.54 Norm of the vector of the gains changing the real part of the first mode . . . . .	48
2.55 Norm of $\mathbf{g}$ changing the real part of the first mode . . . . .	49
2.56 Norm of $\mathbf{f}$ changing the real part of the second mode . . . . .	49
2.57 Norm of $\mathbf{g}$ changing the imaginary part of the second mode . . . . .	50
2.58 Norm of $\mathbf{f}$ changing the imaginary part of the first mode . . . . .	50
3.1 Root locus of the open loop system . . . . .	54
3.2 V plots of the open loop system . . . . .	55
3.3 Root locus decreasing the real part of the first pair of poles, $V_C = 20 \text{ ms}^{-1}$ , leaving the second pair free . . . . .	56
3.4 Damping plot decreasing the real part of the first pair of poles, $V_C = 20 \text{ ms}^{-1}$ , leaving the second pair free . . . . .	57
3.5 Frequency plot decreasing the real part of the first pair of poles, $V_C = 20 \text{ ms}^{-1}$ , leaving the second pair free . . . . .	57

## LIST OF FIGURES

---

3.6	Root locus, $-30\%$ first pole real part variation, $V_C = 20 \text{ ms}^{-1}$ , two strategies compared . . . . .	58
3.7	Damping plot, $-30\%$ first pole real part variation, leaving the second pair of poles free, different $V_C$ compared . . . . .	58
3.8	Root locus of the second mode, $-30\%$ first pole real part variation, leaving the second pair of poles free, different $V_C$ compared	59
3.9	Root locus increasing the real part of the first pair of poles, $V_C = 20 \text{ ms}^{-1}$ , leaving the second pair free . . . . .	59
3.10	Frequency plot increasing the real part of the first pair of poles, $V_C = 20 \text{ ms}^{-1}$ , leaving the second pair free . . . . .	60
3.11	Damping plot increasing the real part of the first pair of poles, $V_C = 20 \text{ ms}^{-1}$ , leaving the second pair free . . . . .	60
3.12	Damping plot, $30\%$ first pole real part variation, leaving the second pair of poles free, different $V_C$ compared . . . . .	61
3.13	Root locus decreasing the imaginary part of the first pair of poles, $V_C = 20 \text{ ms}^{-1}$ , leaving the second pair free . . . . .	61
3.14	Frequency plot decreasing the imaginary part of the first pair of poles, $V_C = 20 \text{ ms}^{-1}$ , leaving the second pair free . . . . .	62
3.15	Root locus, $-30\%$ first pole imaginary part variation, $V_C = 20 \text{ ms}^{-1}$ , two strategies compared . . . . .	62
3.16	Damping plot, $-30\%$ first pole imaginary part variation, leaving the second pair of poles free, different $V_C$ compared . . . . .	63
3.17	Root locus increasing the imaginary part of the first pair of poles, $V_C = 20 \text{ ms}^{-1}$ , leaving the second pair free . . . . .	63
3.18	Frequency plot increasing the imaginary part of the first pair of poles, $V_C = 20 \text{ ms}^{-1}$ , leaving the second pair free . . . . .	64
3.19	Root locus of the second mode, $30\%$ first pole imaginary part variation, $V_C = 20 \text{ ms}^{-1}$ , two strategies compared . . . . .	64
3.20	Damping plot, $30\%$ first pole imaginary part variation, $V_C = 20 \text{ ms}^{-1}$ , two strategies compared . . . . .	65
3.21	Root locus, $-5\%$ and $-10\%$ first pole real part variation, $V_C = 20 \text{ ms}^{-1}$ , leaving the second pair free . . . . .	66
3.22	Root locus, $-20\%$ and $-30\%$ first pole real part variation, $V_C = 20 \text{ ms}^{-1}$ , leaving the second pair free . . . . .	66
3.23	Root locus decreasing the real part of the second pair of poles, $V_C = 20 \text{ ms}^{-1}$ , placing the first pair . . . . .	67
3.24	Damping plot decreasing the real part of the second pair of poles, $V_C = 20 \text{ ms}^{-1}$ , placing the first pair . . . . .	67
3.25	Frequency plot decreasing the real part of the second pair of poles, $V_C = 20 \text{ ms}^{-1}$ , placing the first pair . . . . .	68

3.26	Root locus increasing the real part of the second pair of poles, $V_C = 20 \text{ ms}^{-1}$ , leaving the first pair free . . . . .	68
3.27	Damping plot increasing the real part of the second pair of poles, $V_C = 20 \text{ ms}^{-1}$ , leaving the first pair free . . . . .	69
3.28	Root locus increasing the real part of the second pair of poles, $V_C = 20 \text{ ms}^{-1}$ , placing the first pair . . . . .	69
3.29	Damping plot increasing the real part of the second pair of poles, $V_C = 20 \text{ ms}^{-1}$ , placing the first pair . . . . .	70
3.30	Root locus decreasing the imaginary part of the second pair of poles, $V_C = 20 \text{ ms}^{-1}$ , leaving the second pair free . . . . .	71
3.31	Root locus increasing the imaginary part of the second pair of poles, $V_C = 20 \text{ ms}^{-1}$ , placing the first pair . . . . .	71
3.32	Root locus, 10% second pole imaginary part variation, placing the first pair, different $V_C$ compared . . . . .	72
3.33	Frequency plot, 10% second pole imaginary part variation, placing the first pair, different $V_C$ compared . . . . .	72
3.34	Norm of the vector of the gains changing the real part of the first mode . . . . .	73
3.35	Norm of <b>f</b> and <b>g</b> changing the real part of the second mode leaving the first pair of poles free . . . . .	74
3.36	Norm of <b>f</b> and <b>g</b> changing the real part of the first mode leaving the second pair of poles free . . . . .	74
3.37	Norm of <b>g</b> changing the real part of the second mode . . . . .	75
3.38	Norm of the vector of the gains changing the imaginary part of the second mode . . . . .	75
3.39	Norm of <b>f</b> and <b>g</b> changing the imaginary part of the first mode leaving the second pair of poles free . . . . .	76

## LIST OF FIGURES

---

# Sommario

Il controllo attivo di un sistema aeroelastico è estremamente importante in quanto permette di manipolare instabilità dinamiche, come il flutter, ed estendere per un ampio range di velocità condizioni di volo stabili.

In questo report il controllo è stato applicato a due modelli aeroelastici con lo scopo di aumentare la velocità di flutter del sistema. Per ottenere questo risultato è stato utilizzato un metodo di posizionamento di poli basato completamente sulle funzioni di trasferimento misurate sperimentalmente chiamato *receptance method*. Questo approccio presenta numerosi vantaggi rispetto ad altre forme di controllo che come il *receptance method* richiedono una formulazione agli stati del problema. Questo metodo, basandosi infatti su funzioni di trasferimento ottenute sperimentalmente attraverso attuatori e sensori, non richiede la stima delle matrici strutturali del sistema (massa, rigidità e smorzamento) e non richiede un'approssimazione della matrice dei coefficienti aerodinamici. Inoltre permette di applicare il controllo senza l'obbligo di conoscere tutti gli stati del sistema e quindi non necessita l'implementazione di un osservatore per la loro ricostruzione.

Nello studio effettuato il lavoro è stato concentrato nell'utilizzo di una legge di controllo proporzionale alla velocità e allo spostamento degli stati disponibili applicando un controllo di retroazione agli stati, in questo modo le equazioni per calcolare i guadagni del controllore si riducono alla risoluzione di un sistema lineare.

L'obiettivo di questo lavoro è quello di ottenere un sistema in anello chiuso con prestazioni migliori applicando questo metodo di controllo, e indagare come l'assegnazione dei poli a un sistema aeroelastico influisca sul suo comportamento al variare della velocità di volo. Per ottenere questo risultato sono stati utilizzati due modelli d'ala, uno rigido e uno elastico, e sono state effettuate varie prove assegnando poli a bassa frequenza, comparando i risultati e controllando il valore dei guadagni ricavati.

**Parole chiave:** Controllo attivo, flutter, *receptance method*, posizionamento dei poli, sistema aeroelastico.

---

# Abstract

The aim of this thesis is to apply the receptance method on a aeroelastic system and investigate how this pole placement control method affects the behavior of the system in relation to the flutter speed. Two different models have been adopted, one rigid and one flexible, and the poles have been placed changing the real or the imaginary part. The control methodology has been applied to different air speeds to find the best strategy to increment the flutter speed of the controlled system.

**Key words:** Active control, flutter, receptance method, poles placement, aeroelastic system.

---



# Chapter 1

## Introduction

The phenomenon of flutter is the more characteristic problem of the aeroelastic analysis, it is a dynamic instability due to the interaction between elastic, inertial and aerodynamic forces: the airplane starts to absorb energy from the surrounding aerodynamic flow and that leads to unstable oscillations and to a catastrophic failure of the aircraft structure [1], [2], [3] .

Flutter analysis consists in studying the stability of the aeroelastic system, the eigenvalues behavior is examined changing the aerodynamic flow conditions. The aerodynamic forces, that are proportional to the airflow velocity and to the degrees of freedom of the system, affect the aeroelastic system modifying the eigenvalues. The eigenvalues, that define the damping ratios and natural frequencies can become unstable, with positive real part, resulting in diverging oscillations.

To avoid the onset of the instability within the flight envelope many control techniques have been developed and the flutter suppression has been achieved with both passive and active means [4], [5]. Passive control methodologies consist in mass balancing, structural modifications in order to increase the structural stiffness, restriction of the speed range, . . . . Even though this techniques are considered very robust in their performance, they introduce additional weight and constraints that may lead to an aircraft performance reduction. Instead active control uses the motion of the structure and the deflection of one or more control surfaces, driven through an appropriate control law [6], in order to introduce additional aerodynamic forces that counteract the occurrence of the instability so that the flutter envelope can be extended during the in-flight operations without damaging the aircraft performance.

The possibility to apply an active control system to suppress flutter using the deflection of a control surface has already been established in previous studies [7], [8], [9], [10]; in general the associated control problem deals in

adjusting the natural frequencies and the damping ratios of the aeroelastic system for achieving the desired closed-loop behavior.

Different control methodologies could be used to obtain the required features of the controlled system: control law based upon optimal control or based directly on pole placement [11], [12] have been developed. In this thesis to achieve the flutter suppression a pole placement control law has been used, based upon a new control methodology known as *Receptance Method* as shown in [13].

## 1.1 Receptance Method

The receptance method is well known in passive structural modification and it may be traced back to the work of Duncan [14] who determined the dynamic behavior, natural frequencies and anti-resonances, of a modified system from the receptances of the initial system and the known modification. Bishop and Johnson [15] and Ram [16] also addressed the direct structural modifications in their work, using the transfer functions of the initial system to obtain the eigenvalues of the modified one.

Still in passive structural modifications, the theory was further developed for the inverse problem of eigenvalue assignment, that consists in determining the modification that grant the desired dynamic behavior, and used for vibration suppression. The employment of transfer functions in assigning eigenvalues can be traced back to Weissenburger [17] who proposed a method based on receptance modeling for the assignment of a single natural frequency by a unit rank modification. Receptance modeling was first applied for the assignment of anti-resonances for vibration suppression by Vincent [18] who developed the Vincent circle theory, afterward extended by Ghandchi Tehrani [19] and then by Mottershead [20], [21] who used measured receptances for the assignment of anti-resonances.

Even if the advantage of passive modification is that the modified system is guaranteed to be stable, the form of the modification that can be realized in practice is restrictive and the number of eigenvalues to be assigned must be matched by the rank of the modification. For these reasons active control has received considerable interest and receptance method was developed and introduced for the first time in active vibration suppression by Ram and Mottershead [22]. The main issue in active control is the stability of the closed-loop system. The theory behind the receptance method has been developed further and can be applied to state-feedback control [22], output-feedback control [23] and include also the assignment of eigenvalues sensitivities respect the control gains [24] determined from the matrix of

measured receptances.

### 1.1.1 Theory of the method

This method is entirely based on measured frequency response function  $\mathbf{H}(i\omega)$ , that can be determined in theory by inverting the dynamic stiffness matrix, and has numerous advantages over the conventional matrix methods such as state-space control based on finite elements. In particular there is no need to evaluate the matrices of structural stiffness  $\mathbf{K}$  and structural mass  $\mathbf{M}$  which are usually well determined by a variational approach but suffer from modeling errors and need to be brought into agreement with test data by model updating, are usually very large and in practice model reduction methods have to be applied, that can result in degraded control performance. There is no need to evaluate the damping matrix  $\mathbf{C}$ : damping evaluation is always difficult, there are different forms of damping such as viscous or friction damping, in a FE approach is often neglected or assumed to be proportional but in active control the damping model is vitally important to complex eigenvalue analysis.

Another problem prevented using measured transfer functions is the modeling of the aerodynamic loads for an aeroelastic system so there is no need to model unsteady aerodynamic forces avoiding further approximations.

Since the method uses receptances rather than dynamic stiffness, the system equations are complete by measuring the states at sensor locations. This means that there is no need for model reduction or the estimation of the unmeasured states by an observer. The transfer functions are usually quite modest in size determined by the numbers of sensors and actuators.

In the following sections the equations for active control state-feedback and output-feedback laws are presented.

### 1.1.2 Output-feedback control

Given a dynamic system defined by the equation

$$\mathbf{M}\ddot{\mathbf{x}}(t) + \mathbf{C}\dot{\mathbf{x}}(t) + \mathbf{K}\mathbf{x}(t) = \mathbf{b}\mathbf{u}(t) + \mathbf{f}(t) \quad (1.1)$$

transformed in the Laplace frequency domain

$$(\mathbf{M}s^2 + \mathbf{C}s + \mathbf{K})\mathbf{x}(s) = \mathbf{b}\mathbf{u}(s) + \mathbf{f}(s) \quad (1.2)$$

Where  $\mathbf{M}$ ,  $\mathbf{C}$  and  $\mathbf{K} \in \mathfrak{R}^{n \times n}$  are the system matrices of mass, damping and stiffness,  $\mathbf{x}$  and  $\mathbf{f} \in \mathfrak{R}^{n \times 1}$  are respectively the vectors of the degrees of freedom and the external forces,  $\mathbf{u} \in \mathfrak{R}^{m \times 1}$  represents the vector of the

control forces and  $\mathbf{b} \in \mathfrak{R}^{n \times m}$  is the control force distribution matrix. The outputs directly in the Laplace domain can be defined as

$$\mathbf{y}(s) = \mathbf{D}\mathbf{x}(s) \quad (1.3)$$

Where  $\mathbf{D} \in \mathfrak{R}^{l \times n}$  is the sensor distribution matrix while the output vector  $\mathbf{y} \in \mathfrak{R}^{l \times 1}$ . For the output-feedback the control law can be determined as

$$\mathbf{u}(s) = -\hat{\mathbf{G}}\mathbf{y}(s) \quad (1.4)$$

Where  $\hat{\mathbf{G}}$  is the gains matrix and depends on the control law used:

- $\hat{\mathbf{G}} = \mathbf{G}$  for a displacement feedback.
- $\hat{\mathbf{G}} = s\mathbf{F}$  for a velocity feedback.
- $\hat{\mathbf{G}} = s^2\mathbf{N}$  for an acceleration feedback.
- any combination of the previous laws.

In the following equations a displacement plus velocity feedback is used to explain the method

$$\mathbf{u}(s) = -(\mathbf{G} + s\mathbf{F})\mathbf{y}(s) \quad (1.5)$$

Replacing equations (1.3) and (1.5) in equation (1.2)

$$(\mathbf{M}s^2 + \mathbf{C}s + \mathbf{K})\mathbf{x}(s) = -\mathbf{b}(\mathbf{G} + s\mathbf{F})\mathbf{y}(s) + \mathbf{f}(s) \quad (1.6a)$$

$$(\mathbf{M}s^2 + \mathbf{C}s + \mathbf{K} + \mathbf{b}(\mathbf{G} + \mathbf{F}s)\mathbf{D})\mathbf{x}(s) = \mathbf{f}(s) \quad (1.6b)$$

And defining the receptance matrix of the open-loop system as the inverse of the dynamic stiffness matrix

$$\mathbf{H}(s) = \mathbf{Z}^{-1} = (\mathbf{M}s^2 + \mathbf{C}s + \mathbf{K})^{-1} \quad (1.7)$$

Premultiplying both side of equation (1.6b) by  $\mathbf{H}(s)$  than gives

$$(\mathbf{I} + \mathbf{H}(s)\Delta\mathbf{Z}(s))\mathbf{x}(s) = \mathbf{H}(s)\mathbf{f}(s) \quad (1.8)$$

where

$$\Delta\mathbf{Z}(s) = \mathbf{b}(\mathbf{G} + \mathbf{F}s)\mathbf{D} \quad (1.9)$$

and finally the receptance of the closed-loop system can be defined in terms of the open-loop receptance as

$$\mathbf{x}(s) = \tilde{\mathbf{H}}(s) = (\mathbf{I} + \mathbf{H}(s)\mathbf{b}(\mathbf{G} + \mathbf{F}s)\mathbf{D})^{-1}\mathbf{H}(s)\mathbf{f}(s) \quad (1.10a)$$

$$\mathbf{x}(s) = \frac{\text{adj}(\mathbf{I} + \mathbf{H}(s)\mathbf{b}(\mathbf{G} + \mathbf{F}s)\mathbf{D})}{\det(\mathbf{I} + \mathbf{H}(s)\mathbf{b}(\mathbf{G} + \mathbf{F}s)\mathbf{D})}\mathbf{H}(s)\mathbf{f}(s) \quad (1.10b)$$

The closed-loop system poles are the roots of the denominator of  $\tilde{\mathbf{H}}(s)$  and can be placed by selecting the terms of the gains matrices to satisfy the characteristic equation

$$\det(\mathbf{I} + \mathbf{H}(\lambda_j)\mathbf{b}(\mathbf{G} + \mathbf{F}\lambda_j)\mathbf{D}) = 0, \quad j = 1, 2, \dots, r \quad r \leq 2n \quad (1.11)$$

Instead the zeros of  $p$ pth term of the closed-loop receptance are the roots of the numerator of  $\tilde{\mathbf{H}}(s)$  and can be determined finding the gains that

$$[\text{adj}(\mathbf{I} + \mathbf{H}(\mu_k)\mathbf{b}(\mathbf{G} + \mathbf{F}\mu_k)\mathbf{D})]_{pp} = 0 \quad (1.12)$$

If the poles and the zeros are placed in complex conjugate pairs the terms in the gains matrix are strictly real [25]. The method for pole-zero placement using receptances leads to the resolution of a non-linear system in the control gains so there may be multiple real solutions or the system can be uncontrollable [26], [23].

For a single input system  $\mathbf{u} \in \Re^{1 \times 1}$  and  $\mathbf{G}, \mathbf{F} \in \Re^{1 \times l}$  where  $l$  is the number of sensors used and that limits the number of pairs of poles and zeros that can be placed. Instead for a multi-input system gains matrices can be diagonal or fully populated. Diagonal gains matrices are the simplest form of gains while fully populated symmetric matrices allow more poles and zeros to be assigned than the number of sensors and actuators or a greater number of solutions to the nonlinear equations (1.11) (1.12) may become available. With more set of gains available a solution that leads to the least control cost or that make the poles and zeros placed least sensitive to changes in the gains term can be chosen.

The receptance matrix obtained in this equations as the inverse of the dynamic stiffness matrix in practice is obtained for experimental tests, that give  $\mathbf{H}(i\omega)$  and, in to apply the theory rational fraction polynomials are fitted to the measured terms in  $\mathbf{H}(i\omega)$  and the coefficients of the numerator and denominator are found solving a least-squares problem [27].

### 1.1.3 State-feedback control

For a multi-input system the state-feedback control leads to the solution of nonlinear equations as in the output-feedback control but for a single-input system where  $\mathbf{u}(s)$  is a number and  $\mathbf{b} \in \Re^{n \times 1}$  the gains to place poles and zeros and even to assign their sensibility respect the gains value are obtained solving a linear system.

Using the same system defined by the equation (1.1) with the same matrices but with  $\mathbf{b} \in \mathfrak{R}^{n \times 1}$  and  $\mathbf{u}(s) = u(s) \in \mathfrak{R}^{1 \times 1}$  and a state-feedback control law defined as

$$u(t) = -\mathbf{f}^T \dot{\mathbf{x}}(t) - \mathbf{g}^T \mathbf{x}(t) \quad (1.13)$$

where  $\mathbf{f}$  and  $\mathbf{g} \in \mathfrak{R}^{n \times 1}$ , it should be noted that each nonzero term in  $\mathbf{f}$  and  $\mathbf{g}$  implies the use of a sensor. Transforming equation (1.13) in the Laplace frequency domain and combining it with equation (1.2) the closed-loop dynamic equation is obtained

$$[\mathbf{M}s^2 + \mathbf{C}s + \mathbf{K} + \mathbf{b}(\mathbf{g} + \mathbf{f}s)^T] \mathbf{x}(s) = \mathbf{f}(s) \quad (1.14)$$

The closed-loop dynamic stiffness matrix differs from the open-loop one by a rank-1 modification  $\mathbf{b}(\mathbf{g} + \mathbf{f}s)^T$  which is a consequence of state-feedback using a single input  $u(t)$ . The closed-loop receptance matrix can be obtained from the open-loop one using the *Sherman-Morrison* formula [28] that gives the inverse of a matrix with a rank-1 modification in terms of the inverse of the original matrix

$$\tilde{\mathbf{H}}(s) = \mathbf{H}(s) - \frac{\mathbf{H}(s)\mathbf{b}(\mathbf{g} + \mathbf{f}s)^T \mathbf{H}(s)}{1 + (\mathbf{g} + \mathbf{f}s)^T \mathbf{H}(s)\mathbf{b}} \quad (1.15)$$

The poles of the closed-loop system are the roots of  $1 + (\mathbf{g} + \mathbf{f}s)^T \mathbf{H}(s)\mathbf{b}$  which is a scalar equation and to assign a complex set of eigenvalues  $\{\lambda_1, \lambda_2, \dots, \lambda_{2n}\}$  the terms of gains matrices have to be found such that

$$(\mathbf{g} + \lambda_k \mathbf{f})^T \mathbf{H}(\lambda_k) \mathbf{b} = -1 \quad k = 1, 2, \dots, 2n \quad (1.16)$$

Equation (1.16) can be rewritten as

$$\mathbf{r}_k^T \mathbf{g} + \lambda_k \mathbf{r}_k^T \mathbf{f} = -1 \quad k = 1, 2, \dots, 2n \quad (1.17)$$

with  $\mathbf{r}_k = \mathbf{H}(\lambda_k)\mathbf{b}$ . In order to obtain the gains term a linear system of  $2n$  equations in  $2n$  unknowns need to be solved

$$\begin{bmatrix} \mathbf{r}_1^T & \lambda_1 \mathbf{r}_1^T \\ \mathbf{r}_2^T & \lambda_2 \mathbf{r}_2^T \\ \vdots & \vdots \\ \mathbf{r}_{2n}^T & \lambda_{2n} \mathbf{r}_{2n}^T \end{bmatrix} \begin{Bmatrix} \mathbf{g} \\ \mathbf{f} \end{Bmatrix} = \mathbf{G} \begin{Bmatrix} \mathbf{g} \\ \mathbf{f} \end{Bmatrix} = \begin{Bmatrix} -1 \\ -1 \\ \vdots \\ -1 \end{Bmatrix} \quad (1.18)$$

If  $\mathbf{G}$  is invertible the system is controllable [22] and if the poles are placed in complex conjugate pairs the gains are strictly real [25].

The characteristic polynomial of the zeros of receptance  $\tilde{H}_{ij}$  is given from

$ij$ th numerator term of the equation (1.15)

$$\mathbf{e}_i^T \left( \mathbf{H}(\mu_k) - \frac{\mathbf{H}(\mu_k)\mathbf{b}(\mathbf{g} + \mu_k\mathbf{f})^T\mathbf{H}(\mu_k)}{1 + (\mathbf{g} + \mathbf{f}\mu_k)^T\mathbf{H}(\mu_k)\mathbf{b}} \right) \mathbf{e}_j = 0 \quad k = 1, 2, \dots, r \quad (1.19)$$

Where  $\mathbf{e}_k$  is the  $k$ th column of the identity matrix  $\mathbf{I} \in \mathfrak{R}^{n \times n}$ , and  $\{\mu_1, \mu_2, \dots, \mu_r\}$  is the set of complex zeros wanted, which are the roots of the numerator of equation (1.19). In order to achieve the zero placement the gains have to satisfy

$$\begin{aligned} & \mathbf{e}_i^T \{ [1 + (\mathbf{g} + \mu_k\mathbf{f})^T\mathbf{H}(\mu_k)\mathbf{b}]\mathbf{H}(\mu_k) - \mathbf{H}(\mu_k)\mathbf{b}(\mathbf{g} + \mu_k\mathbf{f})^T\mathbf{H}(\mu_k) \} \mathbf{e}_j = 0 \\ & [(\mathbf{g} + \mu_k\mathbf{f})^T\mathbf{H}(\mu_k)\mathbf{b}]\mathbf{e}_i^T\mathbf{H}(\mu_k)\mathbf{e}_j - \mathbf{e}_i^T[\mathbf{H}(\mu_k)\mathbf{b}(\mathbf{g} + \mu_k\mathbf{f})^T\mathbf{H}(\mu_k)]\mathbf{e}_j = -\mathbf{e}_i^T\mathbf{H}(\mu_k)\mathbf{e}_j \\ & H_{ij}(\mu_k)(\mathbf{g} + \mu_k\mathbf{f})^T\mathbf{H}(\mu_k)\mathbf{b} - \mathbf{e}_i^T\mathbf{H}(\mu_k)\mathbf{b}(\mathbf{g} + \mu_k\mathbf{f})^T\mathbf{H}(\mu_k)\mathbf{e}_j = -H_{ij}(\mu_k) \quad (1.20) \end{aligned}$$

Where  $H_{ij}$  is the  $ij$ th numerator of the open-loop receptance. Noting that  $\mathbf{e}_i^T\mathbf{H}(\mu_k)\mathbf{b}$  is a scalar as  $H_{ij}$ ,  $\mathbf{t}_k$  is defined as

$$\mathbf{t}_k = H_{ij}(\mu_k)\mathbf{H}(\mu_k)\mathbf{b} - [\mathbf{e}_i^T\mathbf{H}(\mu_k)\mathbf{b}]\mathbf{H}(\mu_k)\mathbf{e}_j$$

The set of equations represented by equation (1.20) can be rewritten in a matrix form

$$\begin{bmatrix} \mathbf{t}_1^T & \mu_1\mathbf{t}_1^T \\ \mathbf{t}_2^T & \mu_2\mathbf{t}_2^T \\ \vdots & \vdots \\ \mathbf{t}_r^T & \mu_r\mathbf{t}_r^T \end{bmatrix} \begin{Bmatrix} \mathbf{g} \\ \mathbf{f} \end{Bmatrix} = \begin{Bmatrix} -H_{ij}(\mu_1) \\ -H_{ij}(\mu_2) \\ \vdots \\ -H_{ij}(\mu_r) \end{Bmatrix} \quad (1.21)$$

It is possible to place poles and zeros simultaneously, given two complex sets  $\{\lambda_1, \lambda_2, \dots, \lambda_p\}$  and  $\{\mu_1, \mu_2, \dots, \mu_r\}$  with  $p + r \leq 2n$ , the gains  $\mathbf{g}$  and  $\mathbf{f}$  are obtained solving the linear system (1.22)

$$\begin{bmatrix} \mathbf{t}_1^T & \mu_1\mathbf{t}_1^T \\ \mathbf{t}_2^T & \mu_2\mathbf{t}_2^T \\ \vdots & \vdots \\ \mathbf{t}_r^T & \mu_r\mathbf{t}_r^T \\ \mathbf{r}_1^T & \lambda_1\mathbf{r}_1^T \\ \mathbf{r}_2^T & \lambda_2\mathbf{r}_2^T \\ \vdots & \vdots \\ \mathbf{r}_p^T & \lambda_p\mathbf{r}_p^T \end{bmatrix} \begin{Bmatrix} \mathbf{g} \\ \mathbf{f} \end{Bmatrix} = \begin{Bmatrix} -H_{ij}(\mu_1) \\ -H_{ij}(\mu_2) \\ \vdots \\ -H_{ij}(\mu_r) \\ -1 \\ -1 \\ \vdots \\ -1 \end{Bmatrix} \quad (1.22)$$

Once again if the poles and the zeros are placed in complex conjugate pairs the terms of the gains matrices are strictly real and as the output-feedback

control the control law used can be based on displacement, velocity or acceleration feedback or any combination of the previous ones.

As said before for each nonzero term in  $\mathbf{g}$  and  $\mathbf{f}$  there should be a sensor, and the the relative state needs to be evaluated, usually only few states are used in the state-feedback control and only the corresponding terms in the gains matrices are different from zero. In order to calculate the correct elements of the gains the rows of  $\mathbf{r}_k$  and/or  $\mathbf{t}_k$ , that coincide to the available states, are selected. If there are  $p$  nonzero terms in each gain matrix, placing  $m = p$  pairs of poles or zeros leads to a unique solution if the dynamic system is controllable, if  $m < p$  the system has infinite solutions and the one with minimum norm is used and if  $m > p$  the system is solved in a least-squares sense.



# Chapter 2

## Rigid wing

In this chapter the receptance method is applied to the model of a rigid wing with two degrees of freedom, the eigenvalues of the aeroelastic system are placed using the theory described in the first chapter and their placement is investigated in order to increase the flutter speed.

A model for the experimental tests has been designed and than a numerical one has been implemented with the same property in order to predict its behavior.

The rigid wing has two degrees of freedom, pitch  $\vartheta$  and heave  $h$ , and can be represented by a two dimensions airfoil as figure 2.1 shows.

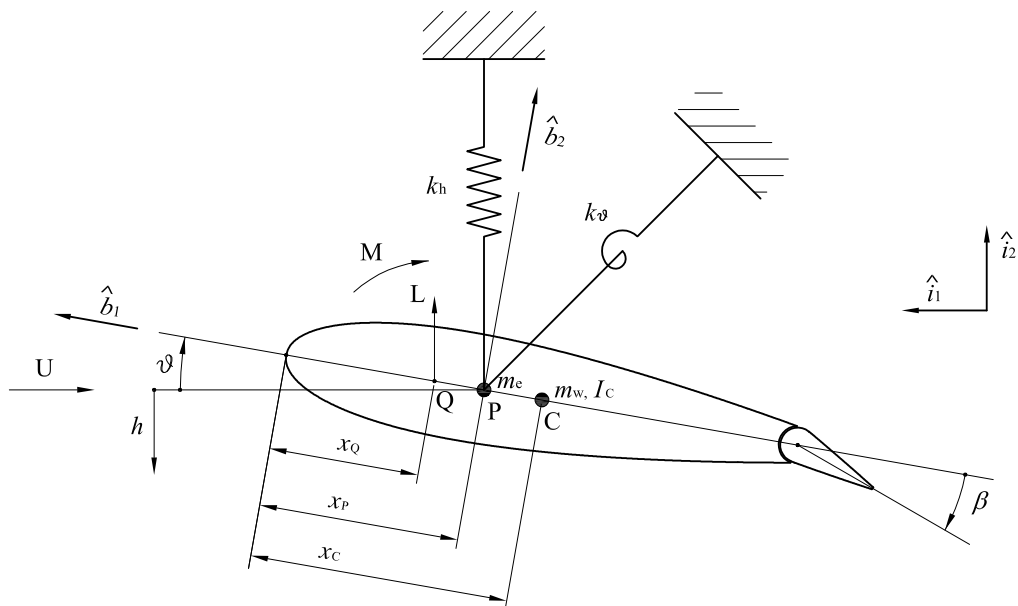


Figure 2.1: Geometry of the wing section with pitch and plunge springs

## 2.1 Experimental model

The experimental model has been designed for wind tunnel tests, given the test section of the wind tunnel used at Liverpool University the support system and the springs has been conceived.

The airfoil used in the test section is a NACA0018, the active control force is given by a flap which length is one fourth of the wing span and its chord is one fifth of the airfoil chord. The control surface is driven by a V-stack piezoelectric actuator allowing a deflection of about  $\pm 7$  degrees, the design of the actuator's geometry and layout is the same adopted by Ardelean et al in [29]; this kind of actuator has already been used and it proved to be successful in the active flutter suppression for an aeroelastic system, as shown in [10], and will be adopted for this study.

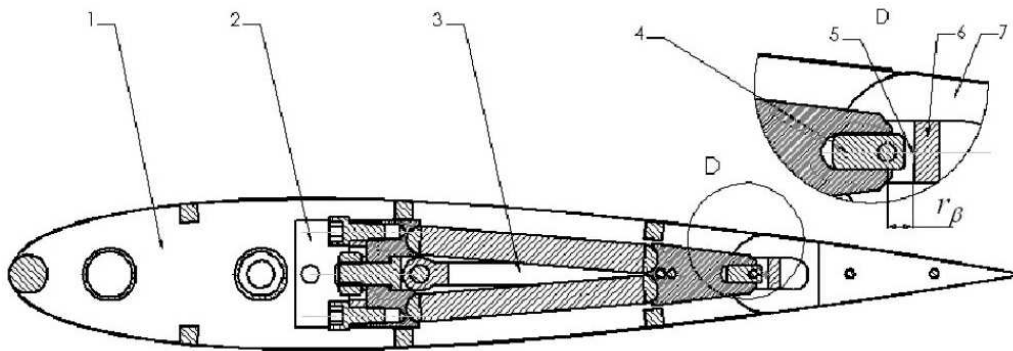


Figure 2.2: V-stack actuator

Figure 2.2 is taken directly from [10] and shows how the actuator is integrated in the wing, the numbers in the figure refer respectively:

1. indicate the wing rib
2. is the actuator support
3. show the actuator
4. is the slider
5. represents the hinge line
6. is the ball-bearing support
7. indicate the flap rib.

The wing is fitted inside the test section of the wind tunnel in order to simulate a two dimensions airfoil and to avoid the effects of the finite wing theory; the model used has been made of balsa wood and has been reinforced with aluminum plates where there is the connection of the piezoelectric actuator, the skin of the airfoil has been made with a film of polymeric material.

The model has been designed so that the parameters are constant over the span length as much as possible, and so that is possible to add additional masses in order to increase the global mass or in order to shift the center of gravity of the airfoil.

In table 2.1 are shown the main features of the wing obtained without additional masses:

Table 2.1: Wing parameters

<i>Parameter</i>	<i>Symbol</i>	<i>Value</i>
Span length [ <i>m</i> ]	$s_w$	1.2
Chord length [ <i>m</i> ]	$c_w$	0.35
Mass [ <i>kg</i> ]	$m_w$	3.6
Moment of inertia [ <i>kgm</i> ]	$I_C$	0.0253
Position of the center of gravity [ <i>m</i> ]	$x_C$	0.1472
Position of the reference point [ <i>m</i> ]	$x_P$	0.1167
Position of the aerodynamic center [ <i>m</i> ]	$x_Q$	0.0875
Flap span length [ <i>m</i> ]	$s_\beta$	0.3
Flap chord length [ <i>m</i> ]	$c_\beta$	0.07

The distances  $x_C$ ,  $x_P$  and  $x_Q$  are measured from the leading edge and refer to the points in figure 2.1;  $P$  is the point where the plunge displacement is measured and it is placed at one third of the chord length while  $Q$  is placed at one quarter of the chord.

The wing moves jointly with a passing aluminum shaft which gives the structural stiffness to the model; the shaft connects the wing to the springs that let it rotate and move upward. The aluminum pole defines the center of rotation  $P$ .

In figure 2.3 is shown an overview of the wind tunnel, the wing supports and the springs designed for this experiment.

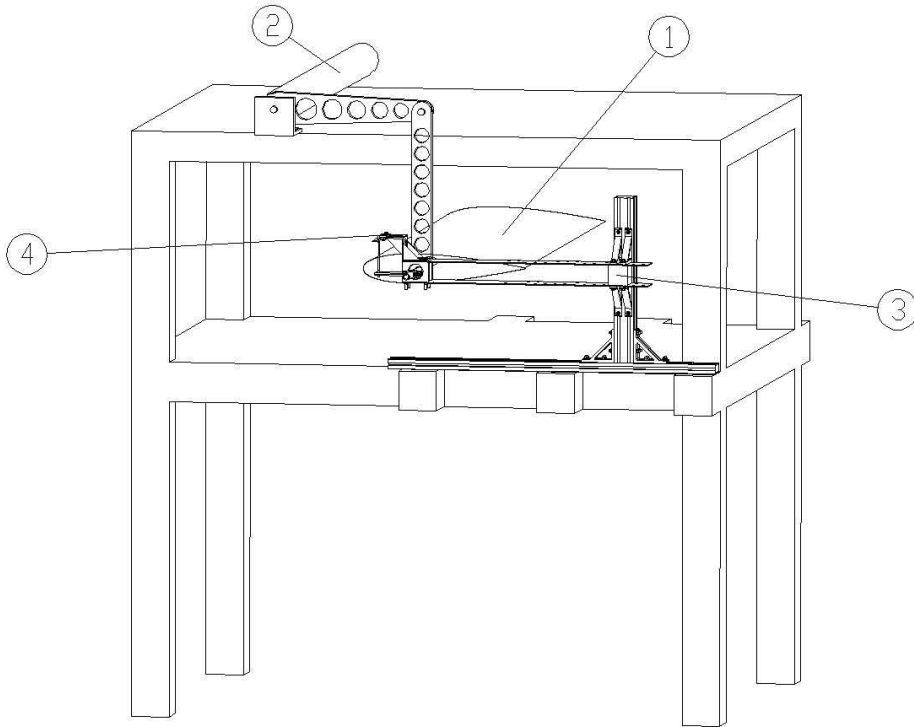


Figure 2.3: Outline of the full test section

In figure 2.3 for clarity only half of the supports are displayed, the same braces configuration is used on the other side of the wind tunnel. The number in the figure refer respectively to:

1. represents the airfoil in the wind tunnel
2. shows the torsional bar
3. indicate the vertical stiffness adjustable spring
4. is the torsional stiffness adjustable spring

The torsional bar is a steel cylindric bar with a high torsional stiffness that provides the same vertical displacements on the two sides of the airfoil. The torsional bar rotate jointly with two horizontal arms that, for small displacements, move upward and downward two vertical arms connected with bearings to the wing's shaft.

The springs, both vertical and torsional, are designed with elastic beam. The vertical springs on one side is fixed to the ground's supports while on the

other other side bear the wing; the airfoil and springs are attached through bearings that allow the shaft to rotate. In figure 2.4 is shown one vertical spring, as said before there is one symmetric spring on the back side of the test section.

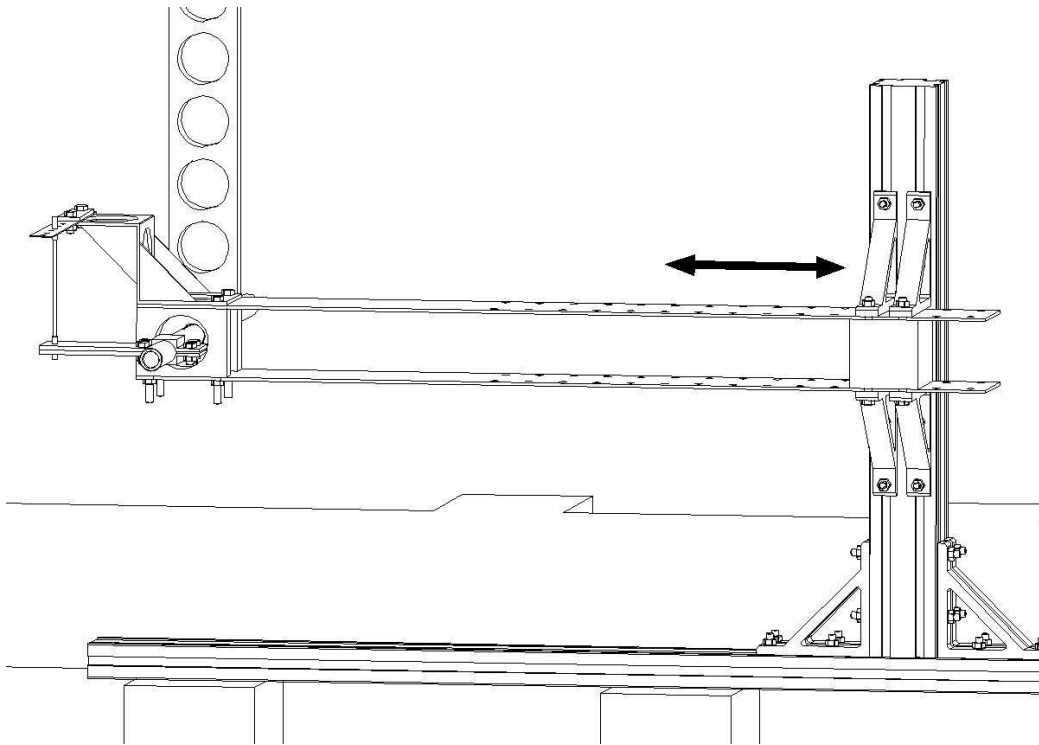


Figure 2.4: Adjustable vertical spring

As said before the experimental model has been designed such that the parameters may be changed easily; in fact by varying the clamp location in the direction shown in the figure, it is possible to vary the stiffness of the vertical spring.

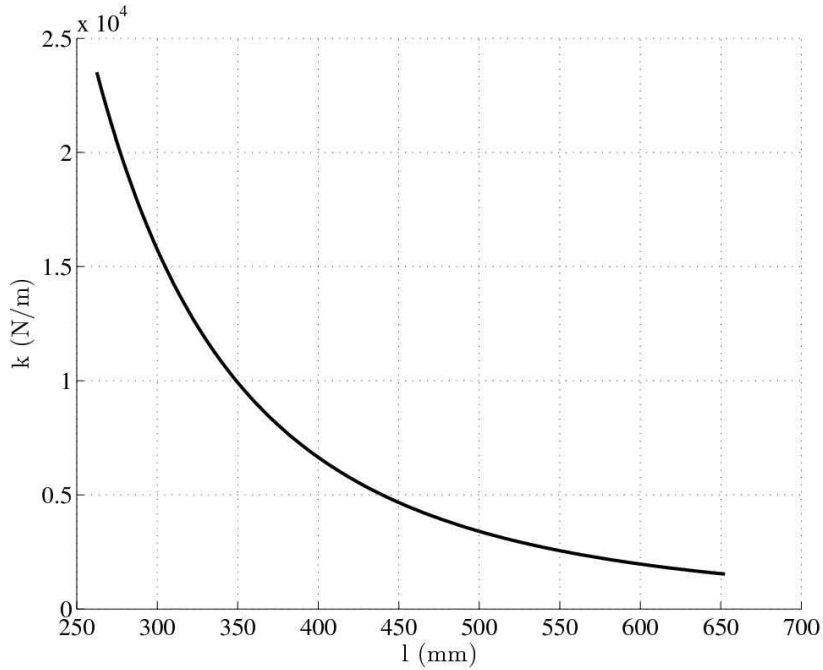


Figure 2.5: Vertical stiffness range

In figure 2.5 is displayed the range of the vertical stiffness versus the beams length, the chart shows the stiffness of the global system and that can vary from  $200 \text{ Nm}^{-1}$  to about  $23000 \text{ Nm}^{-1}$ .

The torsional spring is displayed in figure 2.6; the beam that gives the stiffness to the spring is fixed and moves jointly with the vertical springs beams and it is connected with a string to the aluminum shaft; when the shaft rotates bends the beam.

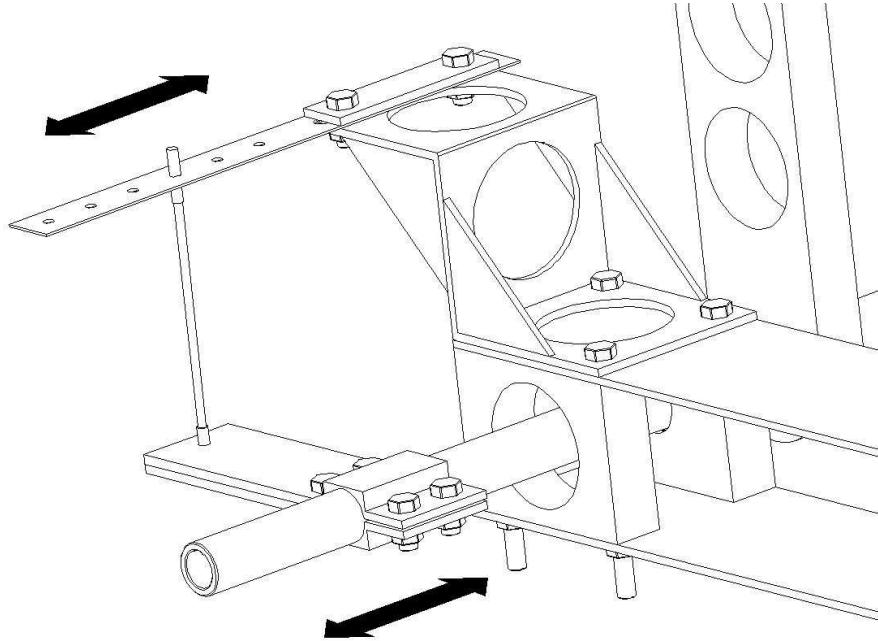


Figure 2.6: Adjustable torsional spring

The torsional spring is adjustable as the vertical one using the same method, by varying the length of the beam. In figure 2.7 is displayed the range of the torsional stiffness versus the beams length that goes from  $10 \text{ Nmrad}^{-1}$  to  $320 \text{ Nmrad}^{-1}$ .

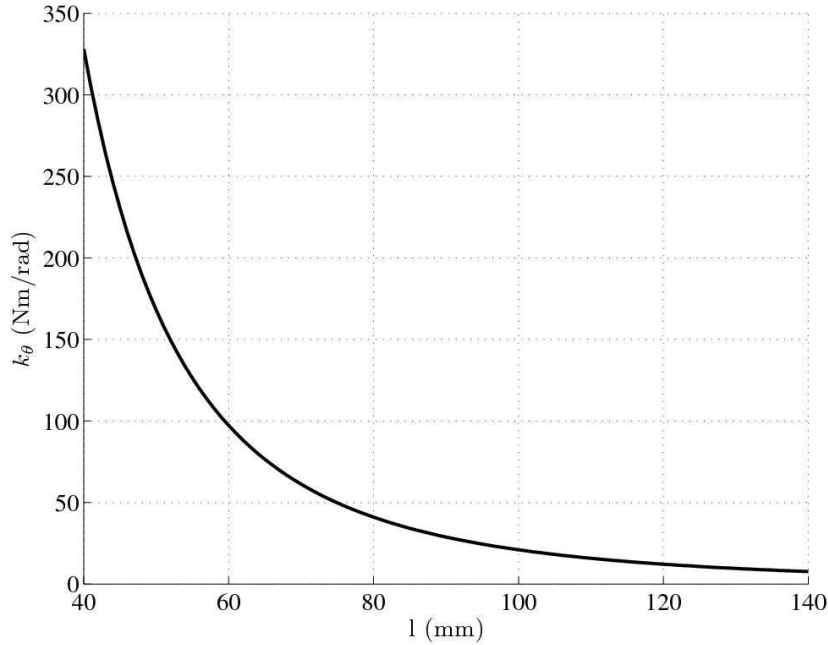


Figure 2.7: Torsional stiffness range

Using these ranges of stiffness, it is possible to vary the flutter speed of the aeroelastic system approximately between  $10 \text{ ms}^{-1}$  to  $70 \text{ ms}^{-1}$ . For the tests the value stiffness adopted are  $5000 \text{ Nm}^{-1}$  for the vertical spring and  $100 \text{ Nmrad}^{-1}$  for the torsional one.

Once designed the supports it is possible to calculate the external mass acting on the system; summing the masses of all the bolts, blocks arms and the inertia of the rotating components as horizontal arms and torsional bar the resulting external mass is equal to about  $6.5 \text{ kg}$  acting on the vertical spring and working for the plunge  $h$  degree of freedom.

## 2.2 Numerical model

A numerical model has been implemented, using *Matlab*, in order to simulate the wind tunnel experiment and foresee the behavior of the airfoil.

The structural matrices of the equations of motions have been obtained with Lagrange equations considering the wing as rigid, adding a external lumped mass  $m_e$  equals to the supports mass that acts on the vertical spring but not including in the model the additional masses that change the center



of gravity of the airfoil and neglecting the structural damping.

The potential energy  $E_p$  is given by:

$$E_p = \frac{1}{2}k_h h^2 + \frac{1}{2}k_\vartheta \vartheta^2 \quad (2.1)$$

where  $k_h$  and  $k_\vartheta$  are respectively the pitch and plunge stiffness,  $h$  is the displacement of  $P$  and  $\vartheta$  is the rotation as in Figure 2.1.

The kinetic energy  $E_k$  is

$$E_k = \frac{1}{2}m_w \mathbf{v}_C^2 + \frac{1}{2}m_e \mathbf{v}_P^2 + \frac{1}{2}I_C \dot{\vartheta}^2 \quad (2.2)$$

where  $m_w$  is the mass of the wing,  $I_C$  is the moment of inertia about  $C$ ,  $\mathbf{v}_C$  and  $\mathbf{v}_P$  are the velocities of  $C$  and  $P$  which can be expressed as

$$\mathbf{v}_C = \mathbf{v}_P + \dot{\vartheta} \hat{\mathbf{b}}_3 \times (x_C - x_P)(-\hat{\mathbf{b}}_1) \quad (2.3)$$

$$\mathbf{v}_P = -\dot{h} \hat{\mathbf{i}}_2 \quad (2.4)$$

so  $\mathbf{v}_C$  becomes

$$\mathbf{v}_C = -\dot{h} \hat{\mathbf{i}}_2 - (x_C - x_P) \dot{\vartheta} \hat{\mathbf{b}}_2 \quad (2.5)$$

The unit vector  $\hat{\mathbf{b}}_2$  can be written as

$$\hat{\mathbf{b}}_2 = -\sin \vartheta \hat{\mathbf{i}}_1 + \cos \vartheta \hat{\mathbf{i}}_2 \quad (2.6)$$

if  $\vartheta$  is small

$$\hat{\mathbf{b}}_2 = -\vartheta \hat{\mathbf{i}}_1 + \hat{\mathbf{i}}_2 \quad (2.7)$$

Substituting equation (2.7) in equation (2.5)

$$\mathbf{v}_C = (x_C - x_P) \dot{\vartheta} \hat{\mathbf{i}}_1 - (\dot{h} + (x_C - x_P) \dot{\vartheta}) \hat{\mathbf{i}}_2 \quad (2.8)$$

substituting equations (2.4) and (2.8) in equation (2.2) and assuming that  $\vartheta$  is small, the higher order term containing  $\vartheta^2 \dot{\vartheta}^2$  can be neglected, so the kinetic energy becomes

$$E_k = \frac{1}{2}m_w (\dot{h}^2 + (x_C - x_P)^2 \dot{\vartheta}^2 + 2(x_C - x_P) \dot{h} \dot{\vartheta}) + \frac{1}{2}m_e \dot{h}^2 + \frac{1}{2}I_C \dot{\vartheta}^2 \quad (2.9)$$

The moment of inertia about  $P$  can be calculated as

$$I_P = I_C + m_w (x_C - x_P)^2 \quad (2.10)$$

so

$$E_k = \frac{1}{2}m_w(\dot{h}^2 + 2(x_C - x_P)\dot{h}\dot{\vartheta}) + \frac{1}{2}m_e\dot{h}^2 + \frac{1}{2}I_P\dot{\vartheta}^2 \quad (2.11)$$

Applying Lagrange's equations

$$\frac{d}{dt} \frac{\partial E_k}{\partial \dot{q}_i} + \frac{\partial E_p}{\partial q_i} = Q_i \quad (i = 1, 2) \quad (2.12)$$

Where  $q_1 = h$ ,  $q_2 = \vartheta$ ,  $Q_1 = -L$  (lift force) and  $Q_2 = M$  (pitching moment), the equations of motion, in a matrix form, result

$$\begin{bmatrix} m_w + m_e & m_w(x_C - x_P) \\ m_w(x_C - x_P) & I_P \end{bmatrix} \begin{Bmatrix} \ddot{h} \\ \ddot{\vartheta} \end{Bmatrix} + \begin{bmatrix} k_h & \\ & k_\vartheta \end{bmatrix} \begin{Bmatrix} h \\ \vartheta \end{Bmatrix} = \begin{Bmatrix} -L \\ M \end{Bmatrix} \quad (2.13)$$

To obtain the aerodynamic forces, lift and pitching moment, a quasi-steady aerodynamic model has been used with forces that depends on the displacements of the degree of freedom and on the relative velocity between the wing and the airflow which leads to a modification of the angle of attack; to include the unsteady behavior of the aerodynamic a term is added:  $M_{\dot{\vartheta}}$  is the unsteady aerodynamic pitching term

The forces acting on all the wing are computed applying the string theory integrating along the wing span the features of each airfoil assuming constant parameters along the wing span.

The expression of the lift and the pitching moment are

$$L = \frac{1}{2}\rho V^2 c_w s_w C_{L,\alpha} \vartheta + \frac{1}{2}\rho V c_w s_w C_{L,\alpha} \dot{h} \quad (2.14)$$

$$M = \frac{1}{2}\rho V^2 c_w s_w C_{L,\alpha} \left( \vartheta + \frac{\dot{h}}{V} \right) (x_P - x_Q) + \frac{1}{8}\rho V s_w c_w^3 M_{\dot{\vartheta}} \dot{\vartheta} \quad (2.15)$$

Where  $V$  is the air speed,  $\rho$  is the air density,  $C_{L,\alpha}$  is the two-dimensional wing lift curve slope,  $c_w$  and  $s_w$  are respectively the wing chord length and the wing span length.

As said before the aerodynamic terms depend on the degrees of freedom and on their derivative and that affects the stiffness and the damping of the system with a term proportional to the velocity of the airflow. The equation of motion of the uncontrolled system can be rewritten as

$$\mathbf{M}\ddot{\mathbf{q}} + (\rho V \mathbf{C}_a + \mathbf{C})\dot{\mathbf{q}} + (\rho V^2 \mathbf{K}_a + \mathbf{K})\mathbf{q} = 0 \quad (2.16)$$

where  $\mathbf{M}$ ,  $\mathbf{C}$  and  $\mathbf{K}$  are respectively the structural mass, the structural damp-

ing (equals to zero in this model) and the structural stiffness, with  $\mathbf{q}$  the degrees of freedom vector while  $\mathbf{C}_a$  is the aerodynamic damping and  $\mathbf{K}_a$  is the aerodynamic stiffness defined as

$$\mathbf{C}_a = \begin{bmatrix} \frac{1}{2}c_w s_w C_{L,\alpha} & 0 \\ -\frac{1}{2}c_w s_w C_{L,\alpha}(x_P - x_Q) & -\frac{1}{8}s_w c_w^3 M_{\dot{\eta}} \end{bmatrix} \quad (2.17)$$

$$\mathbf{K}_a = \begin{bmatrix} 0 & \frac{1}{2}c_w s_w C_{L,\alpha} \\ 0 & -\frac{1}{2}c_w s_w C_{L,\alpha}(x_P - x_Q) \end{bmatrix} \quad (2.18)$$

Now it is possible to check the stability of the uncontrolled system versus the airflow velocity  $V$  by computing the eigenvalues of the system; the aerodynamic matrices depend on the air speed hence when  $V$  is equal to zero the system is undamped and the eigenvalues are purely imaginary.

To obtain the eigenvalues the system is transformed in the state space form

$$\dot{\mathbf{x}} = \begin{Bmatrix} \dot{\mathbf{q}} \\ \ddot{\mathbf{q}} \end{Bmatrix} = \begin{bmatrix} 0 & I \\ -M^{-1}(\rho V^2 \mathbf{K}_a + \mathbf{K}) & -M^{-1}(\rho V \mathbf{C}_a + \mathbf{C}) \end{bmatrix} \begin{Bmatrix} \mathbf{q} \\ \dot{\mathbf{q}} \end{Bmatrix} = \mathbf{A} \mathbf{x} \quad (2.19)$$

Where  $\mathbf{A}$  is the state matrix. There are four eigenvalues in complex conjugate pairs in the form

$$\lambda_{j,j+1} = \omega_j \zeta_j \pm \omega_j \sqrt{1 - \zeta_j^2} \quad j = 1, 2$$

plotting the real part versus the imaginary part of each pole changing the air speed the root locus for the uncontrolled system is obtained as shown in figure 2.8.

While the plots of eigenvalues damping, frequency, real part and imaginary part versus the velocity of airflow are displayed in figure 2.9.

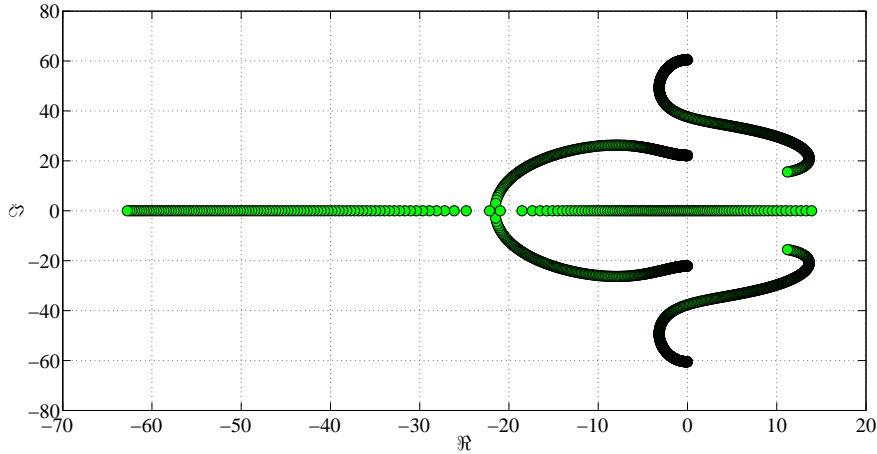


Figure 2.8: Root locus of the uncontrolled system

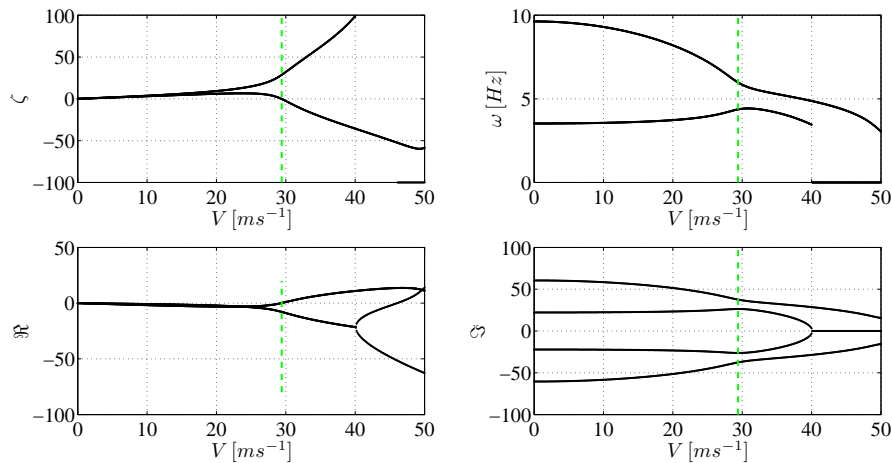


Figure 2.9: Open loop V-plots

For the uncontrolled system the flutter occurs at  $29.4 \text{ m s}^{-1}$ .

## 2.3 Control by the receptance method

The aeroelastic model is controlled through the deflection of the control surface, it is assumed that the flap can move to any prescribed position, within a range of acceptable values, without considering its dynamic so that the deflection  $\beta$  is the input of the system and not a degree of freedom. The control surface acts on the system through the aerodynamic forces, proportional to

its deflection, that are obtained applying the string theory.

$$L_{control} = \frac{1}{2}\rho V^2 c_w s_\beta C_{L,\beta} \beta \quad (2.20)$$

$$M_{control} = \frac{1}{2}\rho V^2 s_\beta (c_w C_{L,\beta} (x_P - x_Q) + c_w^2 C_{M,\beta}) \beta \quad (2.21)$$

Using the data from tables 2.1 and where

$$C_{L,\beta} = \frac{C_{L,\alpha}}{\pi} (\arccos(1 - 2E) + 2\sqrt{E(1 - E)})$$

$$C_{M,\beta} = -\frac{C_{L,\alpha}}{\pi} (1 - E) \sqrt{E(1 - E)}$$

and  $E$  is the chord fraction  $c_\beta/c_w$ .

The control force acting on the aeroelastic system is

$$\mathbf{F} = \mathbf{f}_\beta \beta = \begin{Bmatrix} -L_\beta \\ M_\beta \end{Bmatrix} \beta \quad (2.22)$$

The control law used, based on the state feedback control with the receptance method described in the first chapter, is proportional to the displacements and the velocity of the degrees of freedom

$$\beta = -\mathbf{g}^T \mathbf{q} - \mathbf{f}^T \dot{\mathbf{q}} \quad (2.23)$$

The equation of motion of the controlled system become

$$\mathbf{M}\ddot{\mathbf{q}} + (\rho V \mathbf{C}_a + \mathbf{C} + \mathbf{f}_\beta \mathbf{f}^T) \dot{\mathbf{q}} + (\rho V^2 \mathbf{K}_a + \mathbf{K} + \mathbf{f}_\beta \mathbf{g}^T) \mathbf{q} = 0 \quad (2.24)$$

while the state matrix is

$$\tilde{\mathbf{A}} = \begin{bmatrix} 0 & I \\ -M^{-1}(\rho V^2 \mathbf{K}_a + \mathbf{K} + \mathbf{f}_\beta \mathbf{g}^T) & -M^{-1}(\rho V \mathbf{C}_a + \mathbf{C} + \mathbf{f}_\beta \mathbf{f}^T) \end{bmatrix} \quad (2.25)$$

In a two dimensions model it can be placed up to four poles, two complex conjugate pairs in order to have real gains, assuming to know the four states obtainable with two sensors. The gains have the same dimensions of the generalized coordinates hence when there are four poles placed there is a unique solution to the system, when less poles are placed the linear system is underdetermined and there are infinite solutions, in this case the solutions with minimum norm is chosen.

In the tests the poles have been placed at two control air speed,  $V_C$  equals to  $10 \text{ ms}^{-1}$  and  $20 \text{ ms}^{-1}$  and different strategies have been adopted:

- changing the real or imaginary part of the first pair of poles and leave the other pair unconstrained and vice versa
- changing the real or imaginary part of the first pair of poles and assign to the second pair the same value of the open loop and vice versa

To investigate the effects of the position of the poles the real and the imaginary part have been changed separately; increasing or decreasing the real part of the eigenvalue is equivalent to increase or decrease its damping while acting on the imaginary part affects its frequency because the damping  $\zeta_j \ll 1$ .

Both real and imaginary part have been changed from  $-30\%$  to  $+30\%$  of the respective open loop value, than comparisons have been made between the results.

### 2.3.1 First pairs of poles placed

#### Real part modification

Decreasing the real part of the first pair of poles the damping of the first mode is actually reduced, the poles that go unstable are the second pair and the change affects slightly the path that they follow before the instability, as shown in figure 2.10, hence the flutter speed of the closed loop system is very close to the open loop one even if it is lower as shown in figure 2.11 and in figure 2.12.

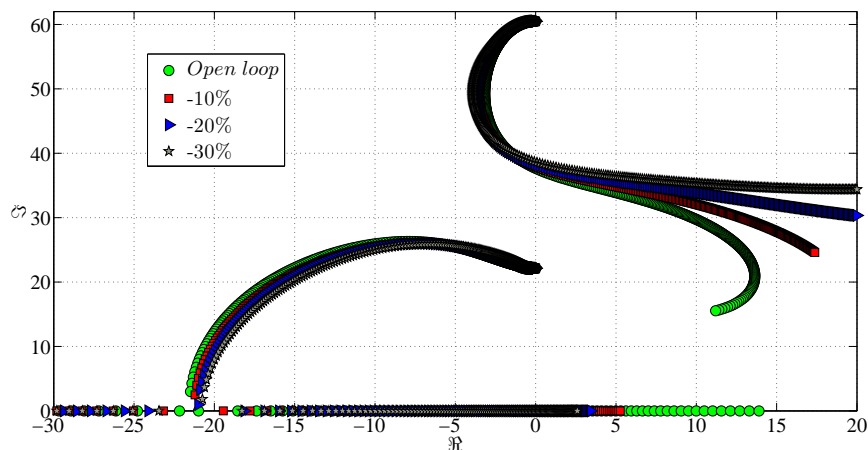


Figure 2.10: Root locus decreasing the real part of the first pair of poles,  $V_C = 10 \text{ ms}^{-1}$ , leaving the second pair free

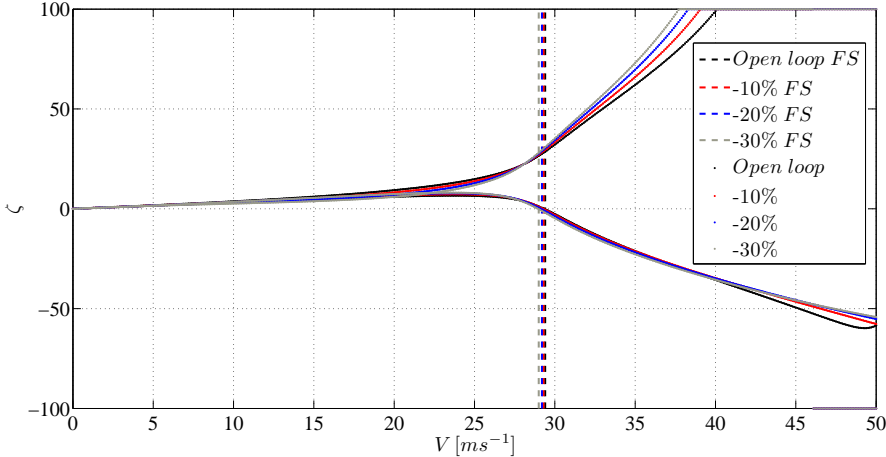


Figure 2.11: Damping plot decreasing the real part of the first pair of poles,  $V_C = 10\text{ ms}^{-1}$ , leaving the second pair free

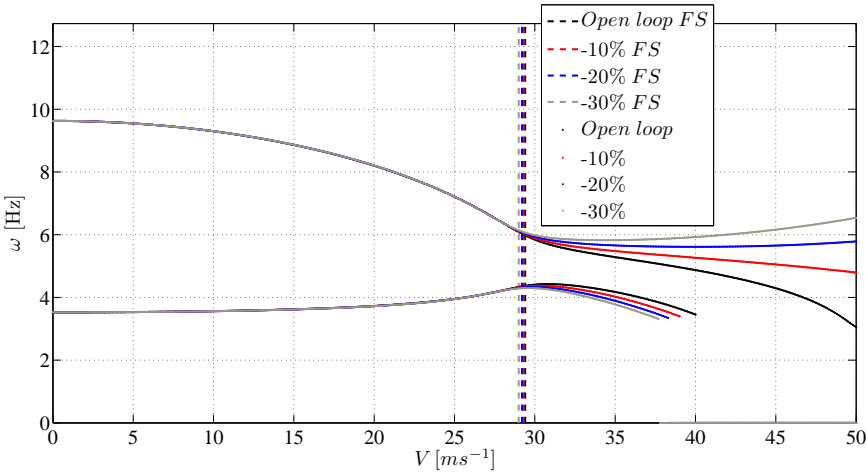


Figure 2.12: Frequency plot decreasing the real part of the first pair of poles,  $V_C = 10\text{ ms}^{-1}$ , leaving the second pair free

As shown in the figures above the change influences the behavior of the second pair of poles after that the instability occurs. In the frequencies plot after the splitting of the first pair of poles, where the imaginary part become zero and there are two real poles instead of two complex conjugate poles, the frequency has been set to zero because the mode described by that pair of poles is no longer oscillatory.

Fixing the second pair poles, forcing them in the same position of the open loop system, and decreasing the real part of the first one the behavior is similar to the previous case as shown in figure 2.13.

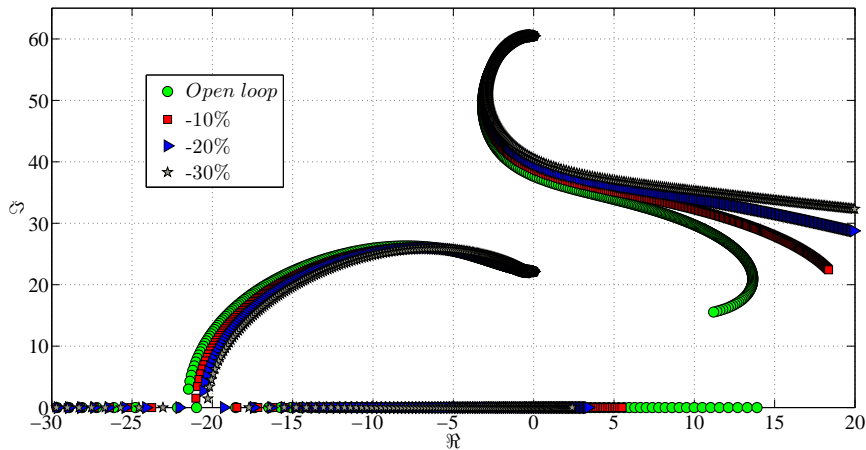


Figure 2.13: Root locus decreasing the real part of the first pair of poles,  $V_C = 10 \text{ ms}^{-1}$ , placing the second pair

Comparing the two strategies it can be seen that fixing the second pole forces it to follow the path of the open loop system up to higher air speeds than the other case and this leads to lower flutter speed due to an anticipated trespassing of the stability threshold. In figure 2.14 is shown the root locus of the second mode using the two strategies for a  $-30\%$  variation of the first pairs of poles real part.

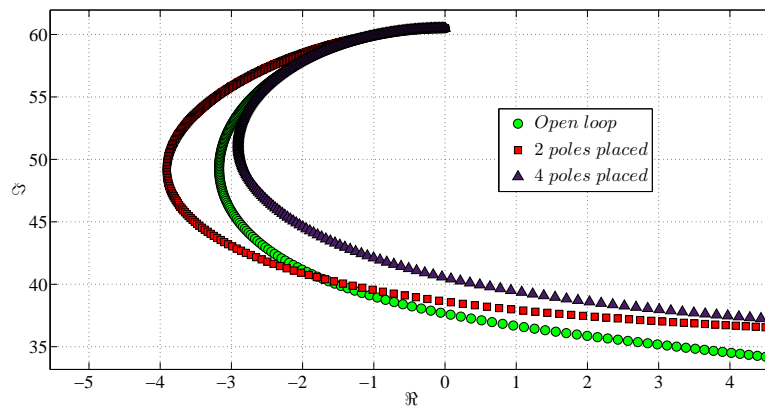


Figure 2.14: Root locus of the second mode,  $-30\%$  first pole real part variation,  $V_C = 10 \text{ ms}^{-1}$ , two strategies compared



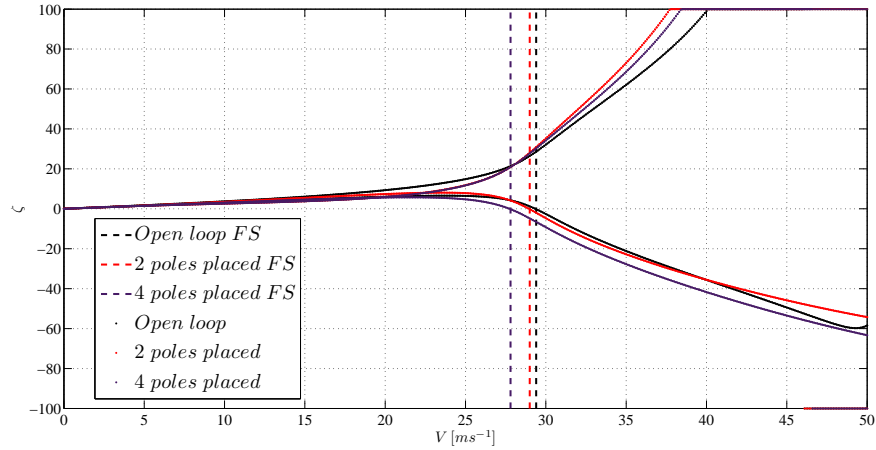


Figure 2.15: Damping plot,  $-30\%$  first pole real part variation,  $V_C = 10 \text{ ms}^{-1}$ , two strategies compared

In figure 2.15 is shown the difference in the flutter speeds using the  $V - \zeta$  plot. Leaving the second pair of poles free gives a flutter speed that is  $1.36\%$  lower than the open loop instability speed instead fixing the second pair gives a  $-5.44\%$  difference.

Test have been made increasing the control speed  $V_C$ , for both strategies the raise of the velocity where the control is applied leads to a reduction of the effects of the control; the closed loop flutter speed is greater for higher control velocity but the global behavior of the poles is the same for both velocities and the closed loop system still become unstable before the uncontrolled one. In figure 2.16 is shown an example of the  $V_C$  modification effect on the flutter speed.

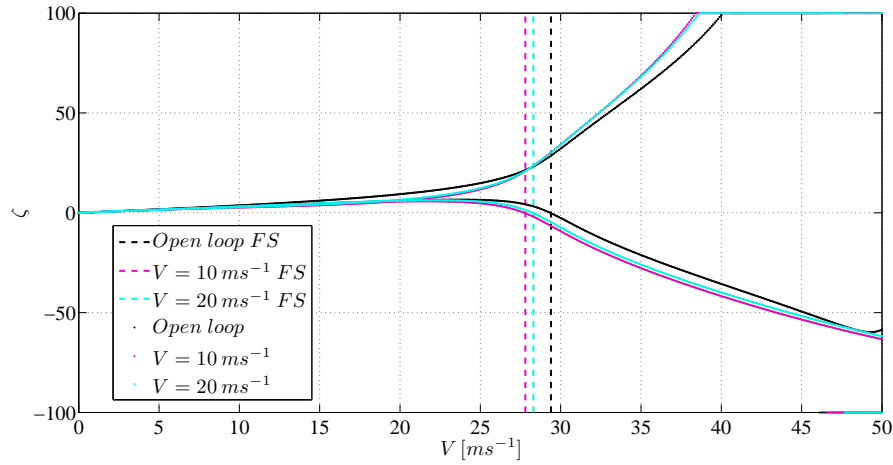


Figure 2.16: Damping plot,  $-30\%$  first pole real part variation, fixing the second pair of poles, different  $V_C$  compared

In figure 2.17 is shown the root locus for the open loop system and the closed loop increasing the real part of the first pair of poles up to the  $30\%$  of the open loop value at  $V_C$ ; as for the previous example these changes affect the poles path significantly only at higher air speed so the flutter occurs almost at the same speed of the uncontrolled system as shown also in figure 2.18.

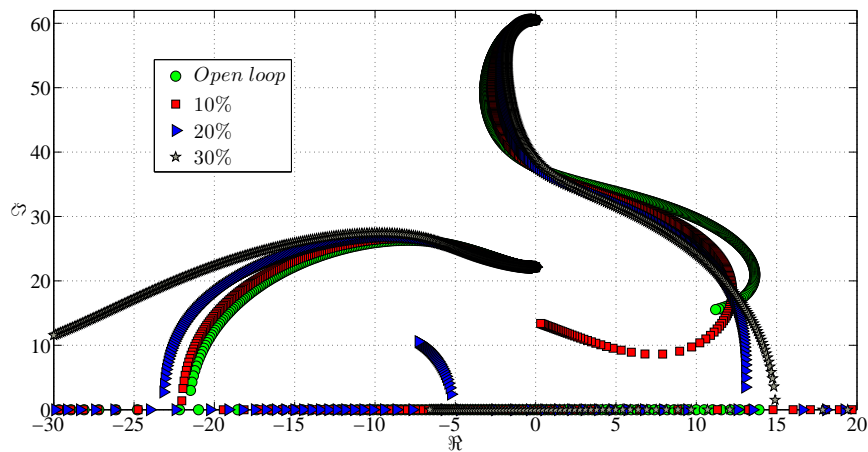


Figure 2.17: Root locus increasing the real part of the first pair of poles,  $V_C = 10 \text{ ms}^{-1}$ , leaving the second pair free

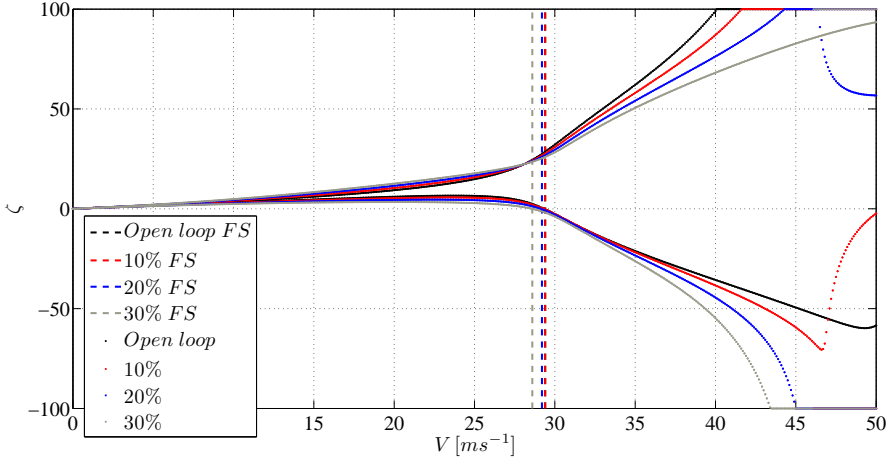


Figure 2.18: Damping plot increasing the real part of the first pair of poles,  $V_C = 10 \text{ ms}^{-1}$ , leaving the second pair free

However increasing the real part shifts the trajectories of the second pair of poles towards the real axis and changes the mode that become non-oscillatory as can be seen in the frequencies plot against the air speed in figure 2.19.

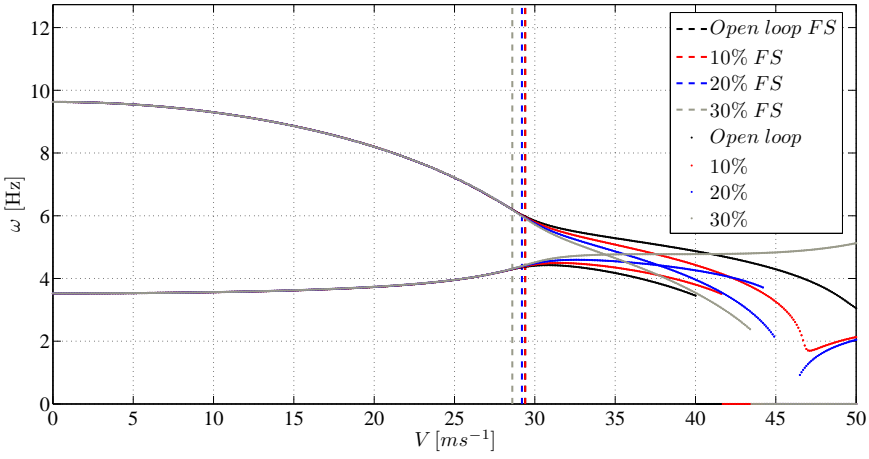


Figure 2.19: Frequency plot increasing the real part of the first pair of poles,  $V_C = 10 \text{ ms}^{-1}$ , leaving the second pair free

Instead fixing the second pair of poles and increasing the damping of the first mode increases the flutter speed of the controlled system; both the path of the first and the second pole shifts raising the percentage change up to 30% of the open loop value at  $V_C$ : the second pole crosses the imaginary axis at higher air speeds as shown in the root locus in figure 2.20 and in the damping plot versus the air speed in figure 2.21.

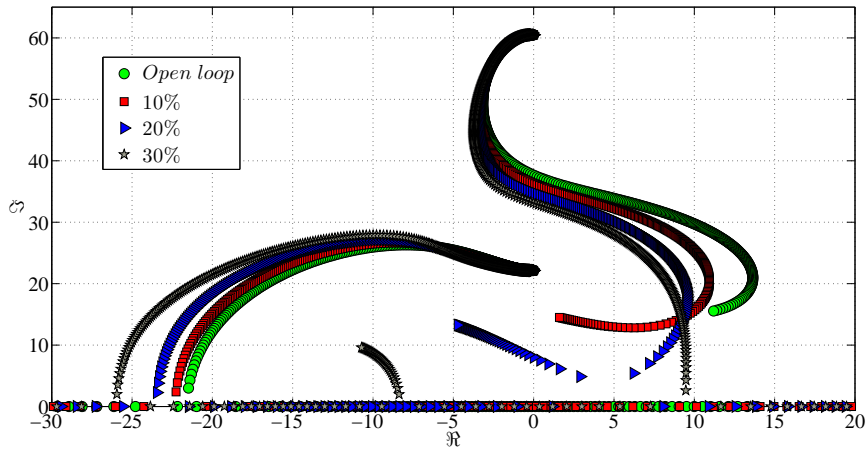


Figure 2.20: Root locus increasing the real part of the first pair of poles,  $V_C = 10 \text{ ms}^{-1}$ , placing the second pair

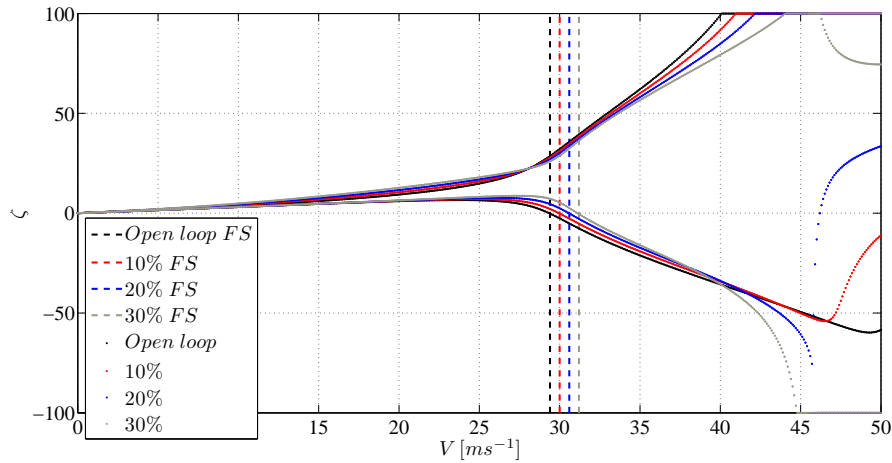


Figure 2.21: Damping plot increasing the real part of the first pair of poles,  $V_C = 10 \text{ ms}^{-1}$ , placing the second pair

As shown in figure 2.21 greater is the variation grater is the effect on the

flutter speed.

Comparing the two techniques applied, leaving the second pair of poles free or fixing it, what happens is that even if the frequencies progress with air speed is similar the damping of the second mode is higher and this leads to a positive increment in the flutter speed as shown in figure 2.22 and in figure 2.23.

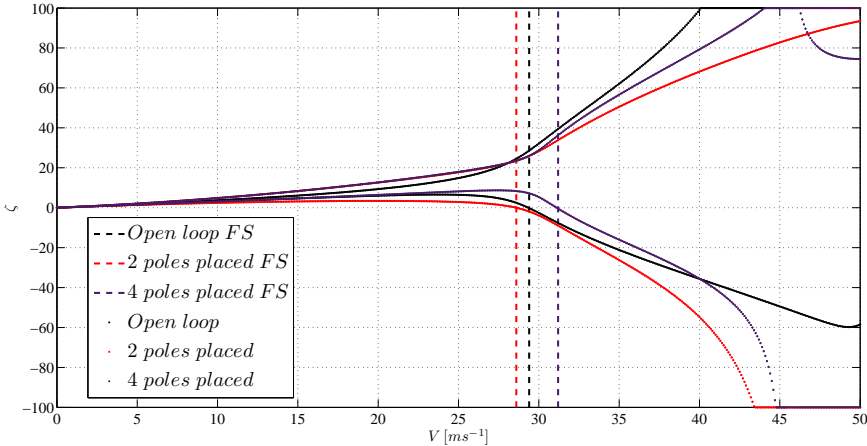


Figure 2.22: Damping plot, 30% first pole real part variation,  $V_C = 10 \text{ ms}^{-1}$ , two strategies compared

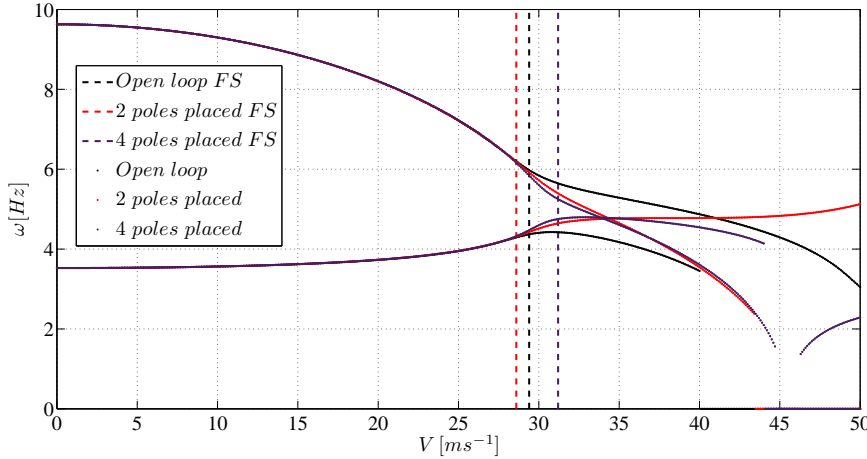


Figure 2.23: Frequency plot, 30% first pole real part variation,  $V_C = 10 \text{ ms}^{-1}$ , two strategies compared

### Imaginary part modification

From the tests made changing the imaginary part of the first pole can infer that the closed loop system is more sensitive to frequency's modifications; the results change significantly depending on the strategy applied and the value of the modification.

Decreasing the imaginary part from  $-5\%$  to  $-10\%$  without fixing the second mode, the flutter speed shifts from  $43.1\text{ m s}^{-1}$  to  $2.2\text{ m s}^{-1}$ .

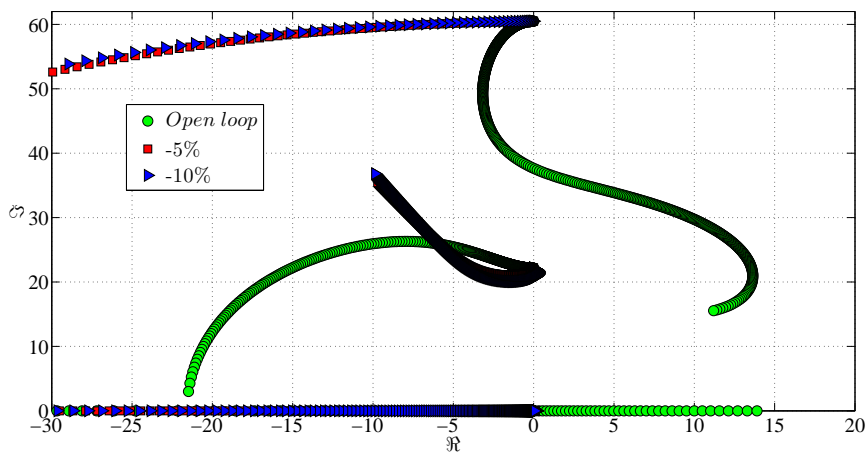


Figure 2.24: Root locus decreasing the imaginary part of the first pair of poles,  $V_C = 10\text{ m s}^{-1}$ , leaving the second pair free

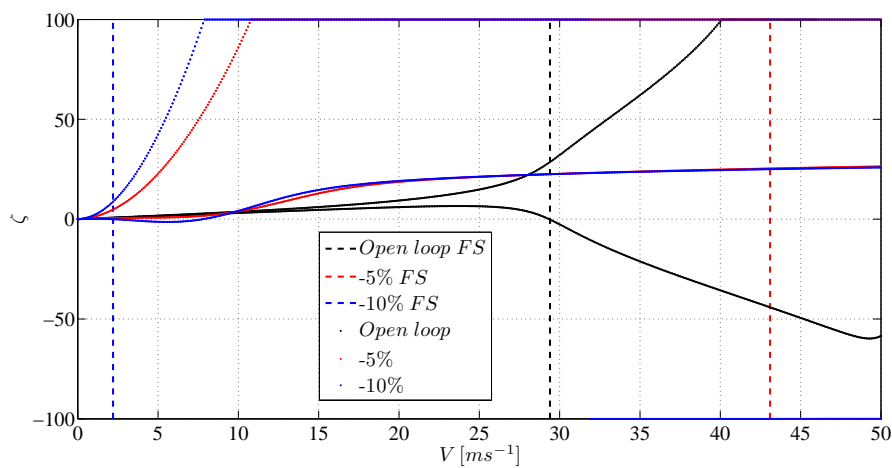


Figure 2.25: Damping plot decreasing the imaginary part of the first pair of poles,  $V_C = 10\text{ m s}^{-1}$ , leaving the second pair free

As shown in figure 2.24 the trajectory of the poles changes completely from the open loop system. Increasing the absolute value of the modification the stability limit gets lower; this is due to the trajectory of the first pole, while decreasing its imaginary part changes its path and goes backward towards the imaginary axis as shown in figure 2.26, where is represented the root locus of the first pole for the initial air speeds.

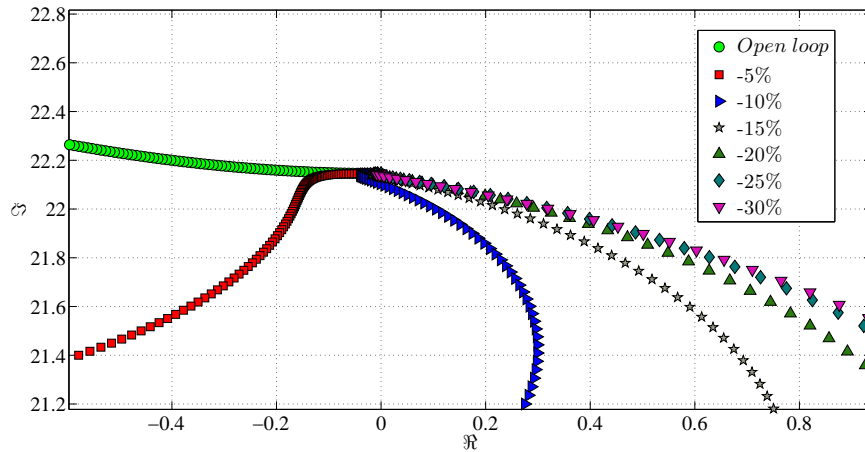


Figure 2.26: Root locus of the first pole decreasing the imaginary part of the first pair of poles,  $V_C = 10 \text{ ms}^{-1}$ , leaving the second pair free

Unlike the tests made modifying the real part, fixing the second pair of poles and decreasing the imaginary part gives a completely different behavior of the poles: the trajectories in the roots plot are similar to the open loop system. For lower variation (in absolute value) the pole that goes unstable is the one with higher frequency instead for greater modifications the first pole is obliged to go too close to the real axis, the assigned frequency is too low, and it splits into two real eigenvalues one of which become unstable.

In figure 2.27 is represented the roots locus for this test.

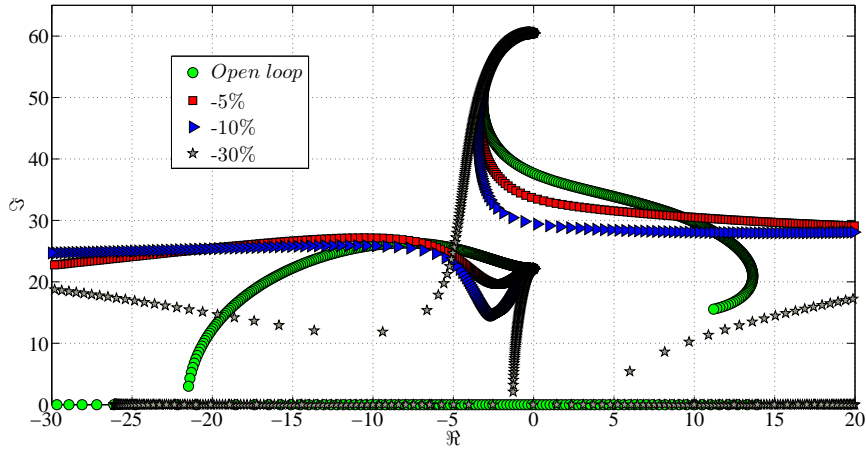


Figure 2.27: Root locus decreasing the imaginary part of the first pair of poles,  $V_C = 10 \text{ m s}^{-1}$ , placing the second pair

Using this strategy the flutter speed is always lower than the closed loop system and bigger is the modification lower is the flutter speed.

Increasing the imaginary part of the first pair of poles without fixing the second one the closed loop system goes unstable almost immediately; as for the previous test where the imaginary part has been reduced, using the same strategy, the first pole's trajectory bends toward the imaginary axis before reaching the assigned pole value creating a ring that cross the imaginary axis before returning stable; but unlike the other tests is the first pole that gives the stability margin because goes unstable at low air speed as shown in figures 2.28 and 2.29.



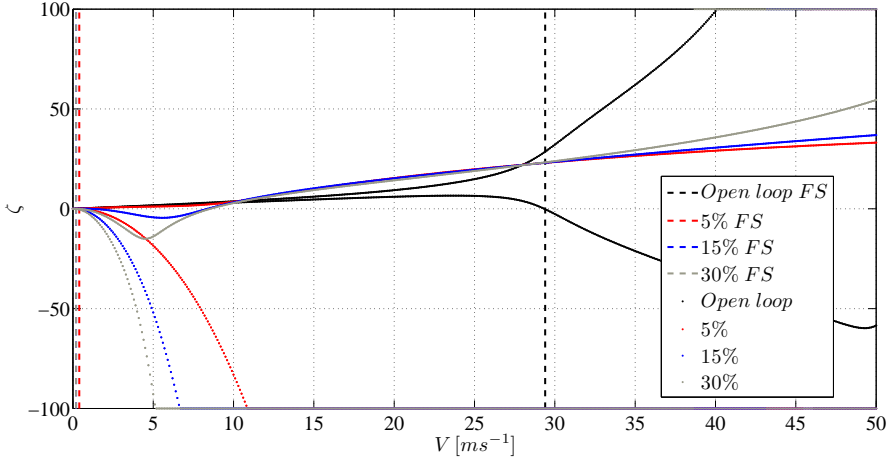


Figure 2.28: Damping plot increasing the imaginary part of the first pair of poles,  $V_C = 10\ ms^{-1}$ , leaving the second pair free

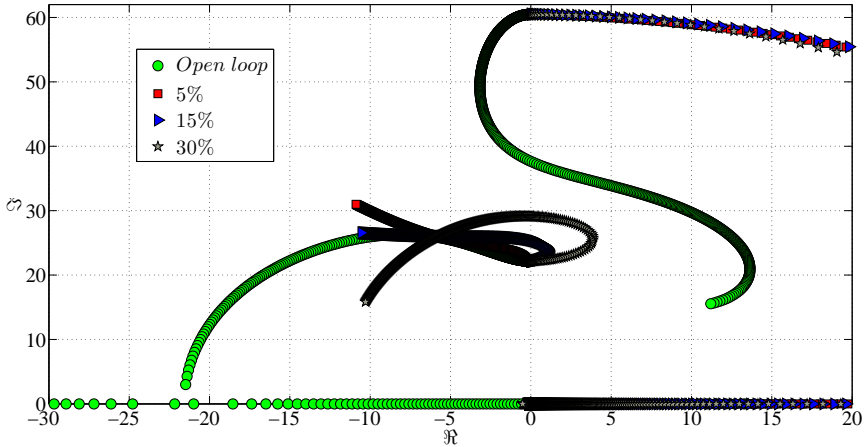


Figure 2.29: Root locus increasing the imaginary part of the first pair of poles,  $V_C = 10\ ms^{-1}$ , leaving the second pair free

Placing the second pair of poles to the same position of the open loop system and applying the same variation of the previous test to the first pole the results are completely different: the flutter speed of the closed loop system is higher than the uncontrolled one. Unlike the open loop system the pole that cause the instability is the first one that reaches the real axis, the poles no longer describes a oscillatory mode and the complex conjugate pair becomes a pair of real poles one of which becomes unstable.

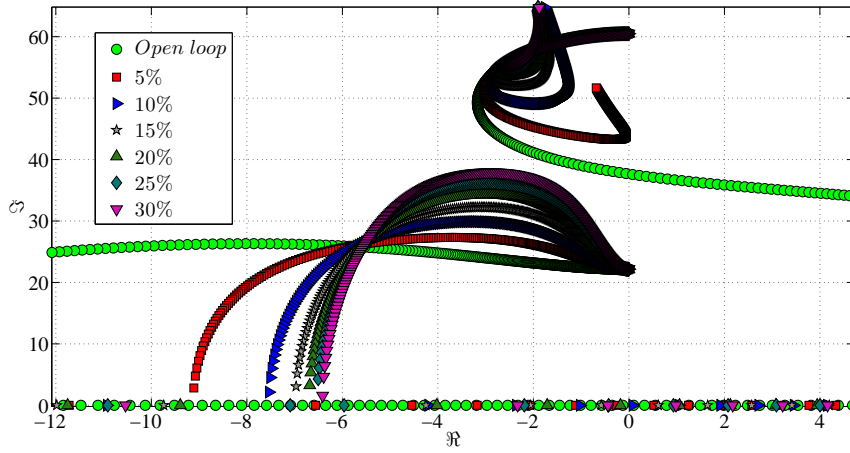


Figure 2.30: Root locus increasing the imaginary part of the first pair of poles,  $V_C = 10 \text{ m s}^{-1}$ , placing the second pair

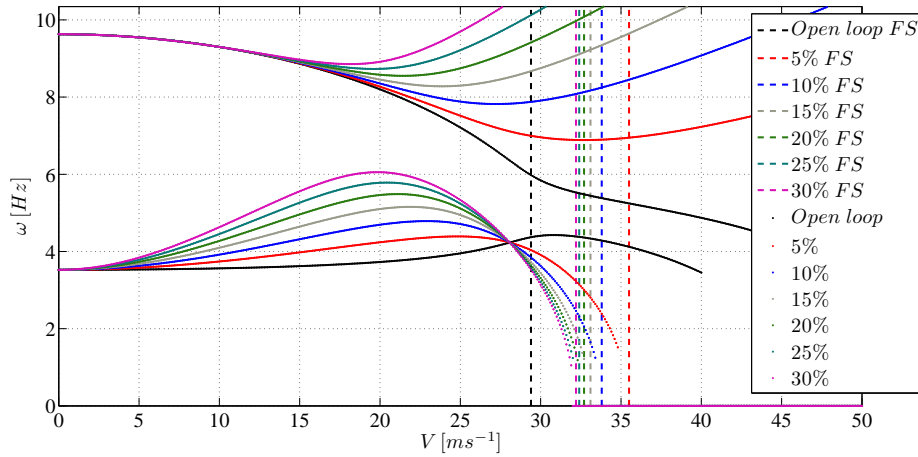


Figure 2.31: Frequency plot increasing the imaginary part of the first pair of poles,  $V_C = 10 \text{ m s}^{-1}$ , placing the second pair

As shown in figure 2.30 and in figure 2.31 the second pole bends upward, and its frequency increases, when the first pole reaches the maximum frequency, after that it does not cross the imaginary axis. From the tests results that for higher variation the flutter speed decreases because the first pair of poles become unstable earlier.

For the tests where the imaginary part has been modified, for both the strategies applied, the increment of the control velocity  $V_C$  does not modify the behavior of the poles but shifts the flutter speed to an higher value than the corresponding instability at  $V_C = 10 \text{ ms}^{-1}$ . In figure 2.32 and in figure

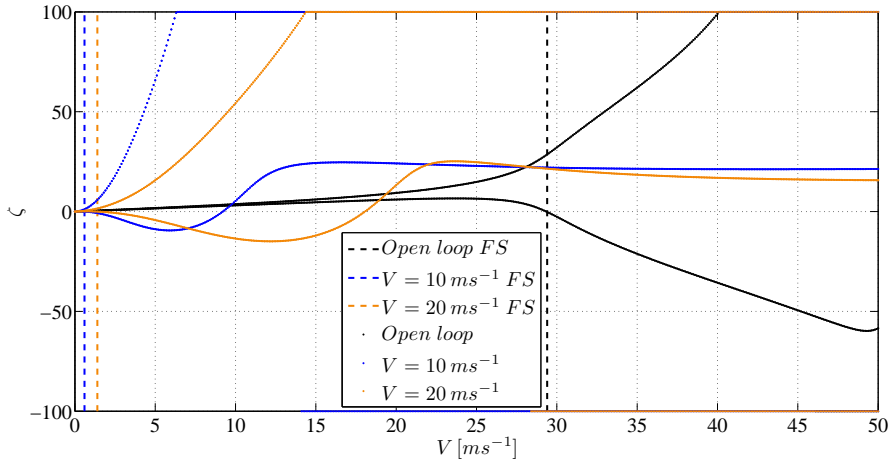


Figure 2.32: Damping plot,  $-30\%$  first pole imaginary part variation, leaving the second pair free, different  $V_C$  compared

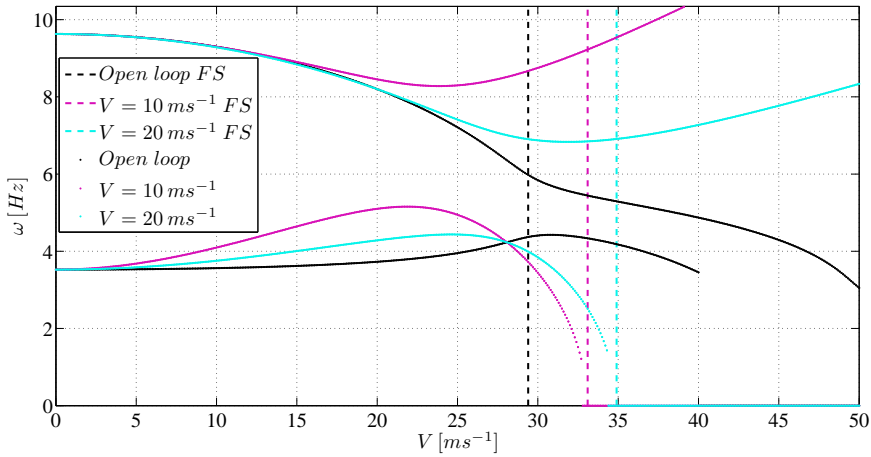


Figure 2.33: Frequency plot,  $+15\%$  first pole imaginary part variation, placing the second one, different  $V_C$  compared

### 2.3.2 Second pair of poles placed

#### Real part modification

Lowering the real part of the second pair of poles corresponds to diminish the damping of the second mode, which is the mode the leads to the instability, as expected decreasing it gives for the closed loop system lower flutter speed and bigger is the modification lower instability speed the aeroelastic system has.

Acting on the real part of this pole does not affect the behavior of the first pair of poles so even without fixing them they are already close to the open loop system and their path differs little from the uncontrolled system; hence for both the strategies applied, fixing the first pole or leaving it free, the results are very similar.

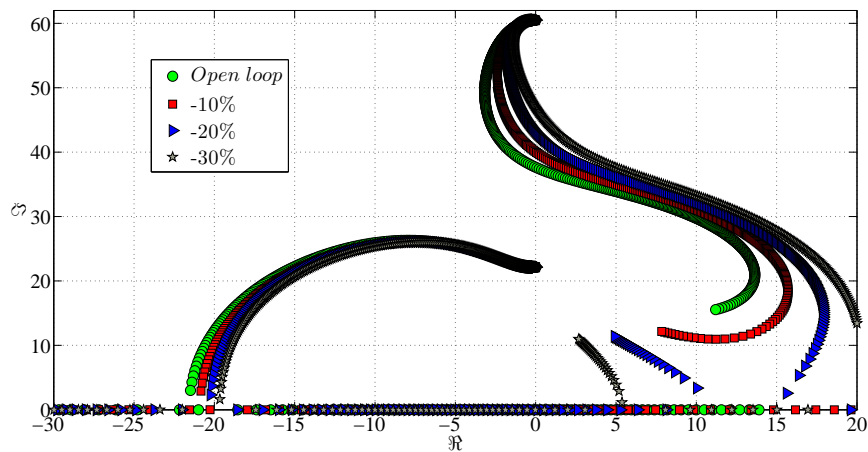


Figure 2.34: Root locus decreasing the real part of the second pair of poles,  $V_C = 10 \text{ ms}^{-1}$ , leaving the first pair free

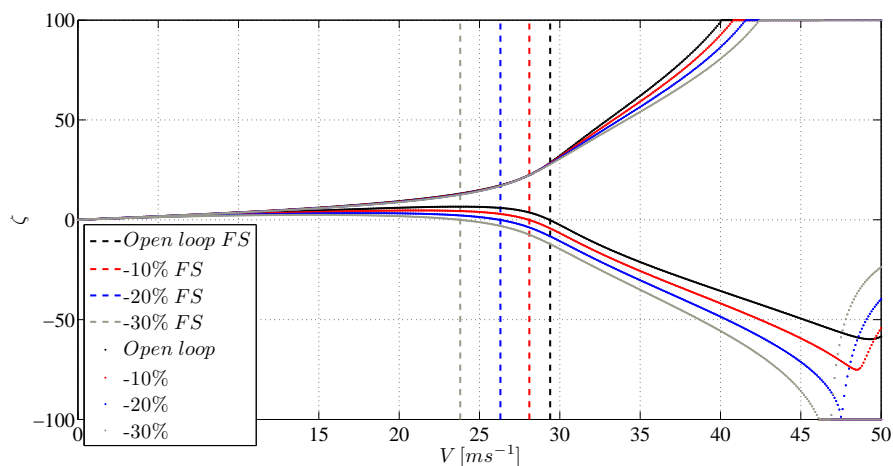


Figure 2.35: Damping plot decreasing the real part of the second pair of poles,  $V_C = 10 \text{ ms}^{-1}$ , leaving the first pair free

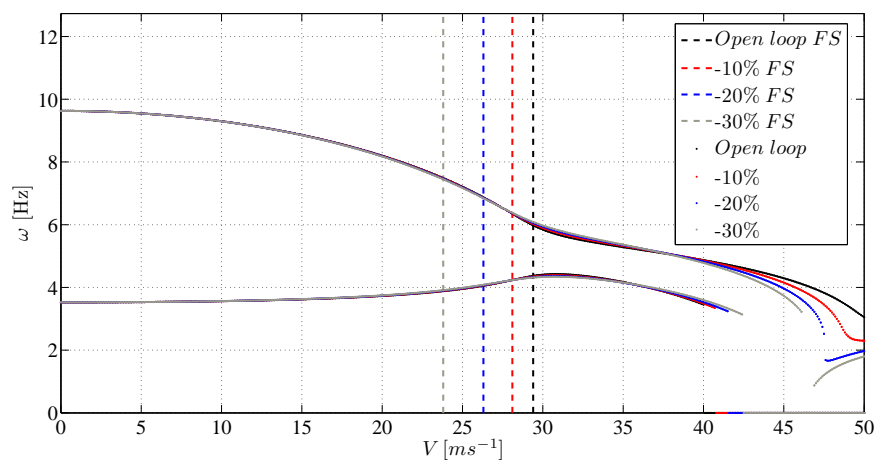


Figure 2.36: Frequency plot decreasing the real part of the second pair of poles,  $V_C = 10 \text{ ms}^{-1}$ , leaving the first pair free

In figure 2.34, figure 2.35 and figure 2.36 there is an example of decreasing the real part while leaving the other pole free, the second pole crosses the imaginary axis at lower speed for higher variation while the frequency is not affected by the modification. In these figures can be also seen how the first pair of poles does not change its behavior.

One example of the closeness of the results between the two strategies applied is shown in figure 2.37; here can be seen that the second pole behave in the same way in both cases.

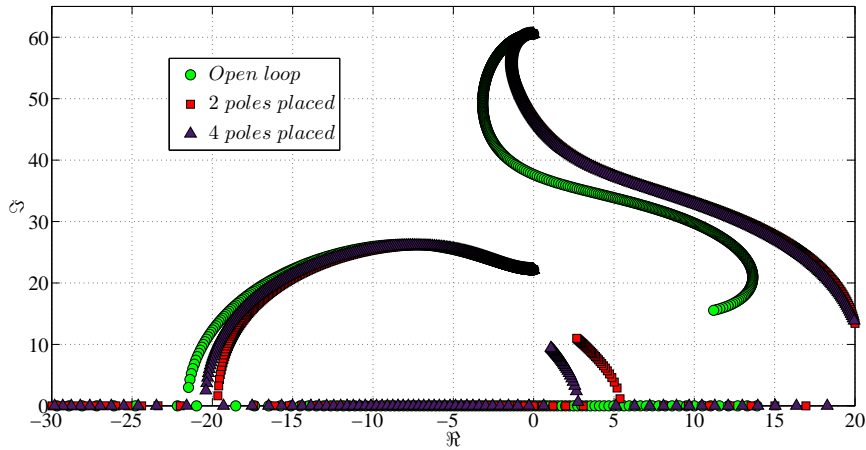


Figure 2.37: Root locus,  $-30\%$  second pole real part variation,  $V_C = 10 \text{ m s}^{-1}$ , two strategies compared

Increasing the control velocity, as in the previous cases, what happens is that there is the same poles behavior but translated to higher air speeds; changing the poles at  $V_C = 20 \text{ m s}^{-1}$  delays the speed at which the instability occurs. However if a reduction of the damping at  $V_C = 10 \text{ m s}^{-1}$  leads to a flutter speed lower than the open loop system a decrease of the real part at  $V_C = 20 \text{ m s}^{-1}$  still brings to the instability at lower velocity than the uncontrolled one. An example is shown in figure 2.38 and in figure 2.39.

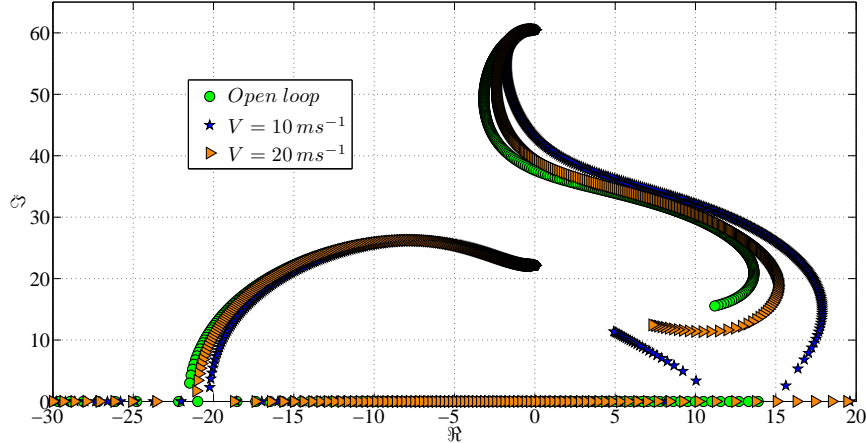


Figure 2.38: Root locus,  $-20\%$  second pole real part variation, leaving the first pair free, different  $V_C$  compared

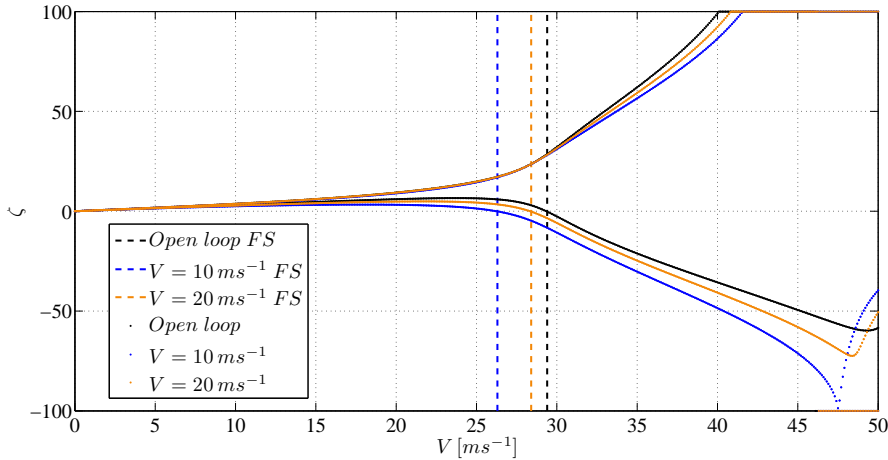


Figure 2.39: Damping plot,  $-20\%$  second pole real part variation, leaving the first pair free, different  $V_C$  compared

The two strategies gives the same results also at  $V_C = 20 \text{ ms}^{-1}$ .

On the contrary increasing the real part raise the damping of the second mode and that increases the flutter speed of the closed loop system; as the previous tests the first pair of poles are slightly affected by this variation and their path is similar to the uncontrolled system so once more the two strategies gives very close results. With higher damping increments there are higher flutter speeds as can be seen in figures 2.40 and 2.41.

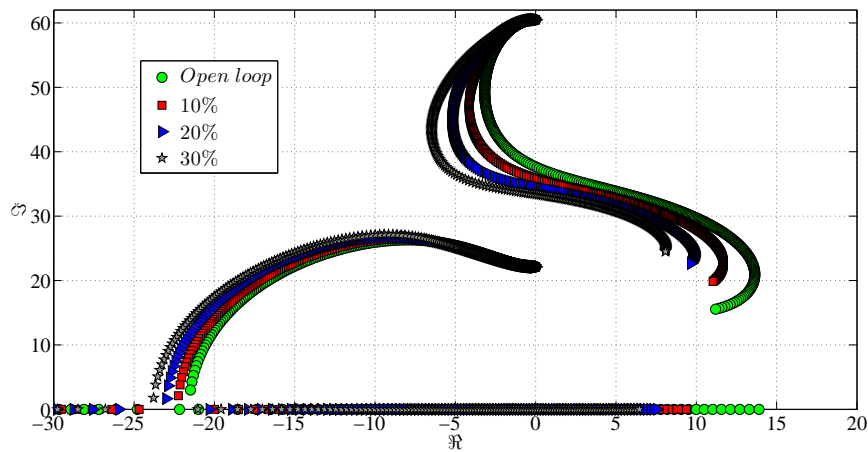


Figure 2.40: Root locus increasing the real part of the second pair of poles,  $V_C = 10 \text{ ms}^{-1}$ , leaving the first pair free

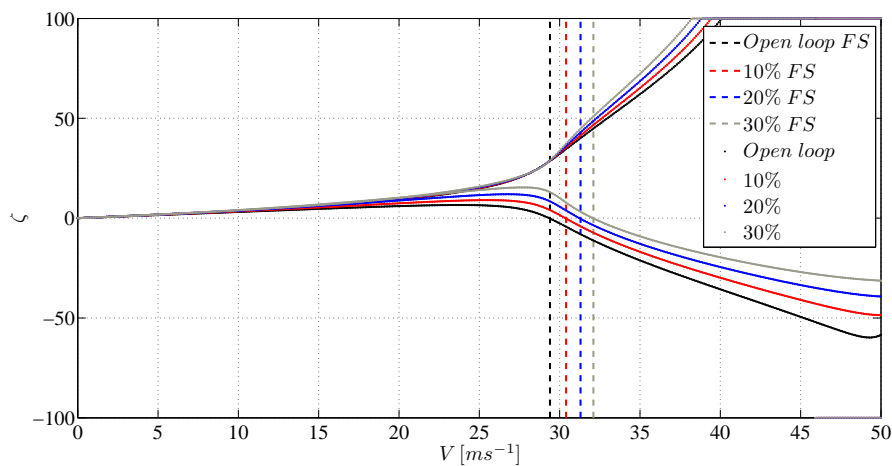


Figure 2.41: Damping plot increasing the real part of the second pair of poles,  $V_C = 10 \text{ ms}^{-1}$ , leaving the first pair free



Like the cases with the real part reduction these tests show that increasing  $V_C$  up to  $20\text{ ms}^{-1}$  the effects of the control are lowered and the controlled system behavior gets closer to the open loop system. In figure 2.42 and in figure 2.43 there is an example of this comparison with an increment of the 30% of the open loop value but the same thing happens for all the other variation and for both strategies.

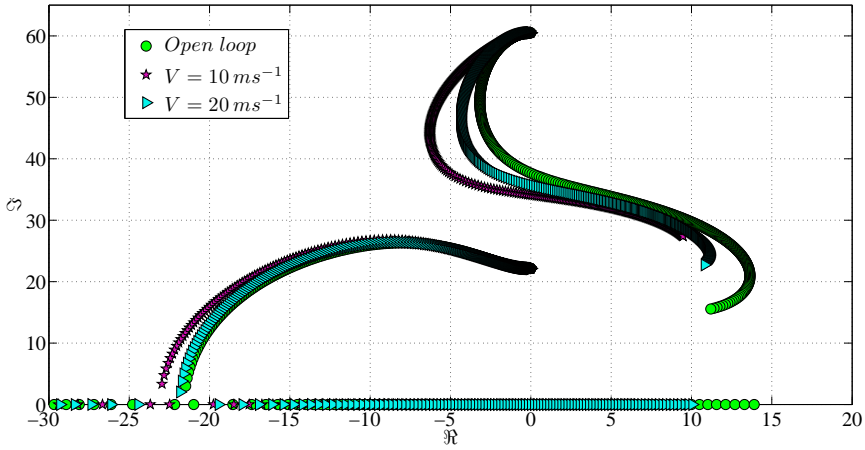


Figure 2.42: Root locus, 30% second pole real part variation, placing the first pair, different  $V_C$  compared

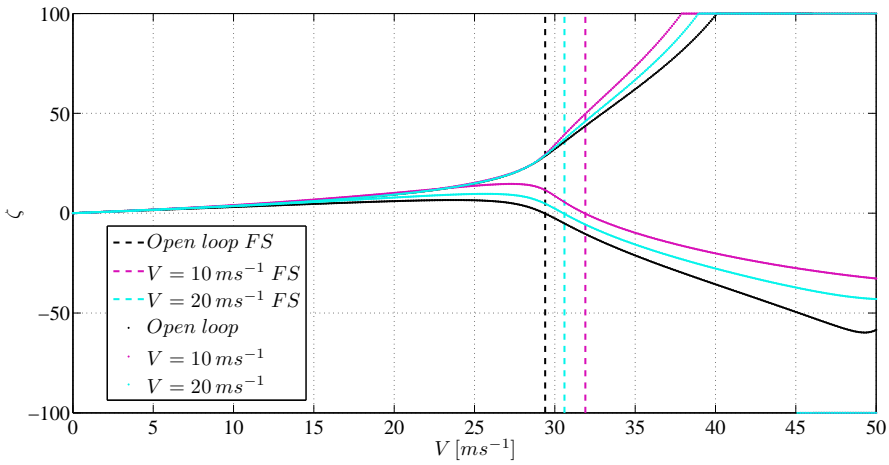


Figure 2.43: Damping plot, 30% second pole real part variation, placing the first pair, different  $V_C$  compared

In all the cases where the real part of the second pair of poles has been

modified the frequency trend with the air speed for all the poles remain the same in the closed and open loop system.

### Imaginary part variation

Changing the imaginary part of the second pair of poles shows how the aeroelastic system is more sensitive to frequency variation than damping modifications, as has happened for the first mode.

Decreasing the imaginary part the two poles come closer at lower air speed and this brings to a lower flutter speed than the open loop system; while the second pole travels towards the real axis the first pole interact, reverse its trajectory and goes unstable. This phenomenon happens both leaving the first pole free and placing it, even if placing the first pole force it to go to the prescribed location before it can go unstable and this delay the instability, that is still lower the uncontrolled system.

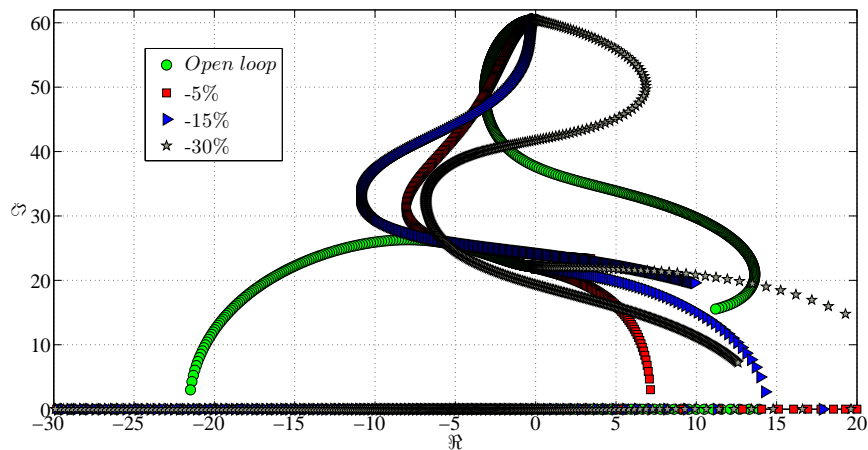


Figure 2.44: Root locus decreasing the imaginary part of the second pair of poles,  $V_C = 10 \text{ m.s}^{-1}$ , leaving the first pair free

In figures 2.44, 2.45, 2.46 and 2.47 are shown the roots plots and the frequencies plots applying both strategies; in figure 2.47 can be seen how the first pair of poles follow the open loop system until higher speeds and delays the flutter speed.

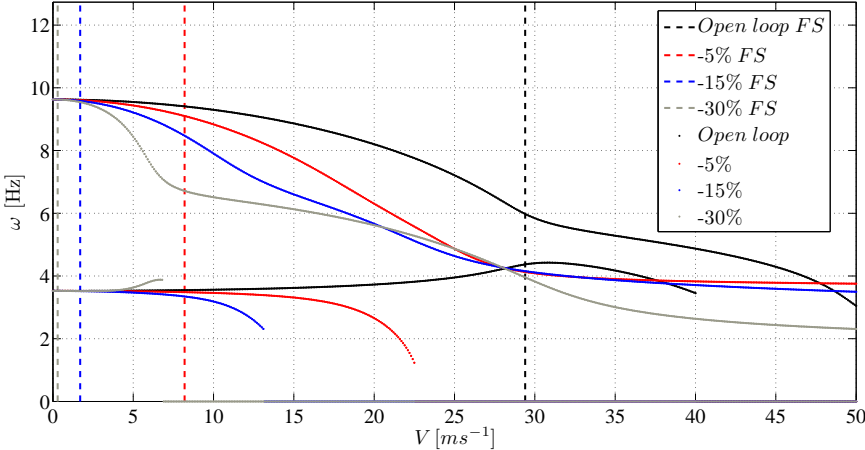


Figure 2.45: Frequency plot decreasing the imaginary part of the second pair of poles,  $V_C = 10 ms^{-1}$ , leaving the first pair free

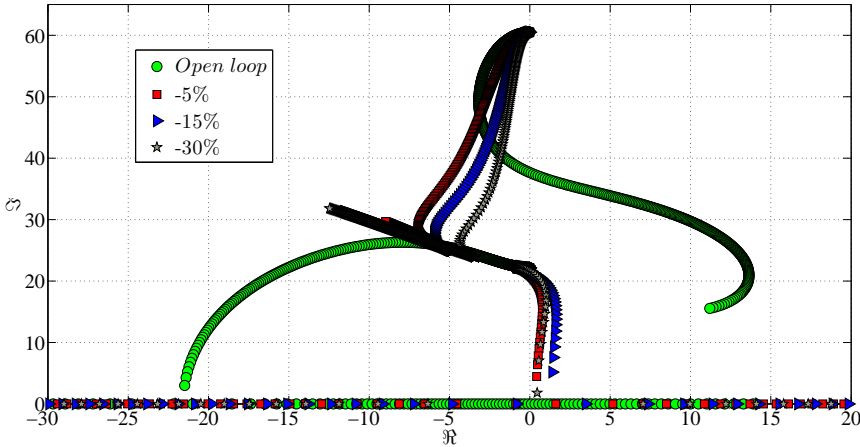


Figure 2.46: Root locus decreasing the imaginary part of the second pair of poles,  $V_C = 10 ms^{-1}$ , placing the first pair

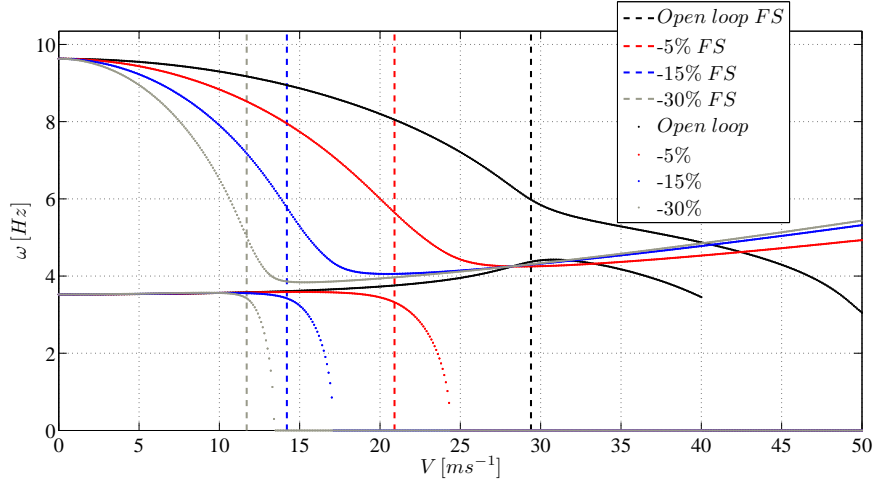


Figure 2.47: Frequency plot decreasing the imaginary part of the second pair of poles,  $V_C = 10 \text{ ms}^{-1}$ , placing the first pair

On the contrary increasing the imaginary part, the poles move away from each other and that prevent them from interacting; the flutter speed increases significantly for each of the cases taken into exam.

For these tests the velocity at which the control is applied change considerably the behavior of the closed loop system. As seen in all the figures above the imaginary part of the second pole decreases from a starting value given considering the only the mechanical properties (the air speed is equal to zero hence there are not aerodynamic forces acting on the system and without structural damping the poles are four complex conjugate without real part) that represents the frequency of the second structural mode; applying the receptance method at  $V_C = 10 \text{ ms}^{-1}$  what happens is that the assigned frequency of the second mode is higher than the starting value so this pole increases its imaginary part moving away from the first pole without stopping.

For both the strategies applied the first pole does not go unstable, in the velocity range taken into exam, but placing the first pair of poles the second one after an initial increment the damping start to decrease and the pole becomes unstable as shown in figures 2.48 and 2.49, instead leaving the first one free the damping of the second mode continue to increase as shown in figures 2.50 and 2.51; in figure 2.51 can be seen that there is no flutter for the closed loop system in the velocity range investigated.

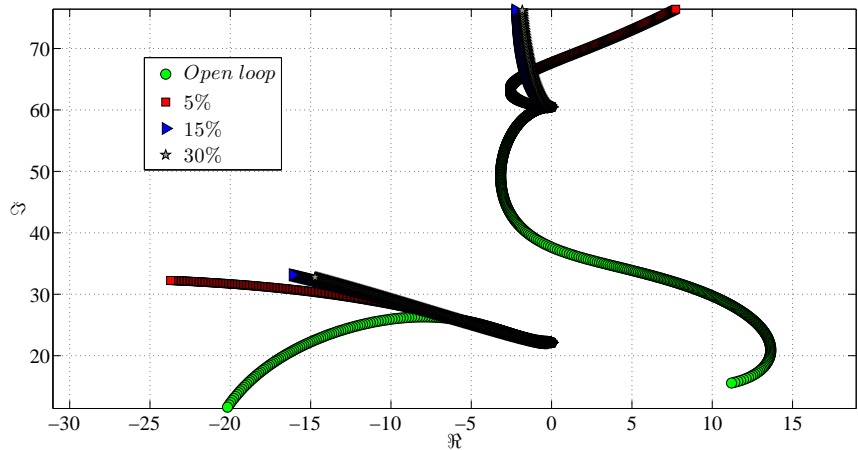


Figure 2.48: Root locus increasing the imaginary part of the second pair of poles,  $V_C = 10 \text{ m s}^{-1}$ , placing the first pair

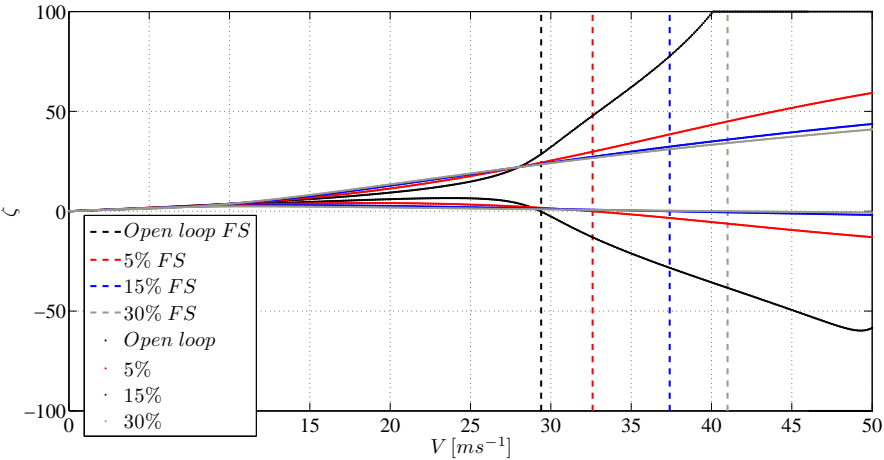


Figure 2.49: Damping plot increasing the imaginary part of the second pair of poles,  $V_C = 10 \text{ m s}^{-1}$ , placing the first pair

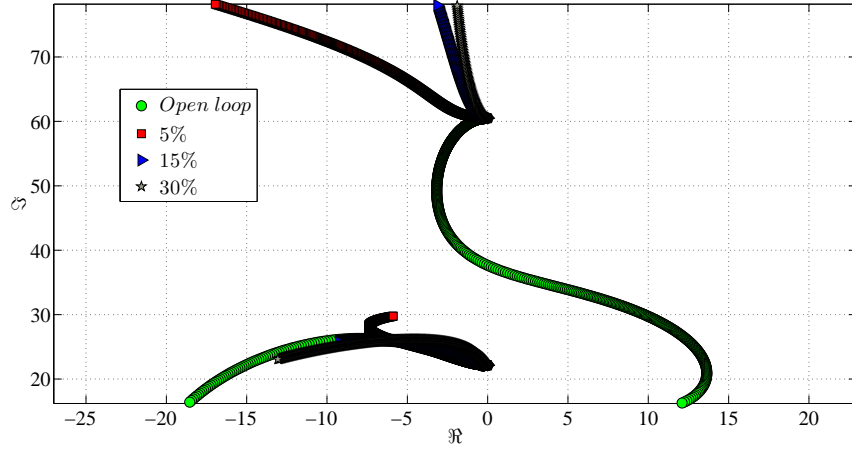


Figure 2.50: Root locus increasing the imaginary part of the second pair of poles,  $V_C = 10 \text{ m s}^{-1}$ , leaving the first pair free

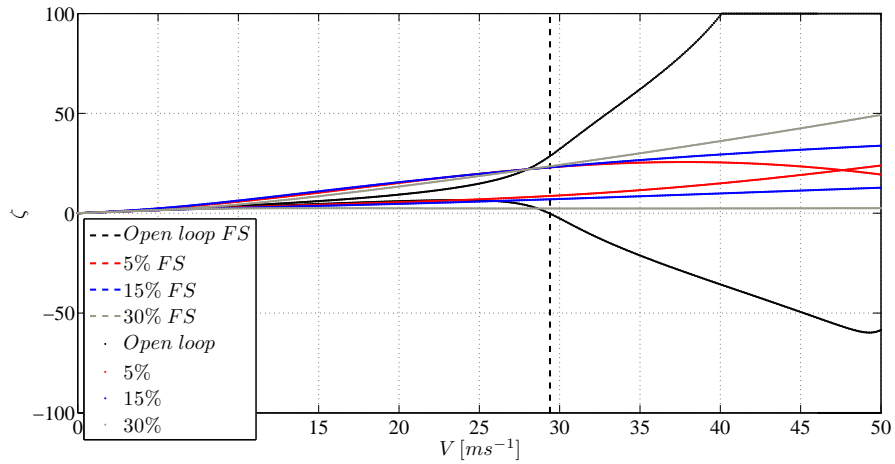


Figure 2.51: Damping plot increasing the imaginary part of the second pair of poles,  $V_C = 10 \text{ m s}^{-1}$ , leaving the first pair free

Instead applying the control at  $V_C = 20 \text{ ms}^{-1}$ , and leaving the first pole free, the results depend on the entity of the variation applied: if the pole is placed to an higher frequency of the starting value (as for a variation of +30% the behavior is the same of the tests made at  $V_C = 10 \text{ ms}^{-1}$ , for lower variation changes the kind of interaction between the poles and changes the pole that leads to the instability as shown in figure 2.52.

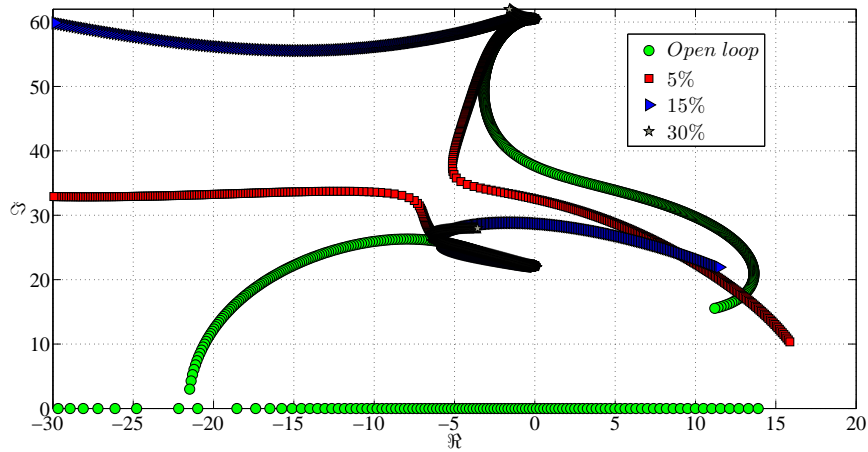


Figure 2.52: Root locus increasing the imaginary part of the second pair of poles,  $V_C = 20 \text{ ms}^{-1}$ , leaving the first pair free

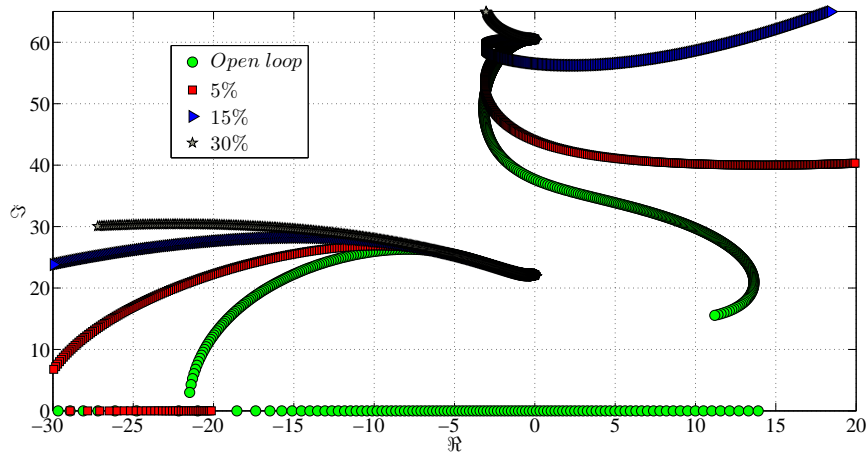


Figure 2.53: Root locus increasing the imaginary part of the second pair of poles,  $V_C = 20 \text{ ms}^{-1}$ , placing the first pair

For all the tests made increasing the imaginary part of the second mode

the flutter speed of the closed loop system is higher than the uncontrolled one and bigger is the increment higher is the flutter speed.

## 2.4 Gains

The deflection that the control surface has to assume to apply the control in reality has fixed structural limitation. According to the control law,  $\beta$  is a function of time and depends on the response of the system, in terms of displacements and velocity of the degrees of freedom, to an external perturbation, multiplied by the gains of the controller; hence if the gains are too big the prescribed deflection needed could exceed the structural limitations and the control would not be applicable.

The comparisons between the gains have been made considering the euclidean norm of the vectors.

In each of the tests considered, the norm of gains vector solution of equation (1.18)  $\begin{Bmatrix} \mathbf{g} \\ \mathbf{f} \end{Bmatrix}$  is greater for tests made changing one pair of poles and fixing the other one in the same position of the open loop system, than the other strategy. Placing only one pair while leaving the other free gives  $\mathbf{g}$  and  $\mathbf{f}$  that are the solution at minimum norm, whereas placing the other mode is a particular case of the previous strategy and that leads to a greater norm. An example is shown in figure 2.54.

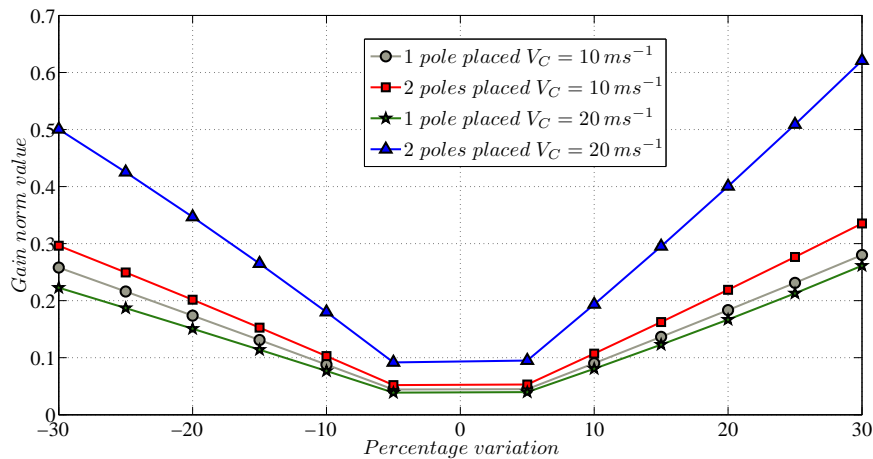


Figure 2.54: Norm of the vector of the gains changing the real part of the first mode

Also for all the tests increasing the absolute value of the real/imaginary part modification gives higher gains, but the gains obtained for a positive



variation might not be equal to the gains obtained with a negative modification with equal in absolute value.

From the trials it appears that changing the real part of the first pair of poles gives similar results as modifying the real part of the second one. In both cases, increasing  $V_C$ , the norms of  $\mathbf{g}$  and  $\mathbf{f}$  decrease placing only one pair while increase placing two modes. Applying the control at the same  $V_C$  fixing all the poles gives a vector  $\mathbf{g}$  with a norm of magnitude  $10^{-1}$  instead leaving one pair free leads to a norm of magnitude  $10^{-2}$  while  $\mathbf{f}$  maintains a norm of magnitude  $10^{-2}$ .

Examples are shown in figures 2.55 and 2.56

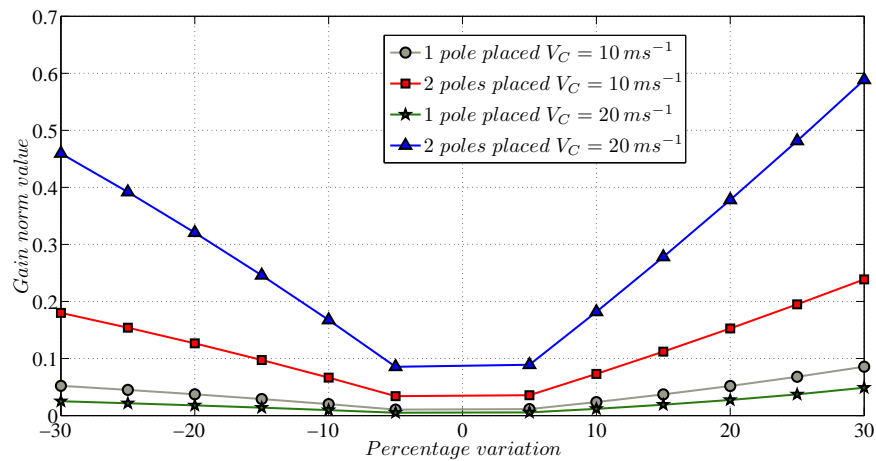


Figure 2.55: Norm of  $\mathbf{g}$  changing the real part of the first mode

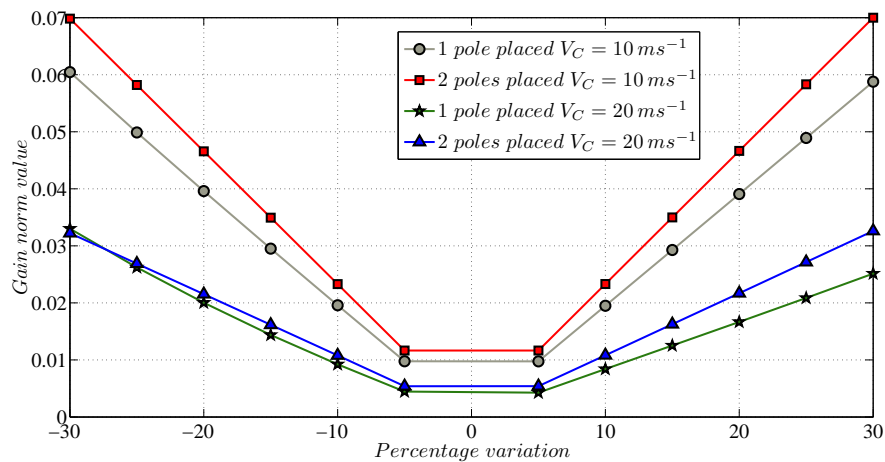


Figure 2.56: Norm of  $\mathbf{f}$  changing the real part of the second mode

Also changing the imaginary part of the poles give the same results for both pair of poles. Placing one or both modes gives very different gains behavior: placing one pair of poles the norm's magnitude of  $\mathbf{f}$  is equal to  $10^1$  while placing all the poles it decreases to  $10^{-1}$ . For both strategies  $\mathbf{g}$  can become very big with a norm of magnitude  $10^2$ .

Also for both strategies increasing the  $V_C$  lowers the value of both gains. In figures 2.57 and 2.58 is shown the trend of the gains changing the imaginary part of the poles.

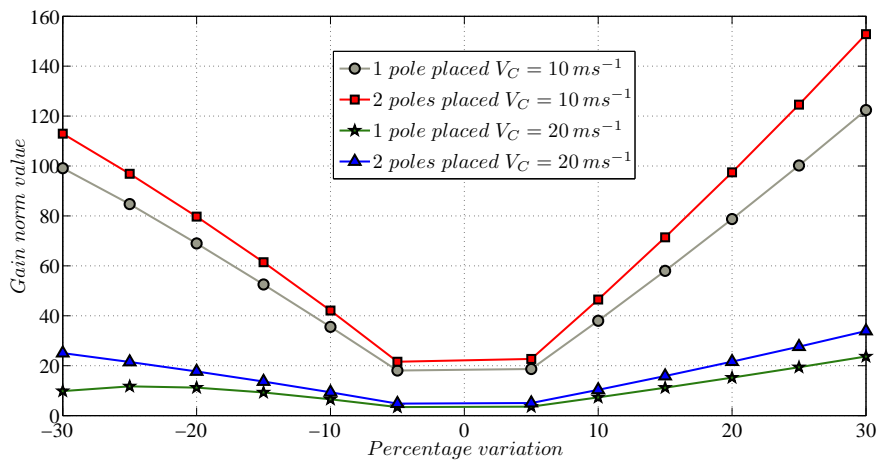


Figure 2.57: Norm of  $\mathbf{g}$  changing the imaginary part of the second mode

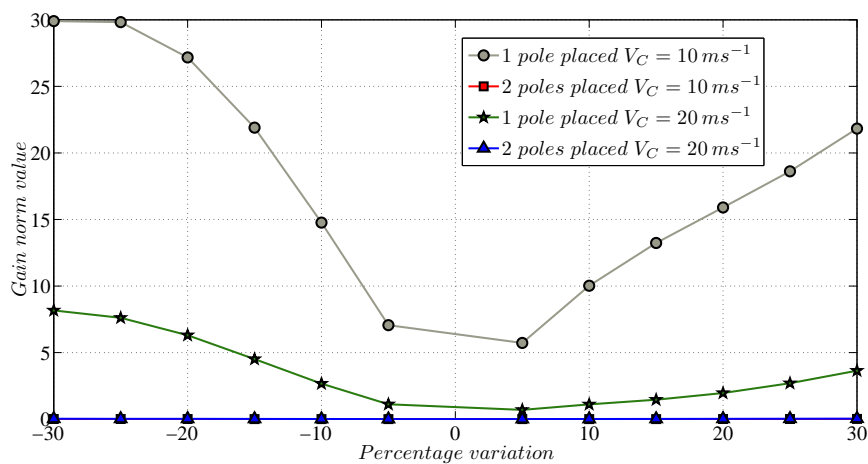


Figure 2.58: Norm of  $\mathbf{f}$  changing the imaginary part of the first mode

What can be seen from the tests is that in almost all the poles placement,

the higher term in the gains vector is the one related to the heave displacement  $h$  and velocity  $\dot{h}$  while the other term is always at least two orders of magnitude lower.

It is also evident that changing the imaginary part of the poles requires more energy than affecting the real part and that the results can differ a lot for the percentage variation adopted.



## Chapter 3

# Cantilever elastic wing

In this chapter the receptance method is applied to a rectangular cantilever wing in order to see what happens applying this control methodology to a multi degrees of freedom system.

The wing has been modeled as an elastic beam, vertical displacements and torsional rotations have been considered in the tests; the model has been implemented using a finite element method used to solve the dynamic equilibrium equation.

The structural and aerodynamic matrices have been obtained using fifteen elements,  $n$ , for the length of the wing span and the degrees of freedom used are the vertical displacement  $w$ , it's derivative along the wing span  $w'$  and the torsional rotation  $\vartheta$  in each element's node. On each element the matrices have been obtained by integration of the shape functions adopted and considering all the parameters constant along the wing span.

The aerodynamic stiffness, damping and control forces for each element have been calculated using the equations (2.14), (2.15), (2.20) and (2.21) described in the second chapter. The global matrices have been obtained expanding the elements matrices and fixing the degrees of freedom of the node relative to the constrain, the system matrices  $\mathbf{M}$ ,  $\mathbf{C}$ ,  $\mathbf{K}$ ,  $\mathbf{C}_a$  and  $\mathbf{K}_a \in \mathfrak{R}^{3n \times 3n}$  while  $\mathbf{f}_\beta$ ,  $\mathbf{g}$  and  $\mathbf{f} \in \mathfrak{R}^{3n \times 1}$ .

### 3.1 Open loop system

The parameters used in the numerical model are listed in the table 3.1

Table 3.1: Elastic wing structural parameters

<i>Parameter</i>	<i>Symbol</i>	<i>Value</i>
Span length [ <i>m</i> ]	$s_w$	7.5
Chord length [ <i>m</i> ]	$c_w$	2
Mass per unit area [ $kgm^{-2}$ ]	$m_w$	100
Position of the center of gravity [ <i>m</i> ]	$x_C$	1
Position of the flexural axis [ <i>m</i> ]	$x_P$	0.96
Position of the aerodynamic center [ <i>m</i> ]	$x_Q$	0.5
Flap span length [ <i>m</i> ]	$s_\beta$	7.5
Flap chord length [ <i>m</i> ]	$c_\beta$	0.2
Flexural rigidity [ $Nm^2$ ]	$k_h$	$27.758 \times 10^6$
Torsional rigidity [ $Nm^2$ ]	$k_\vartheta$	$19.834 \times 10^5$

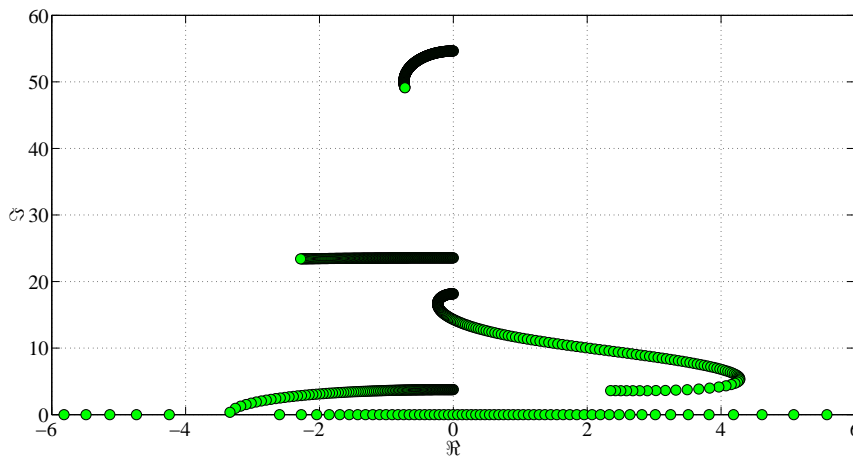


Figure 3.1: Root locus of the open loop system

The system has  $3n$  complex conjugate pairs of poles, the eigenvalues of the open loop system are obtained solving the system defined in equation (2.19) using the matrices obtained from the finite element method, in figure

3.1 and in figure 3.2 are shown the root locus and the  $V$  plots for the uncontrolled system.

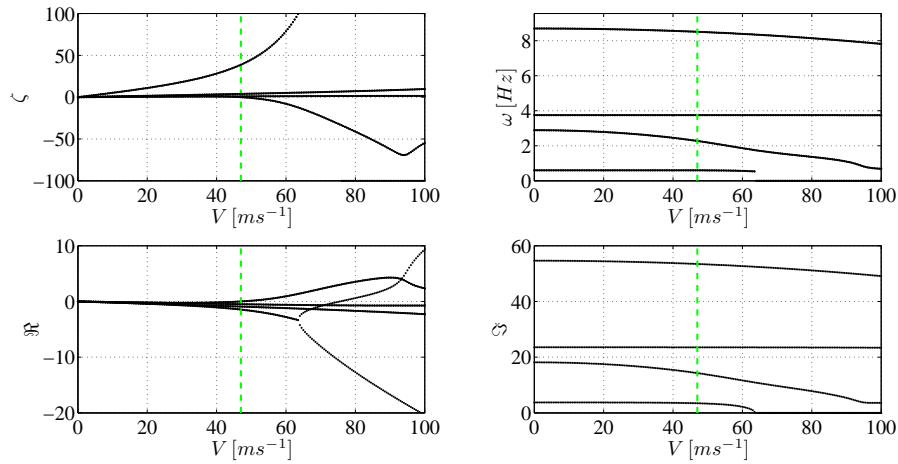


Figure 3.2:  $V$  plots of the open loop system

The uncontrolled system has a flutter speed equal to  $47.5 \text{ ms}^{-1}$  and the mode that causes the instability is the second one.

## 3.2 Controlled System

In the tests shown in this chapter only the first two have been placed using a control law proportional to the displacement and the velocity of the degrees of freedom, such as the one described in the second chapter in equation (2.23), applying the same strategies: changing the real or the imaginary part of one pair of poles and leaving the other free or placing one pair of poles and fixing the second one to the same position of the open loop system. As in the second chapter the velocity where the control is applied  $V_C$  has been changed, the values selected vary from  $V_C = 20 \text{ ms}^{-1}$  to  $V_C = 40 \text{ ms}^{-1}$ .

In these trials, it has assumed the possibility to measure, with some sensors, the vertical displacement and the torsional rotation of the wing tip, that correspond to the degrees of freedom of the last node. In this way the receptance method has been applied selecting the rows of the term  $\mathbf{r}_k = \mathbf{H}(\lambda_k)\mathbf{b}$  of equations (1.16) and (1.17) corresponding to the states available.

The gains value obtained solving the linear system (1.18) are the terms of  $\mathbf{g}$  and  $\mathbf{f}$  vectors corresponding to the selected displacements and velocities while the other terms in the gains matrices are placed equal to zero.

### 3.2.1 First pairs of poles placed

#### Real part modification

Decreasing the real part of the first pair of poles, even if its damping has been lowered the flutter speed of the closed loop system increases because changes the path of the second mode: the turn that makes toward the imaginary axis is wider and the second pair of poles becomes instable at higher speed. On the other hand the behavior of the first pair of poles is almost the same while the control does not affect the other modes at higher frequencies, applying the control changes the damping of the system whereas the frequency is the same of the open loop system. Greater is the variation in absolute value greater is the increment in the flutter speed as shown in figures 3.3, 3.4 and 3.5

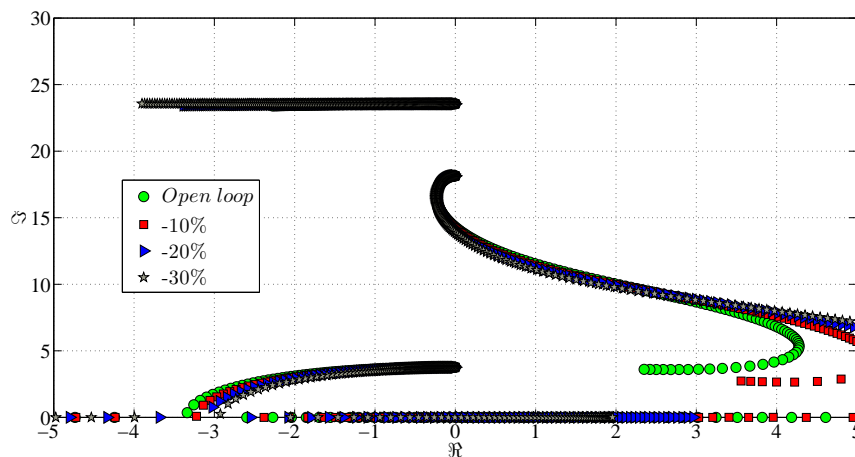


Figure 3.3: Root locus decreasing the real part of the first pair of poles,  $V_C = 20 \text{ m s}^{-1}$ , leaving the second pair free



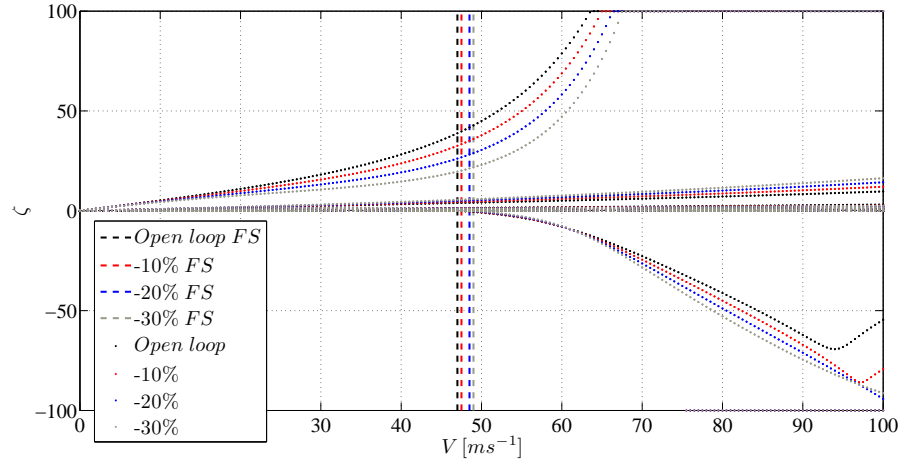


Figure 3.4: Damping plot decreasing the real part of the first pair of poles,  $V_C = 20 m.s^{-1}$ , leaving the second pair free

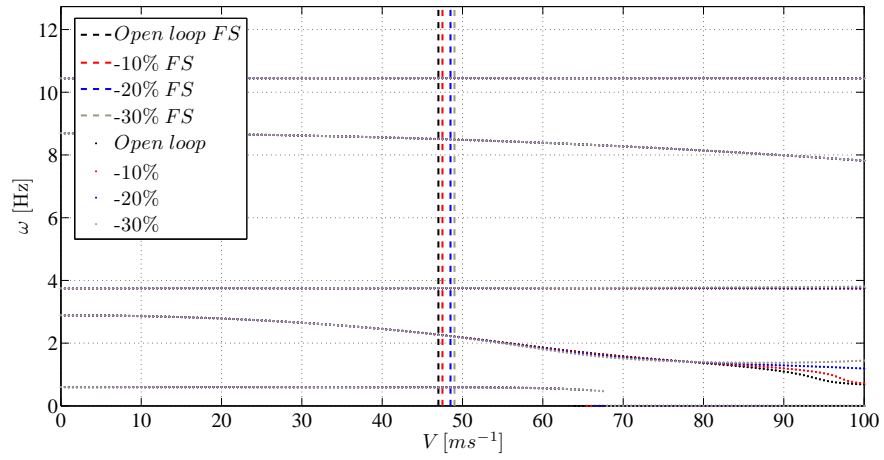


Figure 3.5: Frequency plot decreasing the real part of the first pair of poles,  $V_C = 20 m.s^{-1}$ , leaving the second pair free

Placing the second pair of poles in the same position of the open loop system does not affect the behavior of the poles, the plots of the two strategies compared are overlapping as shown in figure 3.6.

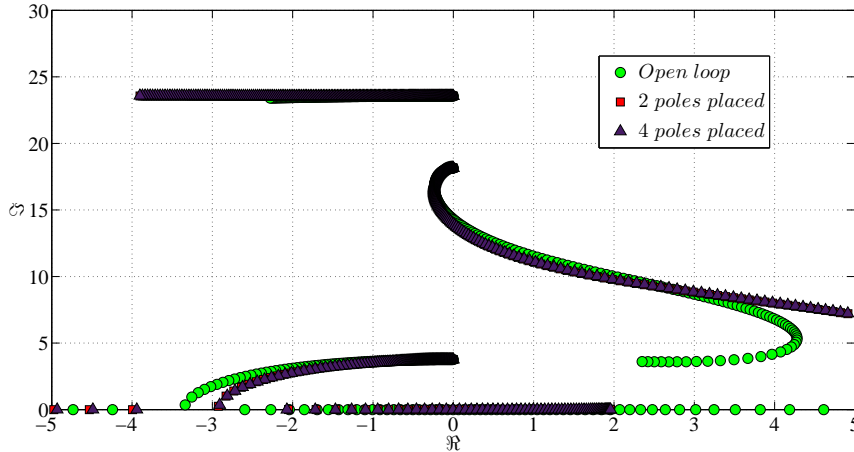


Figure 3.6: Root locus,  $-30\%$  first pole real part variation,  $V_C = 20 \text{ ms}^{-1}$ , two strategies compared

Applying the control at greater  $V_C$  decreases the effects of the control, the flutter speed of the closed loop become lower but still greater than the uncontrolled system. As shown in figures 3.7 and 3.8 the behavior of closed loop system becomes closer to the uncontrolled system increasing  $V_C$ .

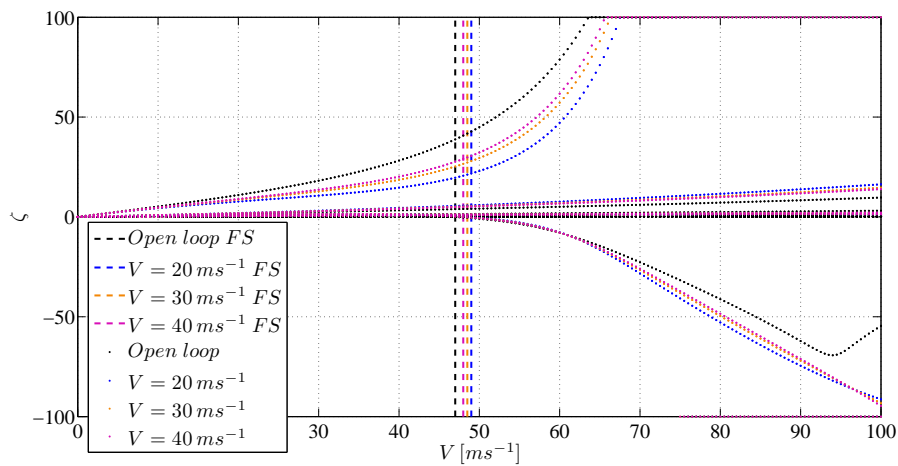


Figure 3.7: Damping plot,  $-30\%$  first pole real part variation, leaving the second pair of poles free, different  $V_C$  compared

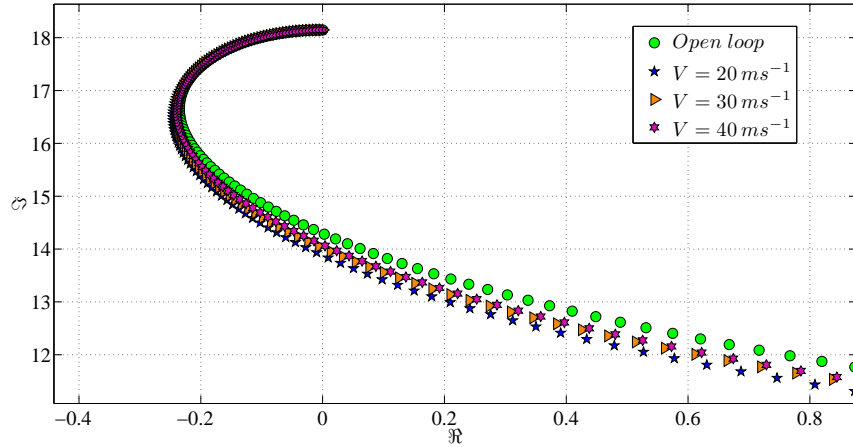


Figure 3.8: Root locus of the second mode,  $-30\%$  first pole real part variation, leaving the second pair of poles free, different  $V_C$  compared

Instead increasing the real part of the first pair of poles the results are the opposite of the previous case: the mode that causes the instability is still the second one, which bends towards the imaginary axis before the open loop system. Higher is the variation grater is the effect. As the former test placing the second pair of poles gives the same results and increasing the  $V_C$  reduces the effects of the control law and the system get closer to the open loop system. The real part increment effects are shown in figures 3.9, 3.10, 3.11 and 3.12.

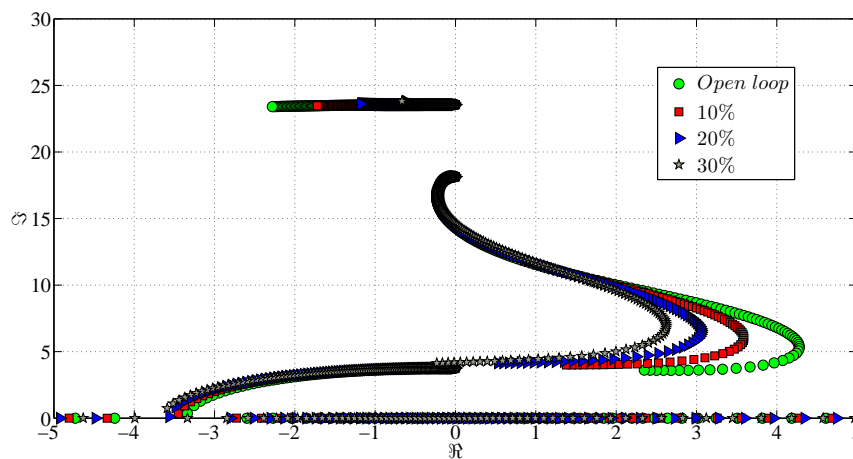


Figure 3.9: Root locus increasing the real part of the first pair of poles,  $V_C = 20 \text{ ms}^{-1}$ , leaving the second pair free

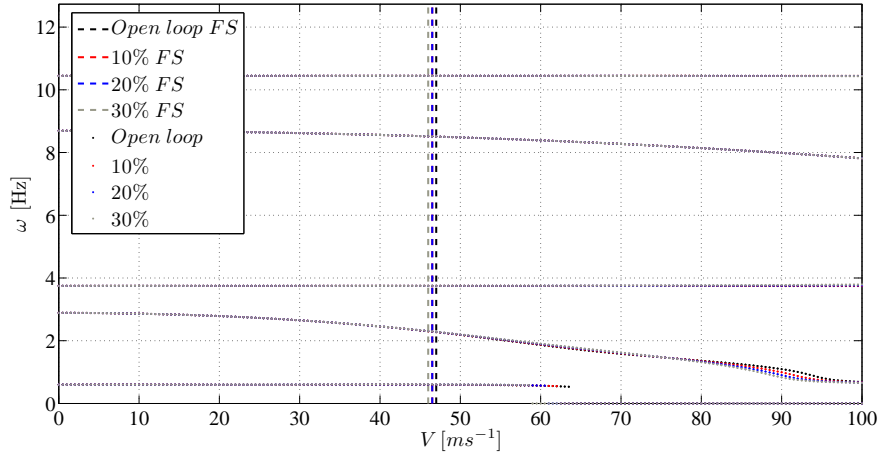


Figure 3.10: Frequency plot increasing the real part of the first pair of poles,  $V_C = 20 ms^{-1}$ , leaving the second pair free

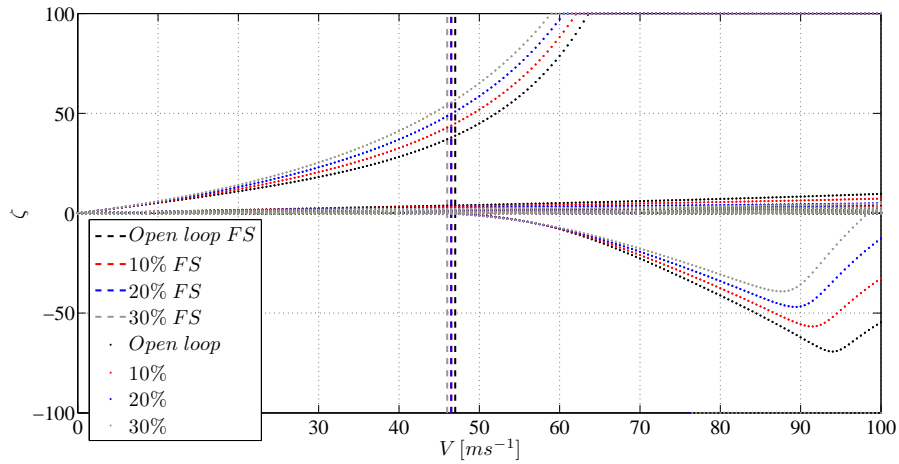


Figure 3.11: Damping plot increasing the real part of the first pair of poles,  $V_C = 20 ms^{-1}$ , leaving the second pair free

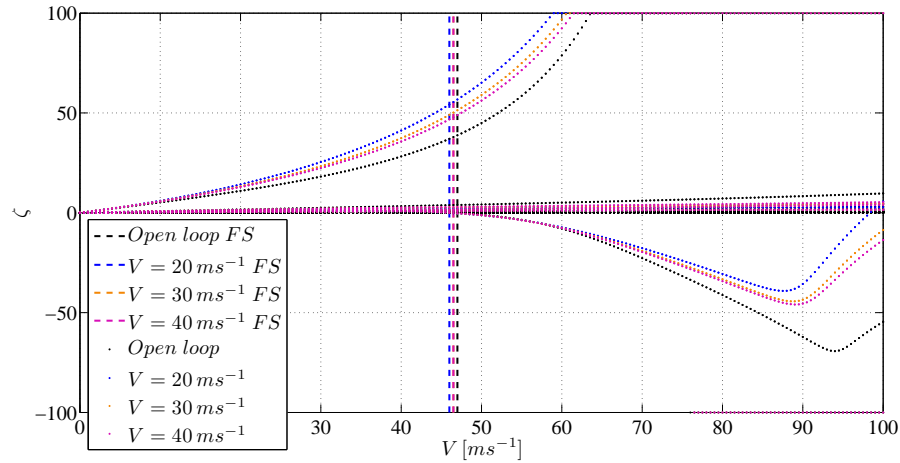


Figure 3.12: Damping plot, 30% first pole real part variation, leaving the second pair of poles free, different  $V_C$  compared

### Imaginary part modification

Decreasing the imaginary part of the first pair of poles there is a drastic fall of the flutter speed of the controlled system, bigger is the variation greater is the loss in the flutter speed value. Lowering the frequency of the first mode it splits into two real eigenvalues one of which become positive at low air speed. Changing the imaginary part of the eigenvalue starts to affect also the modes at higher frequency.

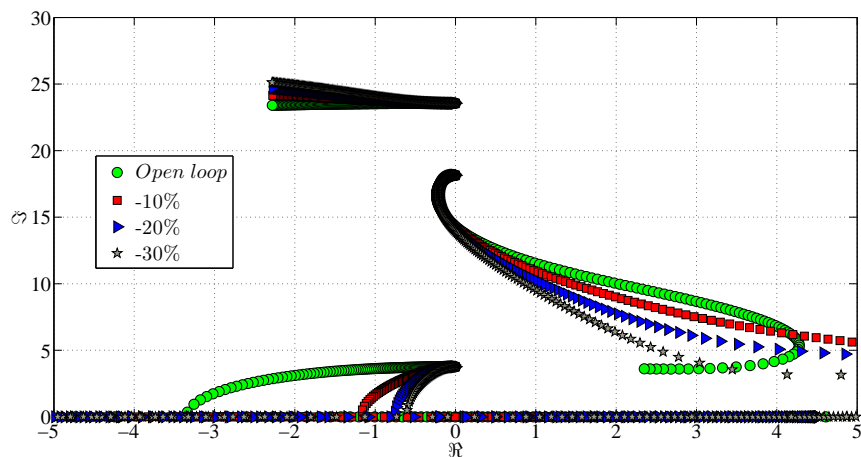


Figure 3.13: Root locus decreasing the imaginary part of the first pair of poles,  $V_C = 20 ms^{-1}$ , leaving the second pair free

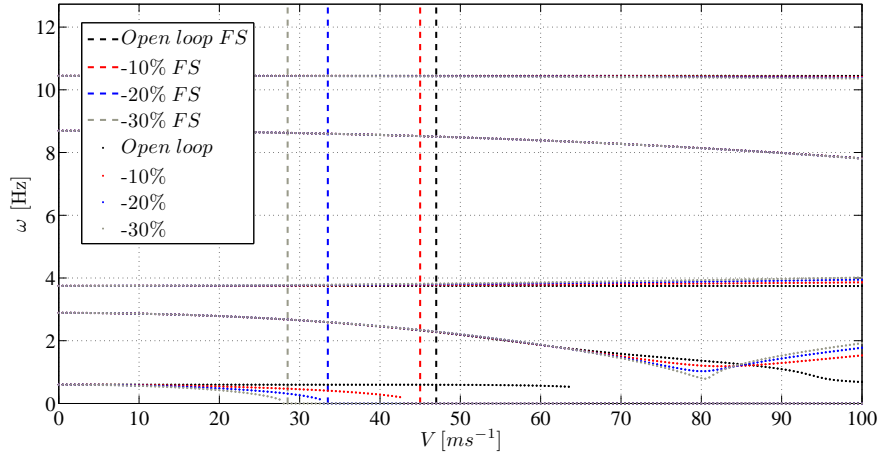


Figure 3.14: Frequency plot decreasing the imaginary part of the first pair of poles,  $V_C = 20 \text{ ms}^{-1}$ , leaving the second pair free

In figures 3.13 and 3.14 is shown the behavior of the closed loop poles acting on the imaginary part, once more changing the strategy does not affect the system properties and increasing  $V_C$  decreases the effects of the control as shown in figures 3.15 and 3.16.

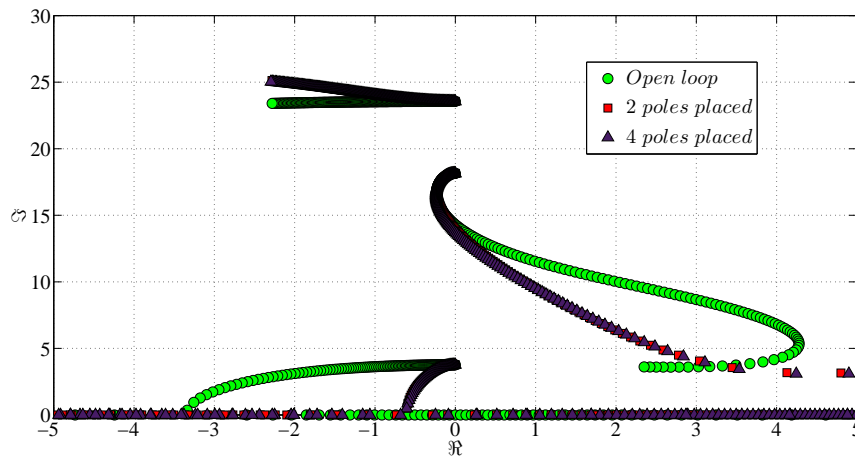


Figure 3.15: Root locus,  $-30\%$  first pole imaginary part variation,  $V_C = 20 \text{ ms}^{-1}$ , two strategies compared

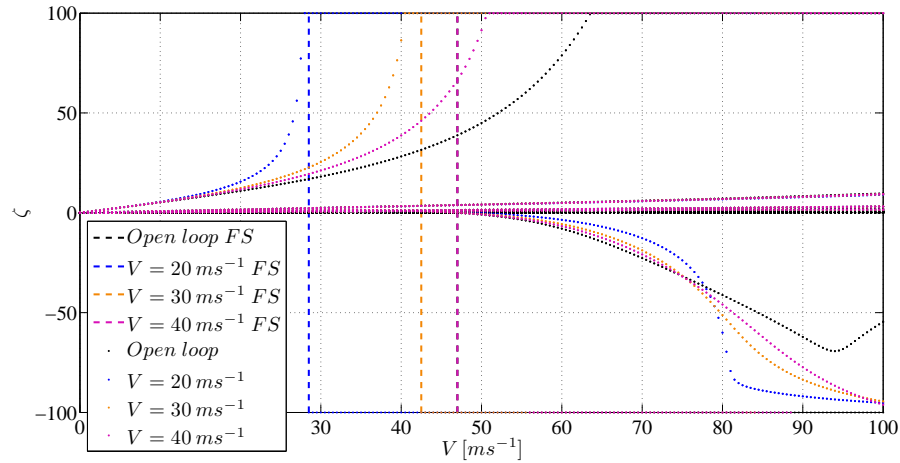


Figure 3.16: Damping plot,  $-30\%$  first pole imaginary part variation, leaving the second pair of poles free, different  $V_C$  compared

Increasing the imaginary part while leaving the second pair of poles free does not change the stability of the aeroelastic system, the control does not affect the poles behavior before the system become unstable. However pushing the poles together they starts to interact and the second mode bend upwards influencing itself the third mode, the global behavior changes significantly even if the flutter speed remains the same of the open loop system.

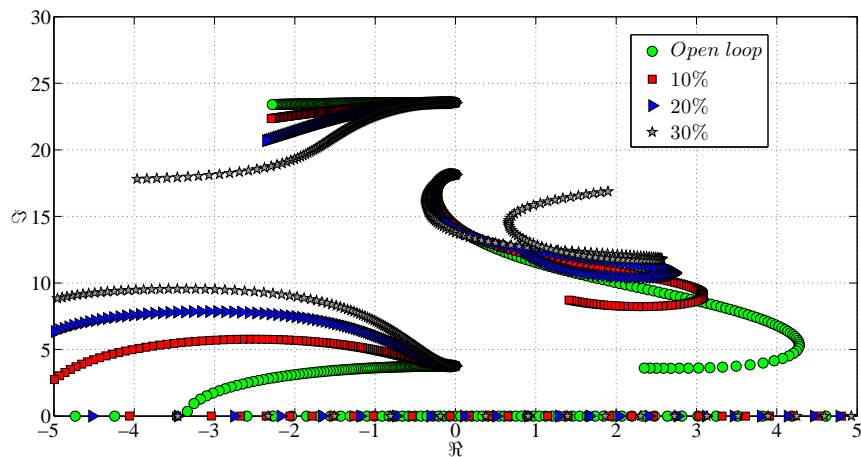


Figure 3.17: Root locus increasing the imaginary part of the first pair of poles,  $V_C = 20 \text{ ms}^{-1}$ , leaving the second pair free

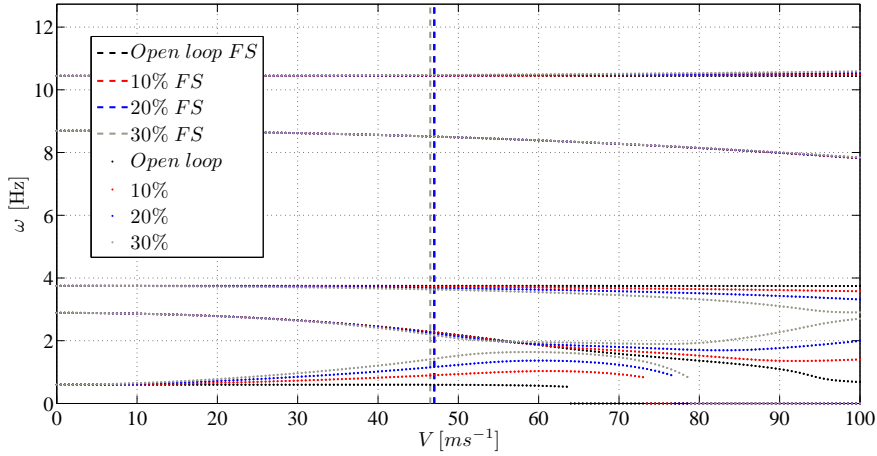


Figure 3.18: Frequency plot increasing the imaginary part of the first pair of poles,  $V_C = 20 \text{ ms}^{-1}$ , leaving the second pair free

Instead placing also the second mode the flutter speed decreases because the second mode is forced to follow the path of the open loop system and interacting with the first one accelerates (for each step of velocity the increment of the real part is greater) and becomes unstable.

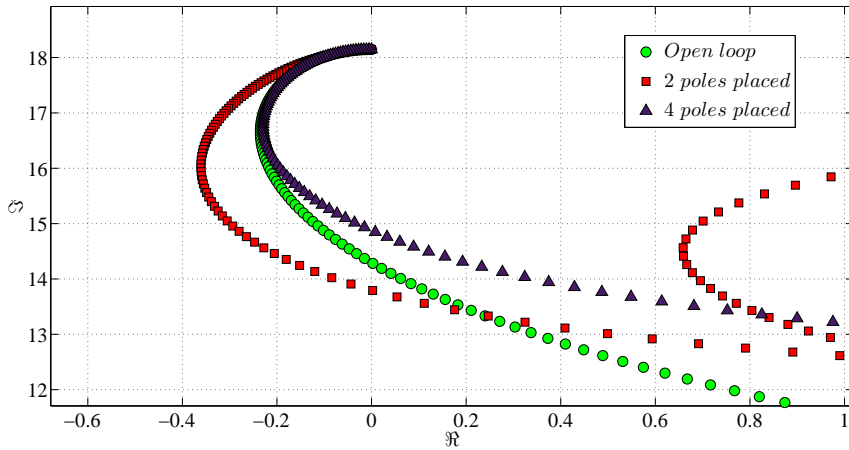


Figure 3.19: Root locus of the second mode, 30% first pole imaginary part variation,  $V_C = 20 \text{ ms}^{-1}$ , two strategies compared



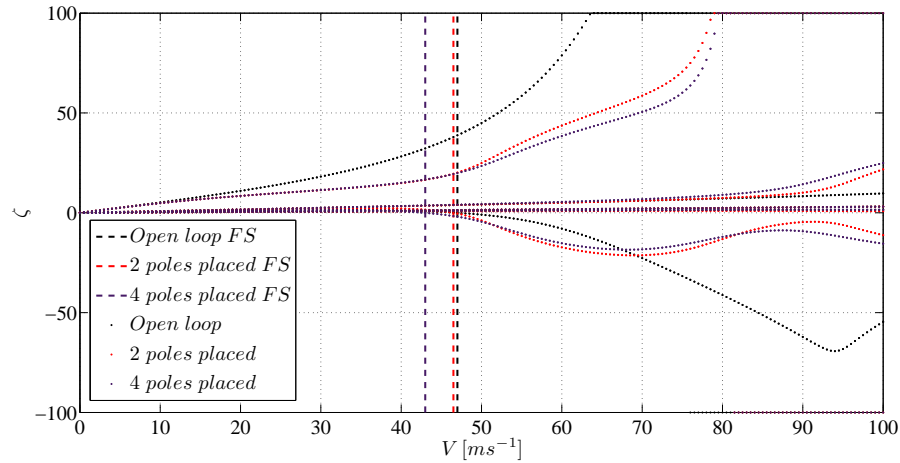


Figure 3.20: Damping plot, 30% first pole imaginary part variation,  $V_C = 20 \text{ m/s}^{-1}$ , two strategies compared

Increasing  $V_C$  diminish the effect of the control as in all the cases taken into exam.

### 3.2.2 Second pairs of poles placed

#### Real part modification

Decreasing the real part of the second pole leaving the first one free the flutter speed gets lower. For variation up to  $-10\%$  of the corresponding open loop value the flutter speed decreases because the second pole has a lower damping than the open loop system and crosses the imaginary axis at a lower speed, while for higher variation in absolute value the effects is more drastic: the first pole bends backwards and it becomes unstable almost immediatly before splitting into two real poles as shown in the figures below.

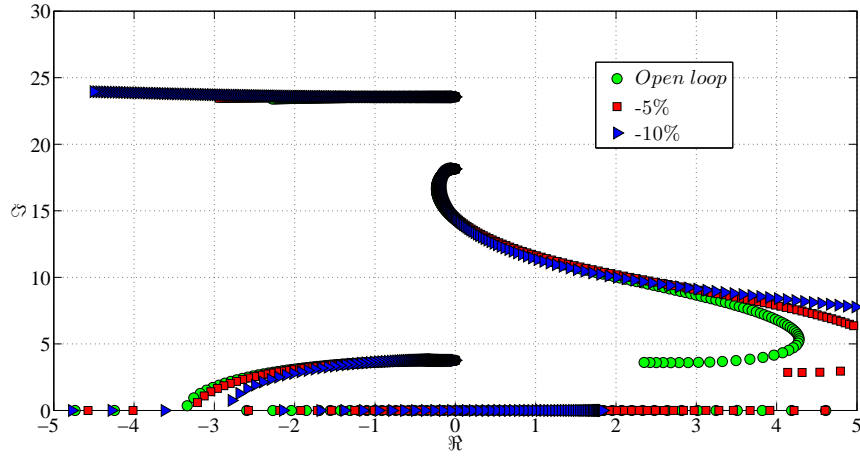


Figure 3.21: Root locus,  $-5\%$  and  $-10\%$  first pole real part variation,  $V_C = 20\text{ms}^{-1}$ , leaving the second pair free

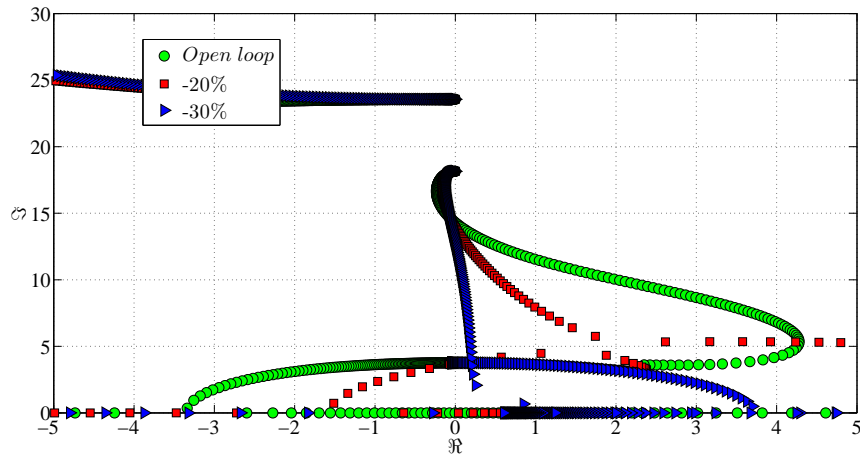


Figure 3.22: Root locus,  $-20\%$  and  $-30\%$  first pole real part variation,  $V_C = 20\text{ms}^{-1}$ , leaving the second pair free

Placing the first mode the behavior of the closed loop system is similar to the uncontrolled one even though decreasing the damping of the mode that causes the instability lower the flutter speed.

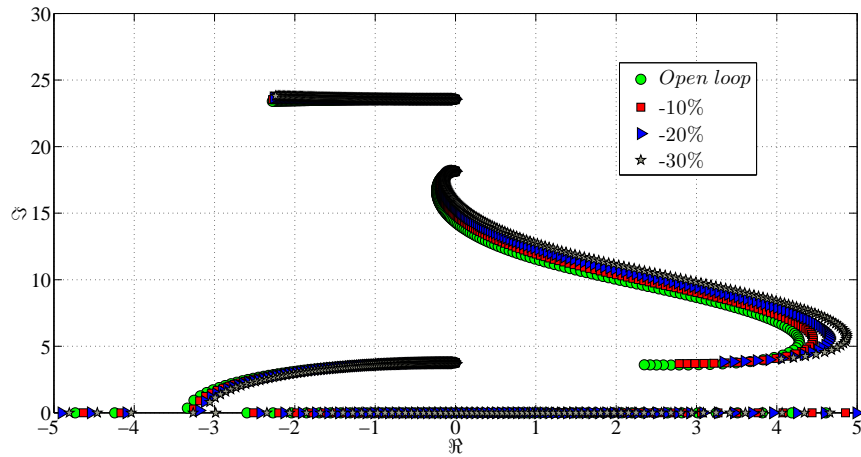


Figure 3.23: Root locus decreasing the real part of the second pair of poles,  $V_C = 20 \text{ ms}^{-1}$ , placing the first pair

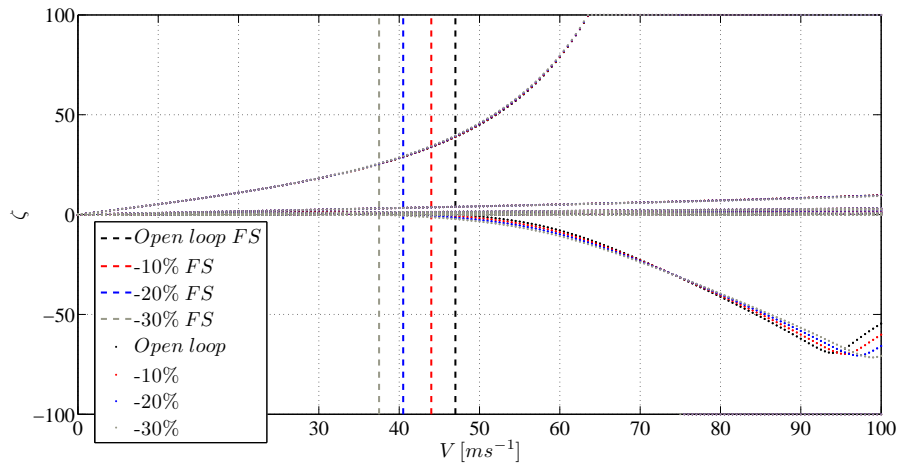


Figure 3.24: Damping plot decreasing the real part of the second pair of poles,  $V_C = 20 \text{ ms}^{-1}$ , placing the first pair

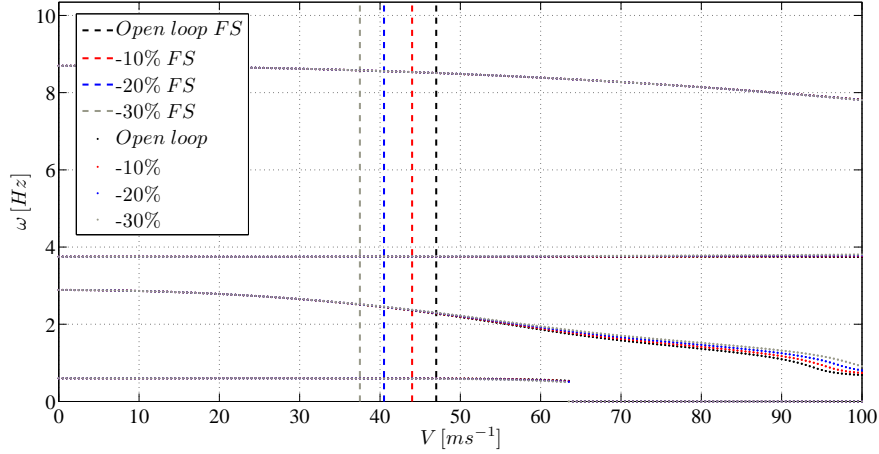


Figure 3.25: Frequency plot decreasing the real part of the second pair of poles,  $V_C = 20 \text{ ms}^{-1}$ , placing the first pair

Increasing  $V_C$  the effects of the controller are lower, for each level of real part variation and for each strategy applied, placing only the second mode and for high variation the poles still interact as shown in figure 3.22.

Increasing the real part gives the same poles behavior for the closed loop system: placing only the second mode and incrementing its damping up to +10% of the open loop value the first poles does not interact and the flutter speed become greater while for higher variation the two poles interact and the flutter occurs at low air speed as shown in figures 3.26 and 3.27.

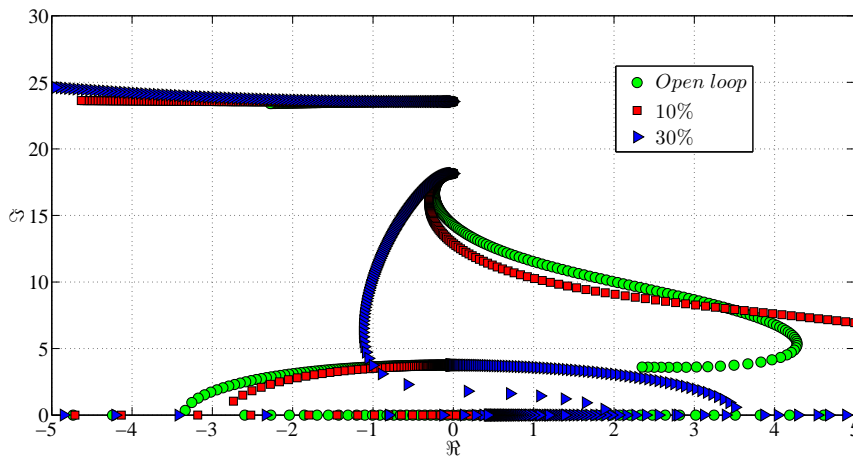


Figure 3.26: Root locus increasing the real part of the second pair of poles,  $V_C = 20 \text{ ms}^{-1}$ , leaving the first pair free

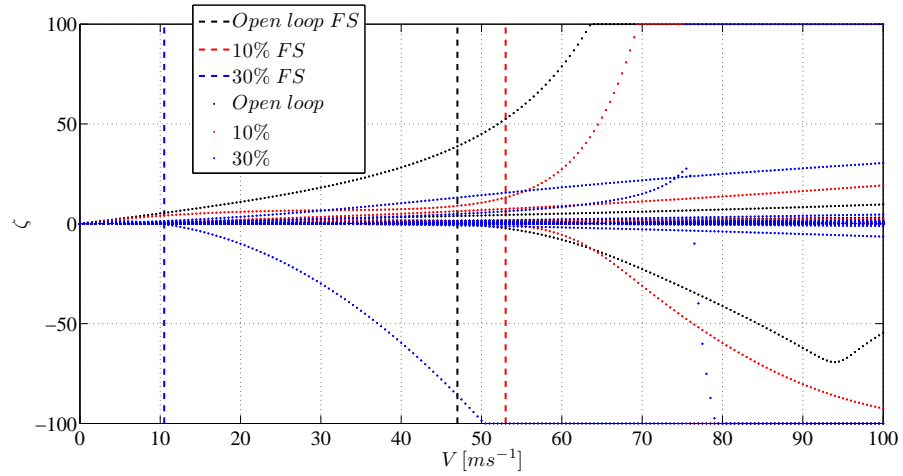


Figure 3.27: Damping plot increasing the real part of the second pair of poles,  $V_C = 20 m s^{-1}$ , leaving the first pair free

Instead applying the other strategy the increment of the real part brings a higher flutter speed for each variation, and bigger is the variation bigger is the flutter speed as shown in figures 3.28 and 3.29.

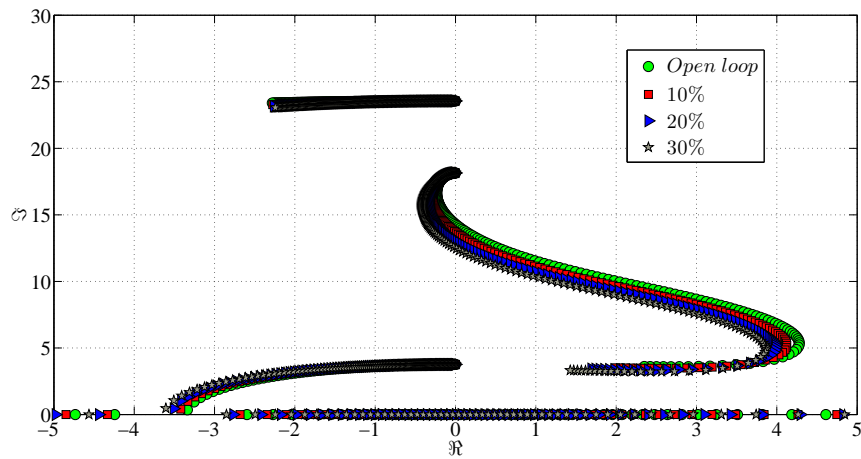


Figure 3.28: Root locus increasing the real part of the second pair of poles,  $V_C = 20 m s^{-1}$ , placing the first pair

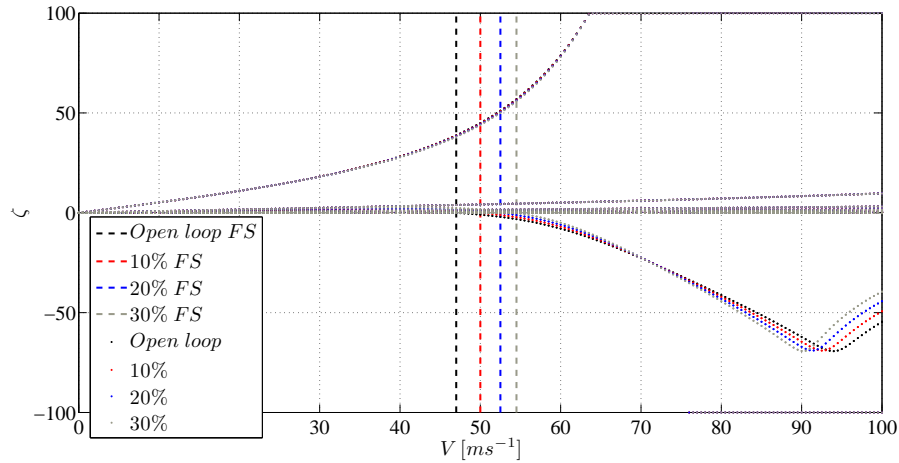


Figure 3.29: Damping plot increasing the real part of the second pair of poles,  $V_C = 20 \text{ m s}^{-1}$ , placing the first pair

Once more increasing  $V_C$  decreases the effects of the control.

### Imaginary part variation

Acting on the imaginary part of the second pair of poles, applying both strategies and increasing or decreasing it, the modes at lower frequency interact and brings the system to the instability almost immediately, in this case the modes that causes the instability are the third and the fourth. The control affects also the poles at higher frequencies, that had not been influenced by the control in previous trials.

Increasing  $V_C$  decreases the effects of the control but still the system become unstable at low air speed.

In the figures below are reported some examples of the imaginary part variation.

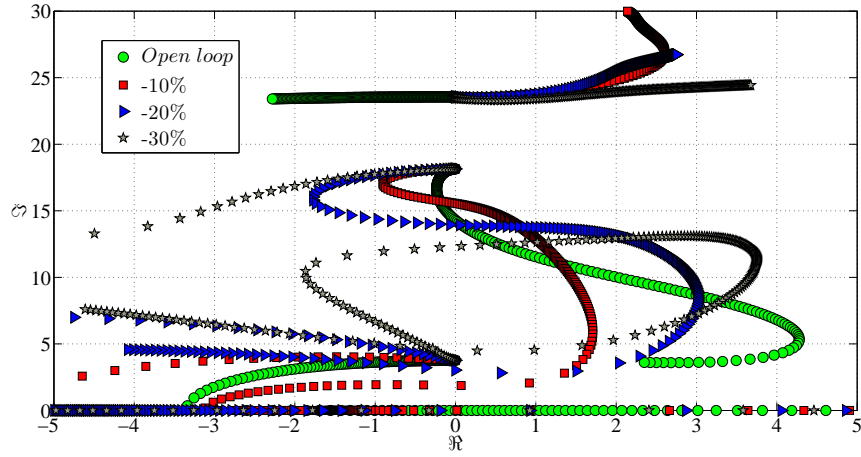


Figure 3.30: Root locus decreasing the imaginary part of the second pair of poles,  $V_C = 20 \text{ ms}^{-1}$ , leaving the second pair free

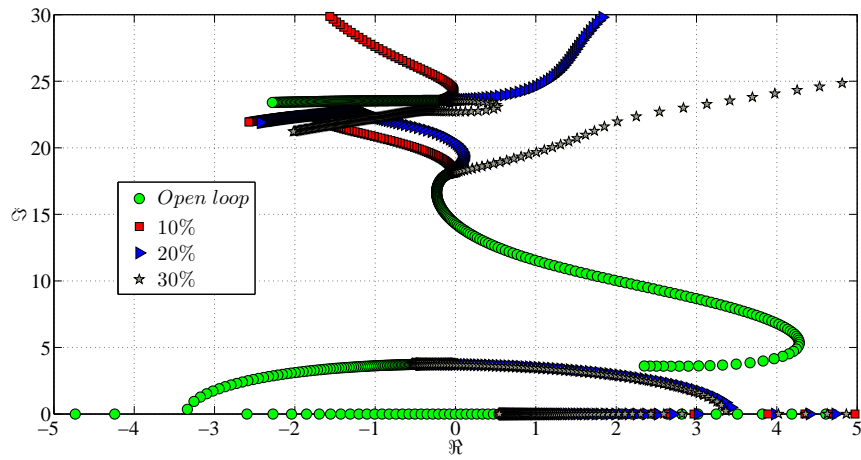


Figure 3.31: Root locus increasing the imaginary part of the second pair of poles,  $V_C = 20 \text{ ms}^{-1}$ , placing the first pair

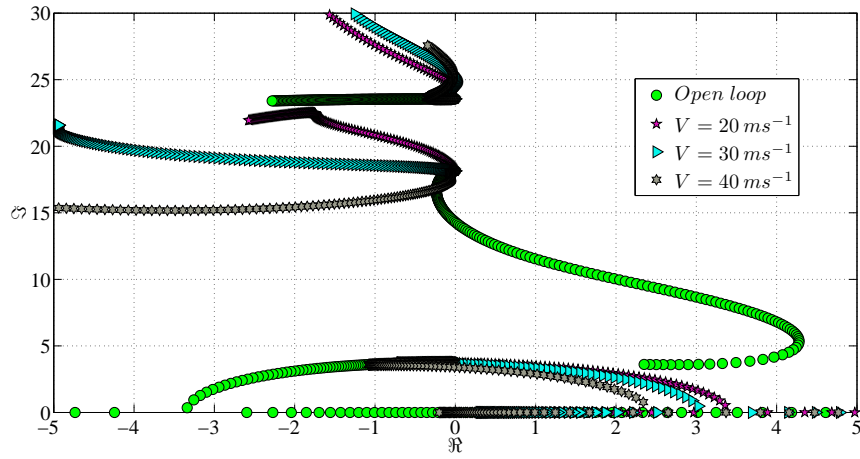


Figure 3.32: Root locus, 10% second pole imaginary part variation, placing the first pair, different  $V_C$  compared

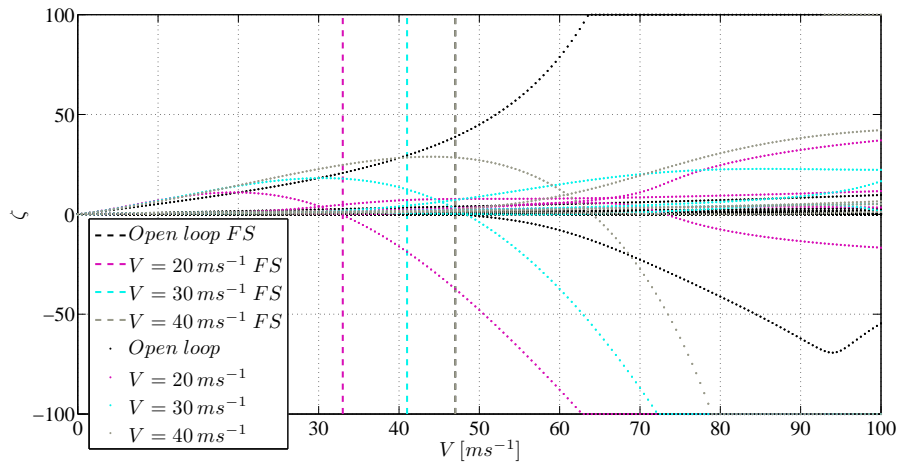


Figure 3.33: Frequency plot, 10% second pole imaginary part variation, placing the first pair, different  $V_C$  compared



### 3.3 Gains

Also for the cantilever wing, as has been done for the tests on the rigid wing, the gains have been inspected because define the deflection that the control surface has to make to apply the control.

The gains has been confronted looking at the euclidean norm of the vectors and what can be seen looking at the results of the trials is that as expected, and as what happened for the tests on the rigid wing, increasing the absolute value of the variation of the imaginary or real part of the poles the norm of the gains increases as shown in figure 3.34.

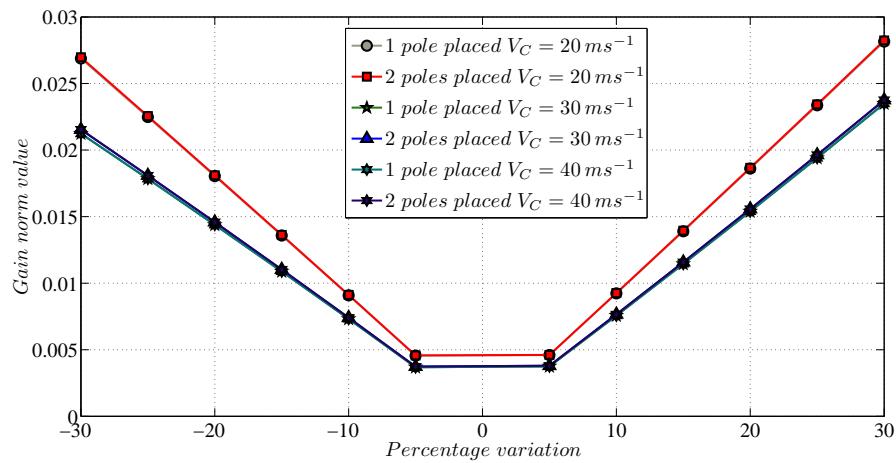


Figure 3.34: Norm of the vector of the gains changing the real part of the first mode

The norm of the gains is always greater if two pairs of poles have been placed instead of placing one pair because the first strategy is a particular case of the second one and placing one mode give the solution with the minimum norm.

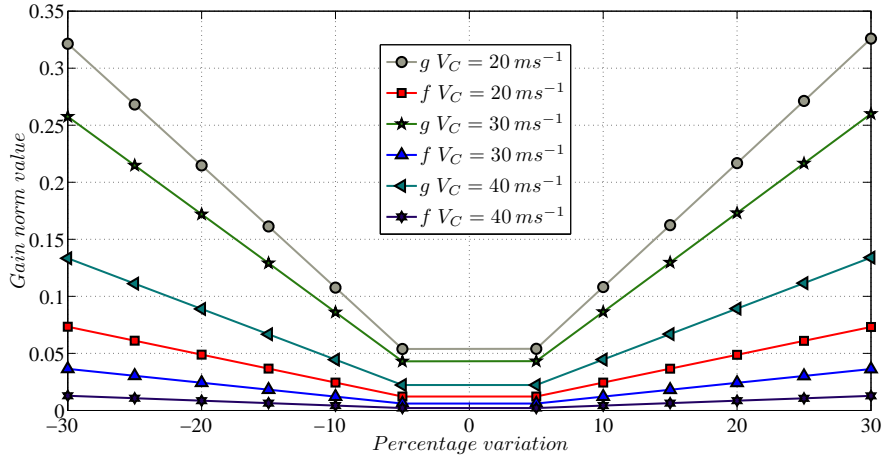


Figure 3.35: Norm of  $\mathbf{f}$  and  $\mathbf{g}$  changing the real part of the second mode leaving the first pair of poles free

One more aspect noted confronting the gains is that for every test (figure 3.35), excepting the real part variation of the first pole, increasing  $V_C$  the norms of the gains diminish. For test with the real part variation of the first pole leaving the second pair free, increasing  $V_C$  the terms in  $\mathbf{g}$  increases as shown in figure 3.36.

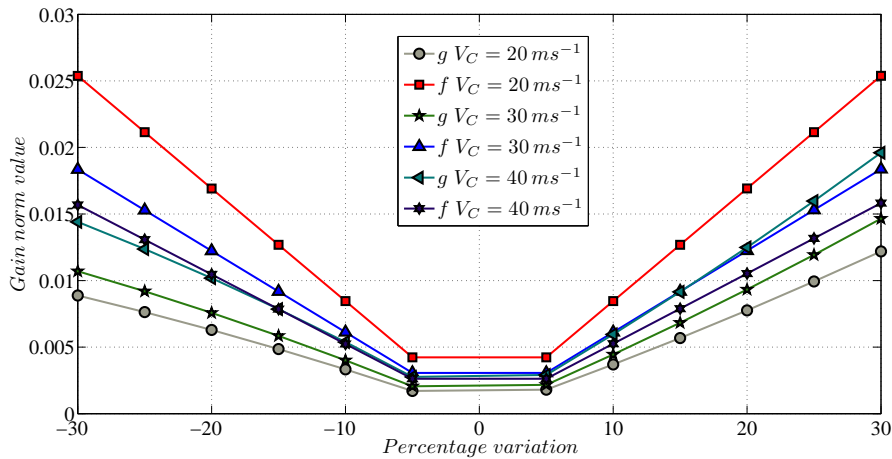


Figure 3.36: Norm of  $\mathbf{f}$  and  $\mathbf{g}$  changing the real part of the first mode leaving the second pair of poles free

The magnitude of the norm of the gains changing the real part is equal to  $10^{-2}$ , for the tests on the first pair of poles, and acting on the second mode gives gains with a magnitude of  $10^{-1}$ .

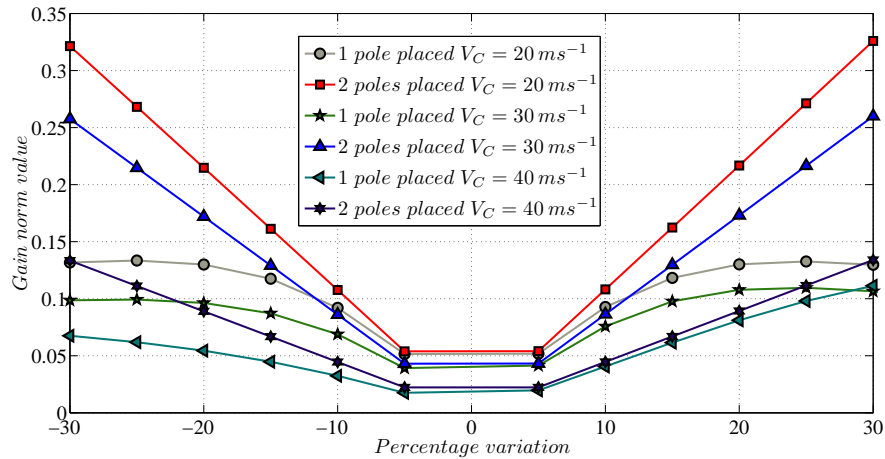


Figure 3.37: Norm of  $\mathbf{g}$  changing the real part of the second mode

Changing the imaginary part of the poles, as what happens for the rigid wing, gives gains with bigger norms sign that the necessary energy to act on the imaginary part is far greater than changing the real part.

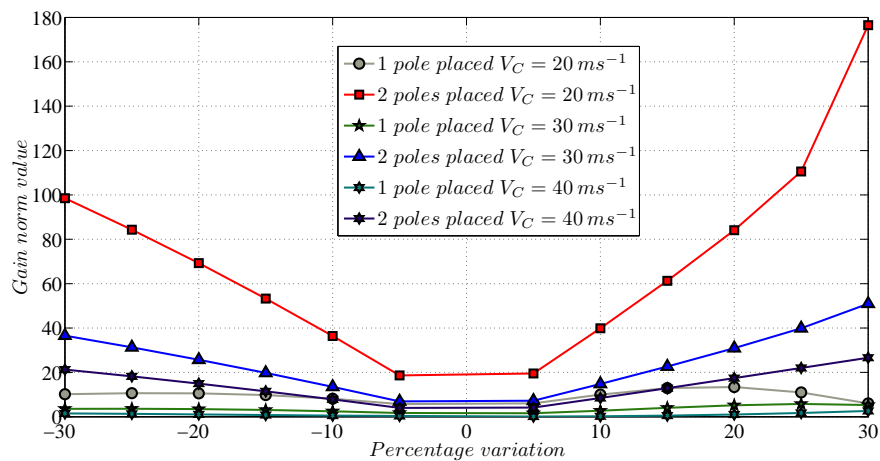


Figure 3.38: Norm of the vector of the gains changing the imaginary part of the second mode

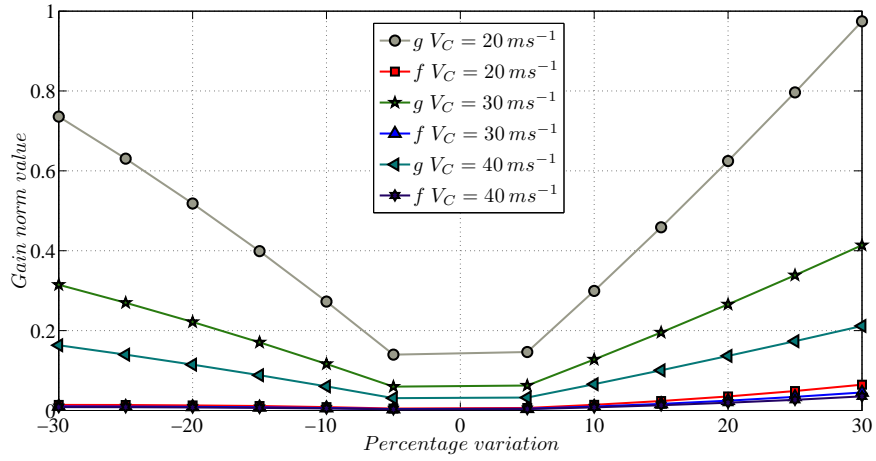


Figure 3.39: Norm of  $f$  and  $g$  changing the imaginary part of the first mode leaving the second pair of poles free

# Chapter 4

## Conclusions and future work

### 4.1 Conclusions

In this thesis the receptance method application on an aeroelastic system has been investigated, the effects of the poles placement have been studied looking for a possible general rule in the behavior of the system stability increasing the airflow speed. This methodology has been applied to different aeroelastic models in order to study effect of the presence of a greater number of modes uncontrolled.

What can be seen from the tests made is that the results depends on the model used, in fact the two numerical models considered have been designed with different parameters but a global common behavior can be seen.

Changing the real part of the poles gives for both models similar results, the behavior of the poles is comparable and is close to the behavior of the open loop system. In each case where the real part has been modified the frequencies of the system do not vary from the uncontrolled one while changes only the damping of the poles.

Changing the real part of the first mode does not affect the flutter speed significantly, in both models the instability occurs near the uncontrolled system, while increasing the damping of the second mode, which is the pole that causes the instability, can increase the performances of the system. Obviously that depends on the characteristics of the model considered, as shown in the tests on the cantilever elastic wing an excessive variation might cause an interaction of the poles and bring the system to the flutter.

What can be also seen in the real variation of the poles is that the gains value in both models remain low with a magnitude of  $10^{-2}$  and that is a index of the feasibility of the control, if the gains would be too big the perturbation that the system could afford would be low in terms of angle of deflection beta.

It appears that systems are very sensible to a variation on the imaginary

part of the poles and depending on the model used a variation on the imaginary part might double the flutter speed or bring to the instability at low air speeds. For the cantilever wing any variation of the frequency of the poles gives as result a flutter speed lower than the uncontrolled system, that is because the poles interact also with the modes at higher frequency that are not modeled in the rigid wing tests.

In additions the gains required to change the frequency of the system are a lot bigger than than the ones required to change the damping (they are  $10^3$  times bigger).

In the following tables are reported the results for the tests made on the rigid wing and on the flexible rectangular wing. In these tables are listed only the trials made with the maximum and the minimum variation of the real or the imaginary part. The other results with different variation fall inside the range defined by the +30% and -30% modifications of the open loop values.

In tables 4.3 and 4.4 are reported the results for the rigid wing model while in tables 4.5, 4.6, 4.7 and 4.7 are listed the tests made on the flexible wing model. The frequencies,  $\omega_{1,2}$  and  $\omega_{3,4}$ , and the damping,  $\zeta_{1,2}$  and  $\zeta_{3,4}$ , are the natural frequencies and the damping of the closed loop system at  $V_C$  of the two pairs of poles placed.

While in tables 4.1 and 4.2 are listed the properties of the uncontrolled system for both each model used.

Table 4.1: Rigid wing, open loop properties

$V_C$ [ $ms^{-1}$ ]	$\omega_{1,2}$ [ $Hz$ ]	$\omega_{3,4}$ [ $Hz$ ]	$\zeta_{1,2}$	$\zeta_{3,4}$	$V_{flutter}$ [ $ms^{-1}$ ]
10	3.56	9.299	3.719	3.1024	29.4
20	3.73	8.2	9.3195	6.0305	

Table 4.2: Flexible wing, open loop properties

$V_C$ [ $ms^{-1}$ ]	$\omega_{1,2}$ [ $Hz$ ]	$\omega_{3,4}$ [ $Hz$ ]	$\zeta_{1,2}$	$\zeta_{3,4}$	$V_{flutter}$ [ $ms^{-1}$ ]
20	$5.9896 \cdot 10^{-1}$	2.7851	$1.0972 \cdot 10^1$	1.1168	47
30	$5.9882 \cdot 10^{-1}$	2.6512	$1.8128 \cdot 10^1$	1.4115	
40	$5.9804 \cdot 10^{-1}$	2.4538	$2.8219 \cdot 10^1$	1.0999	

Table 4.3: Results summary placing one pair of poles and leaving the second one free for the rigid wing model

<i>Poles changed</i>	<i>Variation</i>		$V_C$ [ $ms^{-1}$ ]	$\omega_{1,2}$ [ $Hz$ ]	$\omega_{3,4}$ [ $Hz$ ]	$\zeta_{1,2}$	$\zeta_{3,4}$	<i>Gains</i>				$V_{flutter}$ [ $ms^{-1}$ ]
	$\Re$ or $\Im$	%						$g_{11}$	$g_{12}$	$g_{11}$	$f_{12}$	
1,2	$\Re$	-30	10	3.56	9.3	2.6	3.49	$-4.2 \cdot 10^{-2}$	$3.1 \cdot 10^{-2}$	$-2.5 \cdot 10^{-1}$	$-2.3 \cdot 10^{-2}$	29
1,2	$\Re$	30	10	3.56	9.3	4.8	2.43	$7 \cdot 10^{-2}$	$-4.9 \cdot 10^{-2}$	$2.6 \cdot 10^{-1}$	$4 \cdot 10^{-2}$	28.6
1,2	$\Re$	-30	20	3.72	8.21	6.54	7.9	$-1.5 \cdot 10^{-2}$	$2 \cdot 10^{-2}$	$-2.2 \cdot 10^{-1}$	$-2.8 \cdot 10^{-2}$	29.5
1,2	$\Re$	30	20	3.74	8.18	12.1	1.6	$3.4 \cdot 10^{-2}$	$-3.4 \cdot 10^{-2}$	$2.5 \cdot 10^{-1}$	$6.5 \cdot 10^{-2}$	24.3
1,2	$\Im$	-30	10	2.5	0	5.3	100	$-3.1 \cdot 10^1$	$4.4 \cdot 10^1$	$-2.4 \cdot 10^1$	$-1.8 \cdot 10^1$	0.6
1,2	$\Im$	30	10	4.6	0	2.9	-100	3.01	1.6	-9.8	$1.9 \cdot 10^1$	0.2
1,2	$\Im$	-30	20	2.6	0	13.3	100	-4.3	9.4	-7.3	-3.6	1.4
1,2	$\Im$	30	20	4.84	0	7.18	-100	$2.3 \cdot 10^{-1}$	$4.3 \cdot 10^{-1}$	-3	1.9	1.1
3,4	$\Re$	-30	10	3.56	9.3	3.6	2.17	$-6.3 \cdot 10^{-4}$	$-8.8 \cdot 10^{-2}$	$1.6 \cdot 10^{-2}$	$5.8 \cdot 10^{-2}$	23.8
3,4	$\Re$	30	10	3.56	9.3	3.93	4	$3.4 \cdot 10^{-4}$	$4.7 \cdot 10^{-2}$	$5 \cdot 10^{-3}$	$-5.9 \cdot 10^{-2}$	32.1
3,4	$\Re$	-30	20	3.74	8.19	9.33	4.23	$1 \cdot 10^{-3}$	$-6.1 \cdot 10^{-2}$	$2.1 \cdot 10^{-2}$	$2.5 \cdot 10^{-2}$	27.8
3,4	$\Re$	30	20	3.72	8.2	9.7	7.8	$-6 \cdot 10^{-4}$	$3.7 \cdot 10^{-2}$	$2.9 \cdot 10^{-3}$	$-2.5 \cdot 10^{-2}$	30.7
3,4	$\Im$	-30	10	0	6.5	-100	4.43	$1.9 \cdot 10^1$	$9.7 \cdot 10^1$	$-2 \cdot 10^1$	4.4	0.3
3,4	$\Im$	30	10	3.91	12.1	4.4	2.39	5.1	$-1.2 \cdot 10^2$	$-6.2 \cdot 10^{-1}$	$-8.5 \cdot 10^{-2}$	100
3,4	$\Im$	-30	20	0	5.75	-100	8.6	1.6	9.7	$-1 \cdot 10^1$	1.9	0.7
3,4	$\Im$	30	20	3.99	10.7	16.4	4.6	1.3	$-2.4 \cdot 10^1$	$5.6 \cdot 10^{-1}$	$6.6 \cdot 10^{-3}$	100

Table 4.4: Results summary placing both pair of poles for the rigid wing model

<i>Poles changed</i>	<i>Variation</i>		$V_C$ [ $ms^{-1}$ ]	$\omega_{1,2}$ [ $Hz$ ]	$\omega_{3,4}$ [ $Hz$ ]	$\zeta_{1,2}$	$\zeta_{3,4}$	<i>Gains</i>				$V_{flutter}$ [ $ms^{-1}$ ]
	$\Re$ or $\Im$	%						$g_{11}$	$g_{12}$	$g_{11}$	$f_{12}$	
1,2	$\Re$	-30	10	3.6	9.3	2.6	3.1	$-1.8 \cdot 10^{-1}$	$-5.5 \cdot 10^{-3}$	$-2.4 \cdot 10^{-1}$	$1.7 \cdot 10^{-3}$	27.8
1,2	$\Re$	30	10	3.56	9.3	4.8	3.1	$2.34 \cdot 10^{-1}$	$5 \cdot 10^{-3}$	$2.4 \cdot 10^{-1}$	$-1.7 \cdot 10^{-3}$	31.2
1,2	$\Re$	-30	20	3.7	8.2	6.5	6.03	$-4.6 \cdot 10^{-1}$	$-3.6 \cdot 10^{-2}$	$-1.98 \cdot 10^{-1}$	$-3.2 \cdot 10^{-3}$	28.3
1,2	$\Re$	30	20	3.74	8.2	12.1	6.03	$5.87 \cdot 10^{-1}$	$3.8 \cdot 10^{-2}$	$1.98 \cdot 10^{-1}$	$3.2 \cdot 10^{-3}$	30.8
1,2	$\Im$	-30	10	2.5	9.3	5.31	3.1	$-1.2 \cdot 10^2$	$8.8 \cdot 10^{-1}$	$9.6 \cdot 10^{-3}$	$9.5 \cdot 10^{-4}$	14.7
1,2	$\Im$	30	10	4.63	9.3	2.86	3.1	$1.62 \cdot 10^2$	-1.19	$-1.3 \cdot 10^{-2}$	$-1.3 \cdot 10^{-3}$	32.2
1,2	$\Im$	-30	20	2.62	8.2	13.25	6.03	$-4.2 \cdot 10^1$	$-6.6 \cdot 10^{-1}$	$2.7 \cdot 10^{-2}$	$2.7 \cdot 10^{-3}$	28.3
1,2	$\Im$	30	20	4.84	8.2	7.18	6.03	$5.7 \cdot 10^1$	$8.9 \cdot 10^{-1}$	$-3.7 \cdot 10^{-2}$	$-3.7 \cdot 10^{-3}$	33.1
3,4	$\Re$	-30	10	3.56	9.3	3.72	2.17	$-2.8 \cdot 10^{-1}$	$-8.2 \cdot 10^{-2}$	$3.9 \cdot 10^{-2}$	$5.8 \cdot 10^{-2}$	24
3,4	$\Re$	30	10	3.56	9.3	3.72	4.03	$2.6 \cdot 10^{-1}$	$5 \cdot 10^{-2}$	$-3.9 \cdot 10^{-2}$	$-5.8 \cdot 10^{-2}$	31.9
3,4	$\Re$	-30	20	3.728	8.19	9.32	4.22	$-3.5 \cdot 10^{-1}$	$-6.8 \cdot 10^{-2}$	$2 \cdot 10^{-2}$	$2.5 \cdot 10^{-2}$	27.8
3,4	$\Re$	30	20	3.73	8.21	9.32	7.83	$3.3 \cdot 10^{-1}$	$4.4 \cdot 10^{-2}$	$-2 \cdot 10^{-2}$	$-2.5 \cdot 10^{-2}$	30.6
3,4	$\Im$	-30	10	3.56	6.5	3.72	4.43	$6.4 \cdot 10^1$	$9.3 \cdot 10^1$	$7.7 \cdot 10^{-1}$	$7.6 \cdot 10^{-2}$	11.7
3,4	$\Im$	30	10	3.56	12.1	3.72	2.39	$-8.6 \cdot 10^1$	$-1.26 \cdot 10^2$	-1	$-1 \cdot 10^{-1}$	41
3,4	$\Im$	-30	20	3.73	5.75	9.32	8.6	$1.7 \cdot 10^1$	$1.9 \cdot 10^1$	$4.2 \cdot 10^{-1}$	$4.2 \cdot 10^{-2}$	24.6
3,4	$\Im$	30	20	3.73	10.65	9.32	4.64	$-2.3 \cdot 10^1$	$-2.5 \cdot 10^1$	$-5.7 \cdot 10^{-1}$	$-5.6 \cdot 10^{-2}$	31.5



Table 4.5: Results summary placing one pair of poles and leaving the second one free for the flexible rectangular wing, real part modifications

<i>Poles changed</i>	<i>Variation</i>		$V_C$ [ $ms^{-1}$ ]	$\omega_{1,2}$ [ $Hz$ ]	$\omega_{3,4}$ [ $Hz$ ]	$\zeta_{1,2}$	$\zeta_{3,4}$	<i>Gains</i>				$V_{flutter}$ [ $ms^{-1}$ ]
	$\Re$ or $\Im$	%						$g_{11}$	$g_{12}$	$g_{11}$	$f_{12}$	
1,2	$\Re$	-30	20	0.6	2.79	7.7	1.13	$8.9 \cdot 10^{-3}$	$6.5 \cdot 10^{-5}$	$2.5 \cdot 10^{-2}$	$-3.6 \cdot 10^{-4}$	49
1,2	$\Re$	30	20	0.6	2.79	14.2	1.11	$-1.2 \cdot 10^{-2}$	$-7.2 \cdot 10^{-5}$	$-2.5 \cdot 10^{-2}$	$5.7 \cdot 10^{-4}$	46
1,2	$\Re$	-30	30	0.59	2.65	12.8	1.45	$1.1 \cdot 10^{-2}$	$7.6 \cdot 10^{-5}$	$1.8 \cdot 10^{-2}$	$-7.2 \cdot 10^{-4}$	48.5
1,2	$\Re$	30	30	0.61	2.65	23.3	1.38	$-1.5 \cdot 10^{-2}$	$-8.6 \cdot 10^{-5}$	$-1.8 \cdot 10^{-2}$	$1.16 \cdot 10^{-3}$	46.5
1,2	$\Re$	-30	40	0.59	2.45	20.17	1.2	$1.4 \cdot 10^{-2}$	$9.4 \cdot 10^{-5}$	$1.6 \cdot 10^{-2}$	$-1.5 \cdot 10^{-3}$	48
1,2	$\Re$	30	40	0.61	2.46	35.72	1.02	$-1.96 \cdot 10^{-2}$	$-1.1 \cdot 10^{-4}$	$-1.6 \cdot 10^{-2}$	$2.5 \cdot 10^{-3}$	46.5
3,4	$\Re$	-30	20	0.6	2.79	-8.74	0.782	$-1.5 \cdot 10^{-2}$	$-1.3 \cdot 10^{-1}$	$1.5 \cdot 10^{-1}$	$-9 \cdot 10^{-2}$	11
3,4	$\Re$	30	20	0.59	2.79	-10.02	1.45	$1 \cdot 10^{-2}$	$1.3 \cdot 10^{-1}$	$1.6 \cdot 10^{-1}$	$5.99 \cdot 10^{-2}$	10.5
3,4	$\Re$	-30	30	0.61	2.65	-15.33	0.988	$-2.5 \cdot 10^{-2}$	$-9.5 \cdot 10^{-2}$	$1.14 \cdot 10^{-1}$	$-6.6 \cdot 10^{-2}$	14.5
3,4	$\Re$	30	30	0.59	2.65	-19.76	1.83	$2.08 \cdot 10^{-2}$	$1.04 \cdot 10^{-1}$	$1.3 \cdot 10^{-1}$	$1.1 \cdot 10^{-2}$	13
3,4	$\Re$	-30	40	0.62	2.45	0.197	0.77	$-2.95 \cdot 10^{-2}$	$-6.1 \cdot 10^{-2}$	$5.2 \cdot 10^{-2}$	$-3.7 \cdot 10^{-2}$	41
3,4	$\Re$	30	40	0.56	2.45	8.77	1.43	$4.3 \cdot 10^{-2}$	$1.03 \cdot 10^{-1}$	$3.6 \cdot 10^{-2}$	$-2.9 \cdot 10^{-3}$	50.5

4.1. Conclusions

Table 4.6: Results summary placing one pair of poles and leaving the second one free for the flexible rectangular wing, imaginary part modifications

<i>Poles changed</i>	<i>Variation</i>		$V_C$ [ $ms^{-1}$ ]	$\omega_{1,2}$ [ $Hz$ ]	$\omega_{3,4}$ [ $Hz$ ]	$\zeta_{1,2}$	$\zeta_{3,4}$	<i>Gains</i>				$V_{flutter}$ [ $ms^{-1}$ ]
	$\Re$ or $\Im$	%						$g_{11}$	$g_{12}$	$g_{11}$	$f_{12}$	
1,2	$\Im$	-30	20	0.42	2.79	15.6	1.1	$7.3 \cdot 10^{-1}$	$-2.7 \cdot 10^{-3}$	$-2.3 \cdot 10^{-4}$	$-1.4 \cdot 10^{-2}$	28.5
1,2	$\Im$	30	20	0.78	2.78	8.46	1.406	$-9.7 \cdot 10^{-1}$	$-4.9 \cdot 10^{-3}$	$5.4 \cdot 10^{-5}$	$6.5 \cdot 10^{-2}$	46.5
1,2	$\Im$	-30	30	0.43	2.65	25.5	1.3	$3.1 \cdot 10^{-1}$	$-1.3 \cdot 10^{-3}$	$-3.7 \cdot 10^{-4}$	$-9.9 \cdot 10^{-3}$	42.5
1,2	$\Im$	30	30	0.77	2.64	14.04	1.86	$-4.1 \cdot 10^{-1}$	$-2.2 \cdot 10^{-3}$	$4.5 \cdot 10^{-4}$	$4.5 \cdot 10^{-2}$	48.5
1,2	$\Im$	-30	40	0.44	2.46	38.7	1.01	$1.6 \cdot 10^{-1}$	$-7.4 \cdot 10^{-4}$	$-6.3 \cdot 10^{-4}$	$-8.4 \cdot 10^{-3}$	47
1,2	$\Im$	30	40	0.76	2.44	22.1	1.69	$-2.1 \cdot 10^{-1}$	$-1.1 \cdot 10^{-3}$	$1 \cdot 10^{-3}$	$3.5 \cdot 10^{-2}$	49
3,4	$\Im$	-30	20	1.95	2.26	1.6	45.7	-8.7	$-9.9 \cdot 10^{-1}$	$-5.03 \cdot 10^{-1}$	4.87	4
3,4	$\Im$	30	20	1.41	2.73	2.1	8.76	-5.9	$2.5 \cdot 10^{-1}$	$-5 \cdot 10^{-3}$	1.16	15
3,4	$\Im$	-30	30	1.86	1.98	2.02	53.3	-2.78	$-3.1 \cdot 10^{-1}$	$-2 \cdot 10^{-1}$	2.23	8
3,4	$\Im$	30	30	1.67	3.09	25.4	-13.9	-5.14	$4.8 \cdot 10^{-1}$	$-1.3 \cdot 10^{-1}$	-1.1	5.5
3,4	$\Im$	-30	40	1.72	1.73	1.57	52.1	-1.1	$-1.1 \cdot 10^{-1}$	$-6.9 \cdot 10^{-2}$	1.1	16.5
3,4	$\Im$	30	40	1.07	3.19	64.9	0.85	-1.8	$2.8 \cdot 10^{-1}$	$-3.4 \cdot 10^{-1}$	-2.1	3

Table 4.7: Results summary placing both pairs of poles for the flexible rectangular wing, real part modifications

<i>Poles changed</i>	<i>Variation</i>		$V_C$ [ $ms^{-1}$ ]	$\omega_{1,2}$ [ $Hz$ ]	$\omega_{3,4}$ [ $Hz$ ]	$\zeta_{1,2}$	$\zeta_{3,4}$	<i>Gains</i>				$V_{flutter}$ [ $ms^{-1}$ ]
	$\Re$ or $\Im$	%						$g_{11}$	$g_{12}$	$g_{11}$	$f_{12}$	
1,2	$\Re$	-30	20	0.6	2.79	7.7	1.12	$8.8 \cdot 10^{-3}$	$-4.2 \cdot 10^{-4}$	$2.5 \cdot 10^{-2}$	$-2.5 \cdot 10^{-3}$	49
1,2	$\Re$	30	20	0.6	2.79	14.2	1.12	$-1.2 \cdot 10^{-2}$	$7.9 \cdot 10^{-4}$	$-2.5 \cdot 10^{-2}$	$2.5 \cdot 10^{-3}$	46
1,2	$\Re$	-30	30	0.6	2.65	12.8	1.41	$1 \cdot 10^{-2}$	$-7.5 \cdot 10^{-4}$	$1.8 \cdot 10^{-2}$	$-4.2 \cdot 10^{-3}$	48
1,2	$\Re$	30	30	0.6	2.65	23.3	1.41	$-1.4 \cdot 10^{-2}$	$1.7 \cdot 10^{-2}$	$-1.8 \cdot 10^{-2}$	$4.2 \cdot 10^{-3}$	46.5
1,2	$\Re$	-30	40	0.59	2.45	20.17	1.1	$1.4 \cdot 10^{-2}$	$-2.2 \cdot 10^{-4}$	$1.6 \cdot 10^{-2}$	$-7.1 \cdot 10^{-3}$	47.5
1,2	$\Re$	30	40	0.61	2.45	35.72	1.1	$-1.9 \cdot 10^{-2}$	$2.6 \cdot 10^{-3}$	$-1.6 \cdot 10^{-2}$	$7 \cdot 10^{-3}$	47
3,4	$\Re$	-30	20	0.6	2.79	10.9	0.78	$-2.8 \cdot 10^{-3}$	$-3.2 \cdot 10^{-1}$	$7 \cdot 10^{-4}$	$-7.3 \cdot 10^{-2}$	37.5
3,4	$\Re$	30	20	0.6	2.79	10.9	1.45	$2.8 \cdot 10^{-2}$	$3.3 \cdot 10^{-1}$	$-7.2 \cdot 10^{-4}$	$7.3 \cdot 10^{-2}$	54.5
3,4	$\Re$	-30	30	0.6	2.65	18.1	0.99	$-2.4 \cdot 10^{-3}$	$-2.6 \cdot 10^{-1}$	$9.3 \cdot 10^{-4}$	$-3.6 \cdot 10^{-2}$	42
3,4	$\Re$	30	30	0.6	2.65	18.13	1.8	$2.4 \cdot 10^{-3}$	$2.6 \cdot 10^{-1}$	$-9.4 \cdot 10^{-4}$	$3.6 \cdot 10^{-2}$	52
3,4	$\Re$	-30	40	0.6	2.45	28.2	0.77	$-1.3 \cdot 10^{-3}$	$-1.3 \cdot 10^{-1}$	$7.4 \cdot 10^{-4}$	$-1.3 \cdot 10^{-2}$	45
3,4	$\Re$	30	40	0.6	2.45	28.2	1.43	$1.3 \cdot 10^{-3}$	$1.3 \cdot 10^{-1}$	$-7.4 \cdot 10^{-4}$	$1.3 \cdot 10^{-2}$	49

Table 4.8: Results summary placing both pairs of poles for the flexible rectangular wing, imaginary part modifications

<i>Poles changed</i>	<i>Variation</i>		$V_C$ [ $ms^{-1}$ ]	$\omega_{1,2}$ [ $Hz$ ]	$\omega_{3,4}$ [ $Hz$ ]	$\zeta_{1,2}$	$\zeta_{3,4}$	<i>Gains</i>				$V_{flutter}$ [ $ms^{-1}$ ]
	$\Re$ or $\Im$	%						$g_{11}$	$g_{12}$	$g_{11}$	$f_{12}$	
1,2	$\Im$	-30	20	0.42	2.78	15.6	1.12	$7.3 \cdot 10^{-1}$	$-7.2 \cdot 10^{-2}$	$3.5 \cdot 10^{-5}$	$-4.1 \cdot 10^{-5}$	28.5
1,2	$\Im$	30	20	0.78	2.78	8.46	1.12	$-9.8 \cdot 10^{-1}$	$9.5 \cdot 10^{-2}$	$-4.6 \cdot 10^{-5}$	$5.8 \cdot 10^{-5}$	43
1,2	$\Im$	-30	30	0.43	2.65	25.5	1.41	$3.1 \cdot 10^{-1}$	$-7.3 \cdot 10^{-2}$	$4.1 \cdot 10^{-5}$	$-1.1 \cdot 10^{-4}$	42.5
1,2	$\Im$	30	30	0.77	2.65	14	1.41	$-4.2 \cdot 10^{-1}$	$9.7 \cdot 10^{-1}$	$-5.4 \cdot 10^{-5}$	$1.5 \cdot 10^{-4}$	45.5
1,2	$\Im$	-30	40	0.44	2.45	38.7	1.1	$1.6 \cdot 10^{-1}$	$-7.4 \cdot 10^2$	$2.8 \cdot 10^{-5}$	$-2.8 \cdot 10^{-4}$	47.5
1,2	$\Im$	30	40	0.76	2.45	22.1	1.1	$-2.2 \cdot 10^{-1}$	$9.9 \cdot 10^{-2}$	$-3.67 \cdot 10^{-5}$	$3.8 \cdot 10^{-4}$	46.5
3,4	$\Im$	-30	20	0.59	1.95	10.9	1.6	$4 \cdot 10^{-2}$	$-9.8 \cdot 10^1$	$2.7 \cdot 10^{-1}$	1.16	10
3,4	$\Im$	30	20	0.59	3.62	10.9	0.86	$-3.3 \cdot 10^{-1}$	$1.8 \cdot 10^2$	$-5 \cdot 10^{-1}$	-8.8	1
3,4	$\Im$	-30	30	0.59	1.86	18.13	2.02	$4.3 \cdot 10^{-2}$	$-3.7 \cdot 10^1$	$1.7 \cdot 10^{-1}$	$7.7 \cdot 10^{-1}$	16
3,4	$\Im$	30	30	0.59	3.45	18.13	1.09	$-1.6 \cdot 10^{-1}$	$5 \cdot 10^1$	$-2.4 \cdot 10^{-1}$	-2.6	2.5
3,4	$\Im$	-30	40	0.59	1.72	28.22	1.57	$4.7 \cdot 10^{-2}$	$-1.5 \cdot 10^1$	$1.1 \cdot 10^{-1}$	$5.5 \cdot 10^{-1}$	33
3,4	$\Im$	30	40	0.59	3.19	28.22	0.85	$-1.1 \cdot 10^{-1}$	$1.9 \cdot 10^1$	$-1.5 \cdot 10^{-1}$	-1.2	5

## 4.2 Future work

The studies that could be made on the receptance method applied to an aeroelastic system are numerous:

- A different control law could be applied instead the one used proportional to the states displacement and velocity.
- The receptance method could be applied using an output-feedback control even if the advantage of solving a linear system would be lost.
- The response to an external disturb, such as turbulence or gust, could be computed.
- The tests made could be verified experimentally.

Also the model could be upgraded implementing a more realistic aerodynamic modeling, including a quasi-steady or unsteady aerodynamic description in the frequency domain or a model with augmented states in the time domain.



# Bibliography

- [1] Y. Fung. *An introduction to the theory of Aeroelasticity*. Dover Phoenix Editions, 1955.
- [2] D. H. Hodges and G. A. Pierce. *Introduction to Structural Dynamics and Aeroservoelasticity*. Cambridge University Press, 2002.
- [3] J. R. Wright and J. E. Cooper. *Introduction to Aircraft Aeroelasticity and Loads*. John Wiley, 2007.
- [4] C. Jr. De Marqui, E. M. Belo, and F. D. Marques. Wind-tunnel model and a controller for flutter suppression. *45th AIAA/ASME/ASCE/AHS/ASC Structures, Structural Dynamics & Materials Conference*, 19-22 April 2004.
- [5] J. Njuguna. Flutter prediction, suppression and control in aircraft composite wings as a design prerequisite: A survey. *Structural Control and Health Monitoring*, 14:715–758, 2007.
- [6] E. Nissim. Active flutter suppression using trailing edge and tab control surface. *AIAA Journal*, 14(6):757–762, June 1976.
- [7] P. Palmieri and R. Onori R. *Progetto e Verifica Sperimentale di un Sistema di Controllo Attivo del Flutter*. PhD thesis, Politecnico di Milano, 1988.
- [8] T. E. Noll and L. J. Huttzell. Wing/store active flutter suppression - correlation of analyses and wind tunnel tests. *AIAA Journal*, August 1978.
- [9] S. Raja and A. R. Upadhyaya. Active control of wing flutter using piezoactuated surface. *Journal of aircraft*, 44(1):71–80, January-February 2007.
- [10] E. V. Ardelean, M. A. McEver, D. G. Cole, and R. L. Clark. Active flutter control with v-stack piezoelectric flap actuator. *Journal of Aircraft*, 43(2):482–486, March-April 2006.

## BIBLIOGRAPHY

---

- [11] W. Dressler. Control of an elastic aircraft using optimal control. *Impact of Active Control Technology on Airplanes Design*, AGARD-CP-157.
- [12] J. H. Newson. Control law synthesis for active flutter suppression using optimal control theory. *Journal of Guidance and Control*, 2(5), September-October 1979.
- [13] J. E. Cooper, J. E. Mottershead, L. A. McDonough, and K. V. Singh. Active aeroelastic control using the receptance method. *Proceedings of the ASME 2010 International Mechanical Engineering Congress & Exposition*, 2010.
- [14] W. J. Duncan. The admittance method for obtaining the natural frequencies of systems. *Philosophical Magazine*, 32:401–409, 1941.
- [15] R. E. D. Bishop and D. C. Johnson. *The Mechanics of Vibration*. Cambridge University Press, 1960.
- [16] Y. M. Ram. Dynamic structural modification. *The Shock and Vibration Digest*, 32:11–17, 2000.
- [17] J. T. Weissenburger. Effect of local modifications on the vibration characteristics of linear systems. *Journal of Applied Mechanics*, 90:327–333, 1968. Transactions of ASME.
- [18] A. H. Vincent. A note on the properties of the variation of structural response with respect to a single structural parameter when plotted in the complex plane. Technical report, Westland Helicopters Ltd., September 1973. Report GEN/DYN/RES/010R.
- [19] M. Ghandchi Tehrani, W. Wang, C. Mares, and J. E. Mottershead. The generalized vincent circle in vibration suppression. *Journal of Sound and Vibration*, 292(3-5):661–675, 2006.
- [20] J. E. Mottershead. Structural modification for the assignment of zeros using measured receptances. *Journal of Applied Mechanics*, 68(5):791–798, 2001. Transactions of the American Society of Mechanical Engineers.
- [21] J. E. Mottershead, C. Mares, and M. I. Friswell. An inverse method for the assignment of vibration nodes. *Mechanical Systems and Signal Processing*, 15(1):87–100, 2001.



- [22] Y. M. Ram and J. E. Mottershead. Receptance method in active vibration control. *American Institute of Aeronautics and Astronautics Journal*, 45(3):562–567, 2007.
- [23] J. E. Mottershead, M. Ghandchi Tehrani, S. James, and Y. M. Ram. Active vibration suppression by pole-zero placement using measured receptances. *Journal of Sound and Vibration*, 311:1391–1408, 2008.
- [24] J. E. Mottershead, M. Ghandchi Tehrani, and Y. M. Ram. Assignment of eigenvalue sensitivity from receptance measurements. *Mechanical System and Signal Processing*, 23:1931–1939, 2009.
- [25] E. K. Chu and B. N. Datta. Numerically robust pole assignment for second order system. *International Journal of Control*, 64(4):1113–1127, 1996.
- [26] M. Ghandchi Tehrani. *Passive Modification and Active Vibration Control by the Receptance Method*. PhD thesis, University of Liverpool, October 2007.
- [27] D. Formenti and M. Richardson. Parameter estimation from frequency response measurements using rational fraction polynomials. *Proceedings of the First International Modal Analysis Conference*, 1996. Orlando.
- [28] G. H. Golub and C. F. Van Loan. *Matrix Computations*. Johns Hopkins University Press, 1983.
- [29] E. V. Ardelean, D. G. Cole, and R. L. Clark. High performance v-stack piezoelectric actuator. *Journal of Intelligent Material Systems and Structures*, 15, November 2004.